

**DEVELOPMENT AND INVESTIGATION OF SLURRY
ELECTRODES, NOVEL MATERIALS AND MEMBRANES
FOR TUBULAR VANADIUM REDOX BATTERIES**

**TÜBÜLER VANADYUM REDOKS AKIŞ BATARYALARI
İÇİN BULAMAÇ ELEKTROT, YENİ MATERYAL VE
MEMBRANLARIN ARAŞTIRMA VE GELİŞTİRMESİ**

KORCAN PERÇİN

PROF. DR. AHMET R. ÖZDURAL

Supervisor

Submitted to the Graduate School of Science and Engineering
of Hacettepe University as a Partial Fulfillment of the Requirements for the
Award of the Degree of Master of Science in Chemical Engineering

2015

This work named "**Development and Investigation of Slurry Electrodes, Novel Materials and Membranes for Tubular Vanadium Redox Batteries**" by Korcan Perçin has been approved as a thesis for the degree of Master of Science in Chemical Engineering by the below mentioned advisors.

Prof. Dr. Deniz Tanyolaç
Head

Prof. Dr. Ahmet R. Özdural
Supervisor

Prof. Dr. Ayla Altınten
Member

Doç.Dr. Zehra Zeybek
Member

Yrd. Doç. Dr. Selis Önel
Member

This thesis has been approved as a thesis for the Degree of **MASTER OF SCIENCE IN CHEMICAL ENGINEERING** by Board of Directors of the Institute for Graduate Studies in Science and Engineering.

Prof.Dr. Fatma Sevin Düz

Director of the Institute of
Graduate Studies in Science

ETHICS

In this thesis study, prepared in accordance with the spelling rules of Institute of Graduate Studies in Science of Hacettepe University,

I declare that

- all the information and documents have been obtained in the base of the academic rules
- all audio-visual and written information and results have been presented according to the rules of scientific ethics
- in case of using others Works, related studies have been cited in accordance with the scientific standards
- all cited studies have been fully referenced
- I did not do any distortion in the data set
- and any part of this thesis has not been presented as another thesis study at this or any other university.

08/01/2015

KORCAN PERÇİN

ABSTRACT

DEVELOPMENT AND INVESTIGATION OF SLURRY ELECTRODES, NOVEL MATERIALS AND MEMBRANES FOR TUBULAR VANADIUM REDOX BATTERIES

Korcan PERÇİN

Master Student, Chemical Engineering

Supervisor: Prof. Dr. Ahmet R. ÖZDURAL

December 2014, 89 pages

The energy is essential for human modern life. The importance of energy is increasing, since the basic needs of humans are requiring better conditions, like faster transportations, technologies or manufacturing processes. The most common energy type that is being used is electrical energy. Since the electrical energy cannot be stored as its own form, applications of the energy storage systems are necessary, to improve the quality and stability of the existing electricity network.

Among the energy storage systems, electrochemical systems play a major role, depending on their common usage areas. One of the most promising electrochemical energy storage systems is redox flow batteries (RFB). These batteries contain two electrolyte solutions in a cell, which is separated by a proton exchanging membrane (PEM). Electrical energy is stored in form of chemical energy in electrolytes. Storing electricity in a solution is comparatively easy and cheap to adapt on large scale applications. During this study Vanadium RFB will be investigated.

Vanadium RFB systems are based on different oxidation level of vanadium. The battery contains two half cells. Positive half cell is circulated with V^{4+} and negative half cell is circulated with V^{3+} . During the charge, negative cell produces V^{2+} and positive cell produces

V^{5+} . Discharging procedure is reverse of these reactions. Half cells are separated with a PEM membrane and different electrode materials are being used.

First part of this master thesis study will be the development of a PEM. Nafion type membranes are mostly being used as separator. Due to the high cost and low H^+/V selectivity of Nafion, sulfonated poly-ether-ether-ketone (SPEEK) membranes were produced. SPEEK has lower costs and higher selectivity between H^+/V ions which makes it more suitable than Nafion type membranes. In order to increase selectivity and mechanical stability of SPEEK membranes, polyaniline (PANI) was mixed with SPEEK. After producing SPEEK/ PANI blended membranes characterization methods was applied. Significant performance improvements were obtained with SPEEK membranes when compared to the commercialized Nafion membranes. Furthermore, addition of PANI polymer into the blend resulted a tighter polymer matrix, thus higher selectivity between H^+/V ions. However, lower chemical stability of PANI affected the long-term performance of the cell negatively, this might be attributed to the high effectiveness of $V(V)$. Battery performance values, such as energy, coulombic and voltage efficiencies were obtained around 90 % which might be acceptable as optimum values. Moreover Open Circuit Potential (OCP) performance of the membranes had shown that longer self-discharge might be achieved.

In the second part in this study, a tubular Vanadium RFB was build in order to develop the power density of the planar RFBs. Graphite, carbon and titanium materials were employed as tubular electrodes. After using different types of Membrane Electrode Assembly (MEA), titanium macroporous tubes (as positive electrode) and graphite tubes (as negative electrode) were decided as a suitable assembly for Vanadium RFB. As it was expected the current density of tubular battery was found to be 4 mA/cm^2 , which is lower than planar RFB's ($20\text{-}50 \text{ mA/cm}^2$). At this point slurry electrode was introduced into this tubular RFB to increase the contact area between electrode and electrolyte. Slurry electrode was made from dispersion of conductive particles in electrolyte solution. Activated carbon and graphite powder were used as slurry electrodes. Slurry electrodes were mixed in different ratios with the electrolyte solution. Graphite powder was found to be more suitable for titanium macroporous tubes, due to the fact that large dimensions of the activated carbon particles caused a blockage inside the titanium tubes. Significant current density increase was obtained by the addition of slurry electrodes. Power density of the tubular RFB could be improved by this achievement.

Keywords: Electrochemical energy storage systems, vanadium, redox flow battery, tubular electrode, proton exchange membrane, SPEEK, PANI, slurry electrode

ÖZET

TÜBÜLER VANADYUM REDOKS AKIŞ BATARYALARI İÇİN BULAMAÇ ELEKTROT, YENİ MATERYAL VE MEMBRANLARIN ARAŞTIRMA VE GELİŞTİRMESİ

Korcan PERÇİN

Yüksek Lisans, Kimya Mühendisliği

Danışman: Prof. Dr. Ahmet R. ÖZDURAL

Aralık 2014, 89 sayfa

Enerji, insanlığın modern yaşamı için gerekliliğini korumaktadır. İnsanların temel ihtiyaçları olan ulaşım, teknoloji ve üretim süreçleri de dahil olmak üzere hızlı ve konforlu bir yaşam için enerji kullanımının önemi daha da artmaktadır. En temel kullanılan enerji türü elektrik enerjisidir. Elektrik enerjisi günlük yaşam gereksinimlerinin artmasından dolayı yeni zorluklarla karşılaşmaktadır. Elektrik enerjisi kendi formunda depolanamadığı için, enerji depolama sistemleri uygulamaları, hali hazırda bulunan elektrik dağıtım ağının kalitesi ve stabilitesinin geliştirilmesi adına gereklidir.

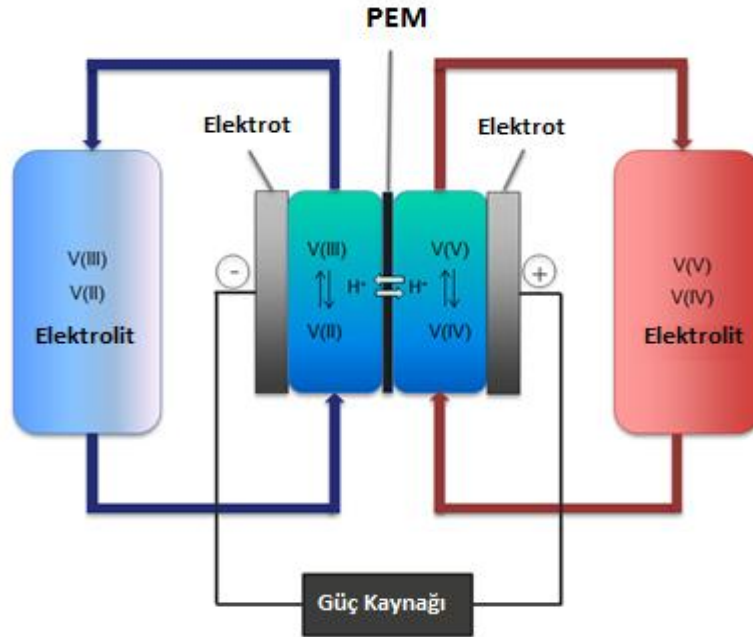
Enerji depolama sistemleri arasında elektrokimyasal enerji depolama sistemleri kullanım alanların göre önemli bir yer kaplamaktadırlar. Aralarından umut vaat edici olanlarından biri ise Redoks Akışlı Batarya (RFB)'dir. Bu bataryalar Proton Değişim Membranı (PEM) yardımıyla ayrılmış iki elektrolit hücrelerinden meydana gelir. Elektrik enerjisi, kimyasal enerji formunda elektrolitlerde depolanır. Enerjiyi elektrolitlerde depolamak, büyük ölçülü sistemlere adapte edildiği zaman daha ekonomik ve ucuz olabilmektedir. Bu çalışmada Vanadyum RFB incelenecektir.

Vanadyum RFB sistemleri, vanadyum elementinin dört farklı oksidasyon seviyesine bağı olarak çalışır. Vanadyum RFB örneği Şekil 1 'de gösterilmektedir. Batarya iki yarı hücre'den oluşur. Pozitif yarı hücrede V^{4+} çözeltisi sirkle edilirken, negatif yarı hücrede V^{3+} çözeltisi sirkle edilir. Şarj sırasında pozitif hücre V^{5+} üretirken, negatif hücre V^{2+} üretir. Deşarj sırasında ise ters işlem gerçekleşir. Yarı hücreler bir PEM ile ayrılmış durumda olup, elektrot olarak farklı materyaller kullanılmaktadır. Vanadyum RFB'de gerçekleşen temel reaksiyonlar aşağıda gösterildiği gibidir.

Şarj



Deşarj



Şekil 1. Vanadyum RFB düzeneği

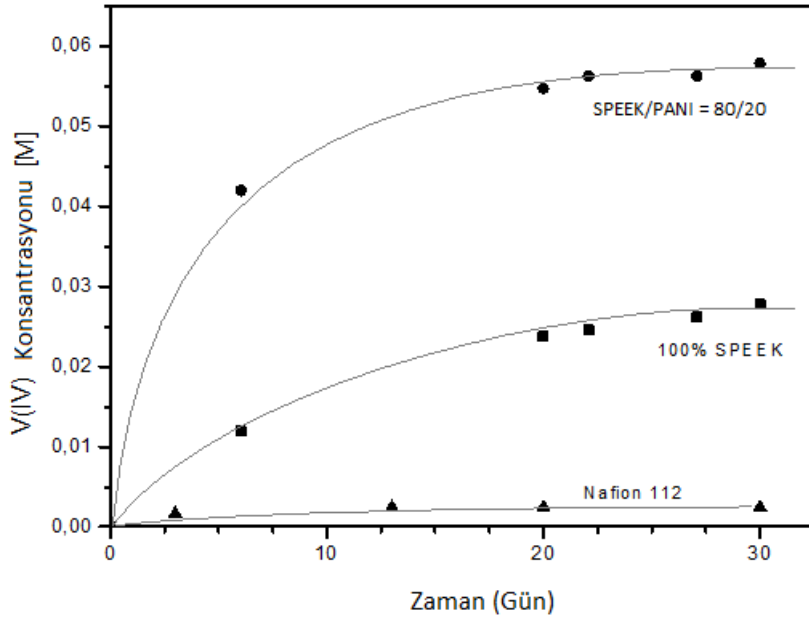
Bu yüksek lisans tez çalışmasının ilk bölümünde bir proton değişim membranı geliştirilecektir. Genellikle Nafion membranlar bu tarz bataryalarda kullanılmaktadırlar. Nafion membranların yüksek maliyetleri ve düşük H⁺/V iyon seçicilikleri dolayısıyla, Sülfonize Poli-Eter-Eter-Keton (SPEEK) membranlar üretilmiştir. Bu polimerin daha düşük maliyete ve daha yüksek seçiciliğe sahip olması, Nafion membranlardan daha uygun bir malzeme olmasını sağlamaktadırlar. Ek olarak SPEEK polimerinin mekanik dayanımını artırıp daha da fazla seçicilik katmak için Polianilin (PANI) polimeri eklenip, karışım membranlar oluşturulmuştur. Farklı oranlarda SPEEK/PANI membranlar üretildikten sonra karakterizasyon metotları uygulanmıştır. Sonuçlar Tablo 1’de verilmiştir.

Tablo 1. Membran karakterizasyon değerleri

	Genişleme Derecesi (%)	Su Hapsetme (%)	İyon Değişim Kapasitesi (mmol g ⁻¹)	Proton İletkenliği (mS cm ⁻¹)	V ⁴⁺ difüzyon katsayısı x 10 ⁷ (cm ² min ⁻¹)
SPEEK-E600	6.66	27.63	1.50 ± 0.06	71.12 ± 7.24	6.88 ± 0.70
SPEEK-E600/PANI = 98/2	6.74	26.88	1.58 ± 0.02	59.86 ± 7.41	4.00 ± 1.45
SPEEK-E600/PANI = 95/5	5.52	26.65	1.54 ± 0.01	57.27 ± 4.74	3.25 ± 0.54
SPEEK-E600/PANI = 80/20	5.56	20.99	1.44 ± 0.01	54.15 ± 4.67	2.67 ± 0.51
Nafion 112	6.83	13.94	0.97 ± 0.11	81.51 ± 0.27	15.9 ± 0.43

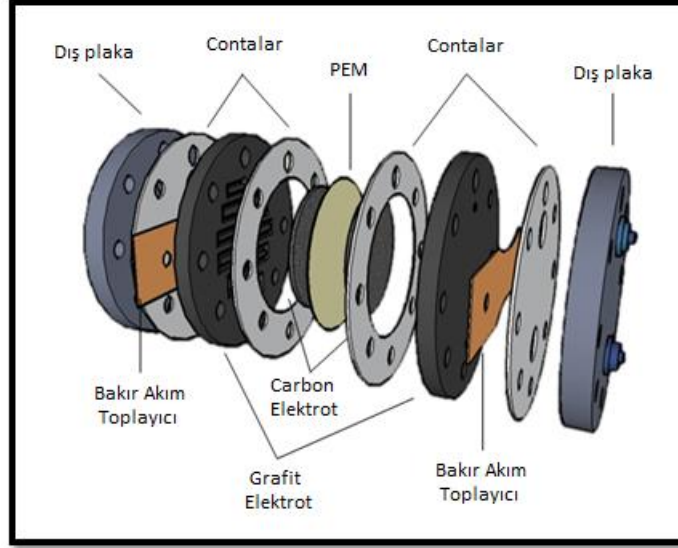
Bu sonuçlar karşılaştırıldığında önemli performans gelişimi olduğu gözlemlenmiştir. V⁴⁺ difüzyon katsayısının, PANI yüzdesi artmasıyla azaldığı gözlemlenmiştir. Böylelikle PANI eklenmiş membranların da daha sıkı bir polimer yapısı gösterdiği, H⁺/ V iyon seçiciliğinin arttığı söylenebilir. Proton iletkenliği PANI yüzdesiyle birlikte azalmıştır, fakat bu azalma iyon değişim kapasitesinin de değişmediği gerçeğiyle birlikte düşünülünce, SPEEK-E600/PANI = 80/20 membranlarının Vanadyum RFB’ler için daha uygun birer membran oldukları sonucu çıkartılabilir. Bunun yanı sıra su hapsetme ve genişleme derecesi olarakta membranlar mekanik olarak daha dayanıklı gözlemlenmişlerdir.

Bir diğerkarakterizasyon metodu olarak kimyasal dayanım testi uygulanmıştır. Bu test batarya içerisinde üretilen V^{5+} çözeltilisinin aşırı etken yapısından dolayı çok önemli bir yer tutmaktadır. Şekil 2’de üç farklı membranın 30 gün boyunca V^{5+} çözeltisi içerisinde bekletilmesiyle oluşturulmuş dayanım grafiğı görölmektedir. Grafik çözelti içerisinde indirgenen V^{4+} miktarını göstermektedir. Bu sonuçlara dayanarak Nafion 112 membranlarının nerdeyse hiçbir bozulma göstermediğini ve en hızlı bozulmayı PANI içeren membranların gösterdiğini söylemek mümkündür.



Şekil 2. Kimyasal Dayanım Testi

Şekil 3’te görölen çizime göre bir Vanadyum RFB tasarlanmış ve ayrı ayrı membranların batarya performansları incelenmiştir.



Şekil 3. Düzlemsel RFB düzeneği

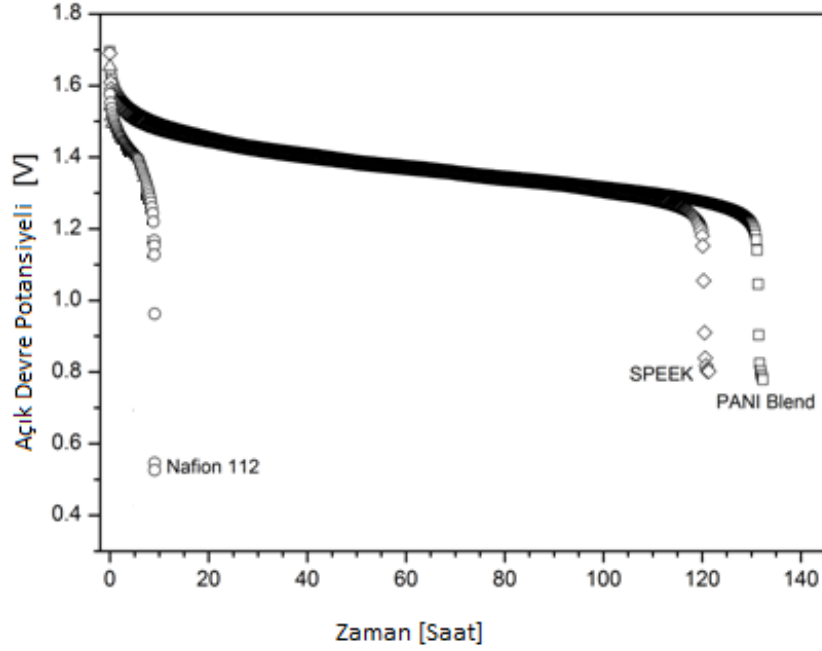
Enerji, coulombic ve voltaj verimliliği gibi batarya performans değerleri, Tablo 2’de görüldüğü üzere optimum düzeylerde bulunmuştur (>90 %).

Tablo 2. Membran Vanadyum RFB performans değerleri

Membran	Coulombic Verim %	Voltaj Verimi %	Enerji Verimi %
SPEEK-E600	98.18	90.67	89.01
SPEEK-E600/PANI=80/20	98.43	92.76	91.31
Nafion 112	85.41	90.98	77.70

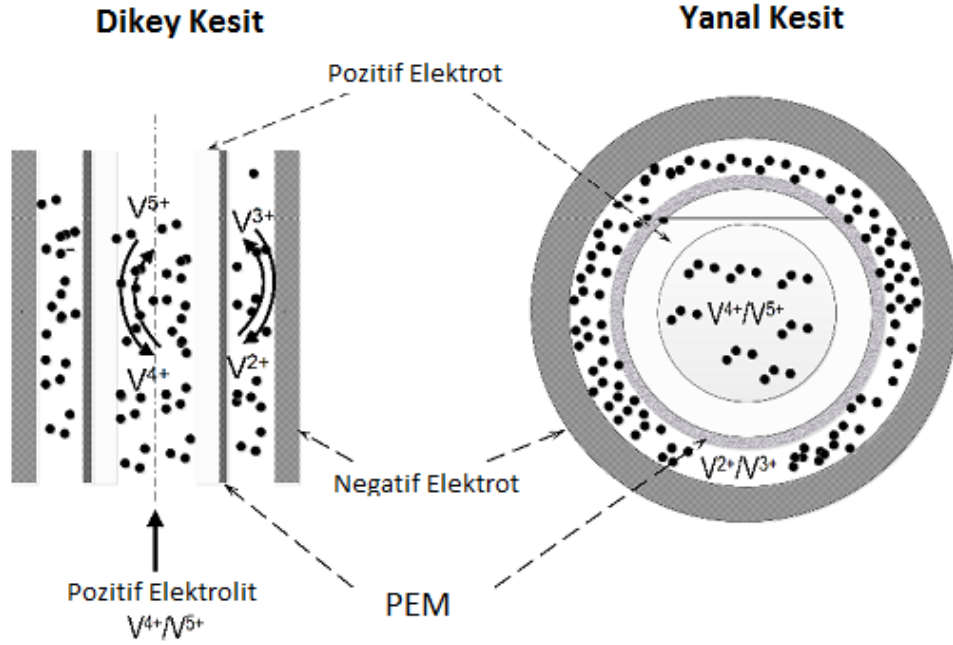
Son olarak, Açık Devre Potansiyel (OCP) performansı, her membran için ayrı ayrı incelenmiştir. Bunu için membran yerleştirilmiş batarya düzenekleri tam şarj edildikten sonra devre açık bırakılarak, ne kadar sürede kendini deşarj edeceği takip edilmiştir. Şekil 4’te de görüldüğü gibi OCP analizi göstermiştir ki, PANI eklenmiş membranlar en yüksek deşarj süresine sahiptirler. Bu sonuçla birlikte SPEEK membranların ve SPEEK/PANI karışım membranlarının performanslarının, sıkça kullanılan Nafion membranlara göre daha yüksek

olduğunu söylemek mümkündür. Fakat SPEEK ve PANI polimerlerinin V^{5+} ile aşırı etkileşmesi membranların bu tarz bataryalarda kullanışlı olmaması anlamına gelmektedir.



Şekil 4. Açık Devre Potansiyeli (OCP)

Bu çalışmanın ikinci kısmında ise, düzlemsel RFB'lerin güç yoğunluklarının artırılabilmesi için sık olarak diğer popüler batarya uygulamalarında tercih edilen, fakat daha önce Vanadyum RFB'lere adapte edilmemiş olan tübüler modül geliştirilmesi planlanmıştır. Şekil 5'te tübüler modül için tasarlanan membran elektrot düzeneği gösterilmektedir. Modül iki tane farklı boyutlarda elektrodun iç içe konumlandırılmasıyla meydana gelir. Büyük çaplı elektrot negatif olarak tasarlanmışken, küçük olan ise pozitif elektrot olarak görev görmektedir. Proton değişim membranı pozitif elektrodun dış yüzeyine kaplanmıştır. V^{4+} , pozitif elektrodun içerisinde sirküle edilirken, V^{3+} ise iki elektrot arasından sirküle edilir.



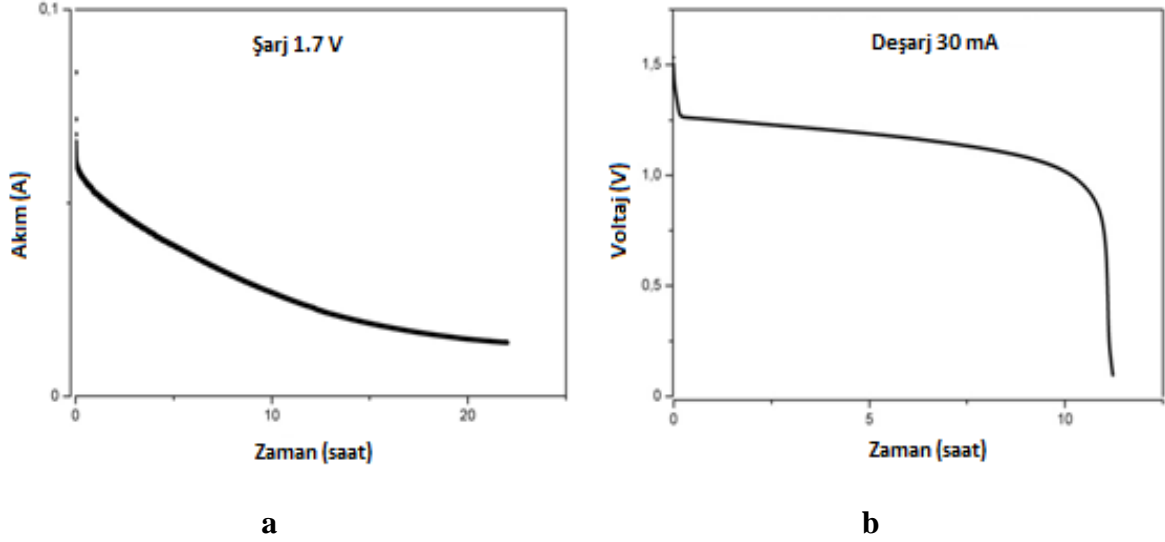
Şekil 5. RFB için tübüler modül tasarımı

Elektrot materyalleri olarak grafit, karbon veya titanyum temelli materyaller, tüp şekillerde elde edilip, elektrot olarak kullanılmışlardır. Membran olarak ise çözelti halinde standart membran kullanılmıştır. Farklı Membran Elektrot Montajlar (MEA) Tablo 3'te gösterildiği gibi uygulandıktan sonra titanyum makro gözenekli tüp (pozitif elektrot) ve grafit tüp (negatif elektrot) tübüler RFB sistemine uygun bulunmuştur.

Tablo 3. MEA yapımında kullanılan elektrot materyalleri

Materyal	Elektrot
CNT	Pozitif & Negatif Elektrot
Karbon Fiber	Negatif Elektrot
Titanyum Keçe	Pozitif Elektrot
Grafit & Epoksi Doyurulmuş Grafit	Negatif Elektrot
Titanyum Makrotüp	Pozitif Elektrot

Şekil 6, tübüler RFB'nin ilk şarj ve deşarj grafiklerini göstermektedir. Görüldüğü üzere tam şarj 22 saatin üzerinde tamamlanmış olup deşarj ise 11 saatte tamamlanmıştır. Bu tübüler bataryanın akım yoğunluğu 4 mA/cm^2 civarında bulunmuştur. Bu değer düzlemsel RFB'lerden oldukça azdır ($20\text{-}50 \text{ mA/cm}^2$).



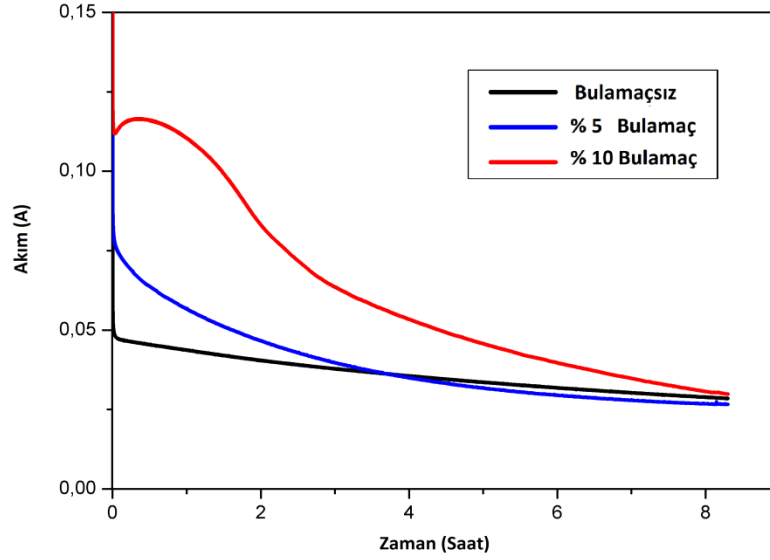
Şekil 6. Tübüler RFB ilk şarj ve deşarjı **a.** 1.7 V ile şarj, **b.** 45 mA ile deşarj

Bu noktada bulamaç elektrot sisteme dahil edilerek, elektrot ve elektrolit yüzey alanının artırılması hedeflenmiştir. Bulamaç elektrot, elektrolit içerisinde iletken partiküllerin dağılımıyla oluşturulmuştur. Aktive edilmiş karbon ve grafit pudrası bulamaç elektrot olarak kullanılmıştır. Karbon partiküllerinin büyük yapısı nedeniyle, makro gözenekli titanyum tüp içerisinde tıkanma olduğu gözlemlenmiştir. Dolayısıyla grafit pudrası, bulamaç elektrot için daha uygun olduğuna karar verilmiştir.

Tübüler RFB öncelikle bulamaçsız, daha sonra ise hacimsel olarak %5 ve %10 olmak üzere üç defa şarj ve deşarj döngüsüne sokulmuştur. Bu döngüler sonucunda Tablo 4'te de görüldüğü gibi akım yoğunluğunda yükselme gözlemlenmiştir. Şekil 7, tübüler elektrodun sabit potansiyel altında şarj grafiğini göstermektedir.

Tablo 4. Akım yoğunluğunun bulamaç elektrot ile deęiřimi

	Bulamaçsız	%5 Bulamaç	%10 Bulamaç
Akım Yoęunluęu, mA/cm²	4.6	7.8	10.2



Şekil 7. Bulamaç oranlarına göre 1,7 V potansiyeldeki bataryanın şarj grafikleri

Şekil 7'den de görüldüğü gibi grafit elektrot yardımıyla tübüler RFB'de temas yüzeyi artırılıp, daha güçlü bir elektrik akımı sağlanmıştır. Fakat hala bu değerler düzlemsel düzeneklere göre düşük kalmaktadırlar. Bu yüzden daha yoğun bir bulamaç elektrot kullanımı gerekmektedir. Düzlemsel RFB standartlarında bir tübüler RFB uygulamaya konulabilmesiyle birlikte, birim hücre başına daha yoğun güç elde edilebilecektir.

Not: Türkçe geniş özet içerisinde yapılmış tüm şekil ve tablo numaralandırmaları tezden bağımsız olarak yapılmıştır.

Anahtar Kelimeler: Elektrokimyasal enerji depolama sistemleri, vanadyum redoks akışlı batarya, tübüler elektrot, proton deęişim membranları, sülfonize eter eter keton, polianilin, bulamaç elektrot.

ACKNOWLEDGMENT

I would like to express my gratitude to my supervising academic members, Dr. Youri Gendel and Dr.Oana David, whose expertise, understanding, and patience, added considerably to my graduate experience. I appreciate their vast knowledge and their assistance in writing this thesis. I would like to thank to Prof.Dr.-Ing. Matthias Wessling for accepting me for this master study as an Erasmus exchange student. In addition I would like to thank the other members of my project group, Tao Luo, Alexandra Romerskirschen and Hannah Roth for the assistance and friendship they provided at all levels of the research project. All the commercial rights, if any, arising to this work goes to RWTH (Rheinisch-Westfaelische Technische Hochschule, Aachen).

A very special thanks to my supervisor Prof.Dr.Ahmet Özdural that he provided me a great support along this period of study. I must also present my gratitude to RWTH, Hacettepe University and European Union Office of HU for providing me this wonderful exchange student opportunity with the program of ERASMUS.

I would also like to thank my family for the support they provided me through my entire life and this period. I must also acknowledge friends that were supporting me during this year, thanks for your kind love and respect.

CONTENTS

	Page
ABSTRACT	i
ÖZET	iv
ACKNOWLEDGMENT	xiii
LIST OF TABLES	xvi
LIST OF FIGURES	xvii
ABBREVIATIONS	xx
1. Energy Storage Systems	1
1.1 Mechanical Energy Storage Systems	4
1.2 Electrochemical Energy Storage (EES) Systems	8
1.2.1 Super Capacitors (SC)	14
1.2.2 Fuel Cells	16
1.2.3 Batteries	20
1.2.4 Redox Flow Batteries (RFB)	21
2. Research Objectives	30
2.1 Incentive	30
2.2 Membrane Development	34
2.3 Tubular Module Development	38
3. Materials and Methods	42
3.1 Membrane Development	42
3.1.1 Membrane Preparation	42
3.1.2 Pre-treatment	44
3.1.3 Characterization Methods	44
3.1.4 Battery Performance	48
3.2 Tubular Module Development	52

3.2.1	Membrane Electrode Assembly	52
3.2.2	Construction of Tubular All-Vanadium RFB	55
3.2.3	Tubular All-Vanadium RFB Operation.....	58
4.	Results and discussion.....	60
4.1	Membrane Development	60
4.1.1	Membrane properties.....	61
4.1.2	Chemical Stability of Membranes.....	64
4.1.3	Single Battery Performance	68
4.2	Tubular Module Development	76
4.2.1	Battery Performances	79
5.	Conclusions	86
5.1	Membrane Development	86
5.2	Tubular Module Development	87
	REFERENCES	88
	CIRRICULUM VITAE.....	94

LIST OF TABLES

	Page
Table 1.1 Battery characteristics[13]	10
Table 1.2 Standard electrode potentials in an aqueous electrolyte at 298 K (Reduction Reactions)[13]	12
Table 1.3 Capacity of some electrode species	13
Table 1.4 RFB redox reaction couples [29]	23
Table 3.1 SPEEK/ PANI wt. ratios for blended membranes	42
Table 3.2 Efficiency equations	52
Table 3.3 Electrode materials	53
Table 3.4 Physical properties of electrode materials	53
Table 3.5 Basic properties of slurry materials	58
Table 4.1 Experimental results for swelling degree, water uptake, proton exchange capacity, proton conductivity and vanadium diffusion coefficient for the membranes characterized at room conditions.	62
Table 4.2 Battery efficiencies of different membranes at a current density of 40 mA cm^{-2}	68
Table 4.3 Densities and efficiencies of the tubular RFB	84
Table 4.4 Current density improvement of graphite addition in electrolyte	85

LIST OF FIGURES

	Page
Figure 1.1 Energy source distribution in Turkey, 2013, TEI [4].....	2
Figure 1.2 Energy consumption during the day in Turkey, July 2014,TEI [5]	2
Figure 1.3 Daily solar energy production of a standard solar panel [6]	3
Figure 1.4 Energy storage system types	4
Figure 1.5 Pumped hydro systems [3]	5
Figure 1.6 Basic scheme of a flywheel energy storage system [8].....	6
Figure 1.7 Compressed air energy storage system [9].....	7
Figure 1.8 Superconducting magnetic energy storage [10]	7
Figure 1.9 Electrochemical energy storage systems.....	9
Figure 1.10 Ragone plot for energy storage systems [16]	14
Figure 1.11 Supercapacitor [18].....	15
Figure 1.12 Basic fuel cell process	16
Figure 1.13 Polymer electrolyte membrane fuel cell [21]	17
Figure 1.14 Comparison of primary batteries [27]	20
Figure 1.15 Comparison of secondary batteries[27].....	21
Figure 1.16 A redox flow battery energy storage system	22
Figure 1.17 All-Vanadium redox flow battery	26
Figure 1.18 Air- Vanadium redox flow battery.....	28
Figure 2.1 Application ranges for energy storage systems [9].....	30
Figure 2.2 Capital costs per energy and power [36].....	31
Figure 2.3 Component cost distribution of a VRFB a. 0.25 MWh system b. 4 MWh system [37].....	32
Figure 2.4 Total capital costs of 1 MW All-Vanadium RFBs a. 0.25 MWh b. 4 MWh [38] ...	33
Figure 2.5 Structure of the Nafion (DuPont).....	35
Figure 2.6 Chemical structure of sulfonated poly ether-ether-ketone	36
Figure 2.7 Chemical structure of polyaniline; if $y=1$ the structure is leucoemeraldine form, if $y=0.5$ the structure is emeraldine form and if $y=0$ the structure is pernigraniline form [48] ...	36
Figure 2.8 Schematic explanation of interaction between SPEEK and PANI [41].....	36

Figure 2.9 Tubular module of RFB	39
Figure 2.10 a. Structure of single-walled CNT, b. Structure of multi-walled CNT	40
Figure 3.1 a. Mixing device, b. Filtration device, c. Degassing pump and vessel	43
Figure 3.2 H-Cell and peristaltic pump.....	45
Figure 3.3 Four-Probe proton conductivity cell	48
Figure 3.4 a. Rectangular redox flow battery design; b. Circular redox flow battery design ...	49
Figure 3.5 a. Rectengular planar RFB; b. Circular planar RFB	50
Figure 3.6. Carbon fibers, CNT and Ti wires.....	55
Figure 3.7 a. CNT and titanium wire with membrane coating b. MEA materials c. Side view of the tubular RFB d. Front view of the tubular RFB	56
Figure 3.8 a. Titanium macroporous tube with membrane coating b. Titanium m. tube with current collectors c. Titanium m. tube, Epoxy impregnated graphite tube with Teflon connectors and epoxy impregnated graphite tube with current collectors d. Tubular RFB with all connections	57
Figure 4.1 a. SPEEK-E600 (100/0) b. SPEEK-E600/PANI = 98/2 c. SPEEK-E600/PANI = 95/5 d. SPEEK-E600/PANI = 80/20.....	61
Figure 4.2 Calibration graph for chemical stability measurement	64
Figure 4.3 Concentration increase of V(IV) with time in acidic vanadium solutions immersed with membranes at room temperature. The initial concentration of acidic vanadium solution is 1 M V(V), 2.5 M H ₂ SO ₄	66
Figure 4.4 a. Newly immersed membrane samples in V (V) solution b. Membrane samples immersed in V (V) for 30 days.....	67
Figure 4.5 a. CE, b. VE, c.EE of batteries with SPEEK-E600/PANI= 80/20 membrane(■), SPEEK-E600 membrane(●), Nafion 112(◆) and Fumapem 14100 membrane (▲) at current densities of 20, 30, 40 and 50 mA cm ⁻²	71
Figure 4.6 a. CE, b. VE, c.EE of batteries with different membranes during charge-discharge cycles (The charge and discharge current densities are both 40 mA cm ⁻² .).....	73
Figure 4.7 Discharge capacity loss graph	75
Figure 4.8 Open circuit voltage of V-RFB batteries with different membranes.	76
Figure 4.9 FeSEM images of Carbon Nanotubes (CNTs) – 50x a. Perspective view b. Cross-sectional view with membrane	76

Figure 4.10 FeSEM images of titanium macrotubes a. Non-pretreated tubes, cross-sectional view b. Non-pretreated tubes, outer surface c. Pre-treated tubes, outer surface d. Pt/Ir coated tubes, outer surface e. Membrane coated tubes, cross-sectional view.....	78
Figure 4.11 Current change graph during the charge at 1.5V	80
Figure 4.12 a. First Charge at 1.7V, b. First Discharge at 30mA	81
Figure 4.13 a. Negative electrolyte, V(II), b. Positive electrolyte, V(V).....	81
Figure 4.14 a. Charge of 5 % slurry mixed electrolyte, b. Discharge of 5 % slurry mixed electrolyte	82
Figure 4.15 Charge with slurry and non-slurry electrode at 1.7V	83
Figure 4.16 Comparison of graphite powder addition to the electrolyte	84

ABBREVIATIONS

CNT	Carbon Nanotubes
CAES	Compressed Air Energy Storage
CE	Coulombic Efficiency
DMFC	Direct Methanol Fuel Cell
EES	Electrochemical Energy Storage
EE	Energy Efficiency
IEC	Ion Exchange Capacity
MEA	Membrane Electrode Assembly
MWCNT	Multi Walled Carbon Nanotubes
OCP	Open Circuit Potential
PANI	Polyaniline
PEMFC	Polymer Electrolyte Membrane Fuel Cell
PEM	Proton Exchange Membrane
PHS	Pumped Hydro Storage
RFB	Redox Flow Battery
RFC	Regenerative Fuel Cell
SWCNT	Single Walled Carbon Nanotubes
SOC	State of Charge
SPEEK	Sulfonated Poly Ether-Ether-Ketone
SD	Sulfonation Degree
SC	Super Capacitors
SMES	Super Conducting Energy Storage
V-RFB	Vanadium Redox Flow Battery
VE	Voltage Efficiency

1. Energy Storage Systems

The electricity network, which is started to build up from the first years of 20th century, is still under development. Due to improvement of this electricity network, industrial revolution expanded to the top after almost a century. The liberalization and deregulation of the electricity systems get new challenges day by day, therefore new inventions, researches and ideas are necessary to face these challenges [1].

Currently electrical systems became a part of our life, such as transportation vehicles, computer technologies and mobile phone systems, etc. They all use electrical energy as their primary power supply. If somehow required electricity couldn't be provided, it would cause a catastrophe [2]. Therefore electrical energy is indispensable for all around the world and it also has to provide some constant items, as flexibility, availability and reliability against the consumer's needs[3].

The main disadvantage of using electricity is to store the electrical energy. Therefore the development and application of energy storage systems is a crucial challenge for the modern science and technology. Moreover, ability to store electrical energy could change and improve all types of electrical device usages [2].

Every land needs power sources to supply sufficient energy to its citizens. Due to fulfill the energy consumption of the land, different types of energy sources are being used. Figure 1.1 shows the distribution of energy sources in Turkey.

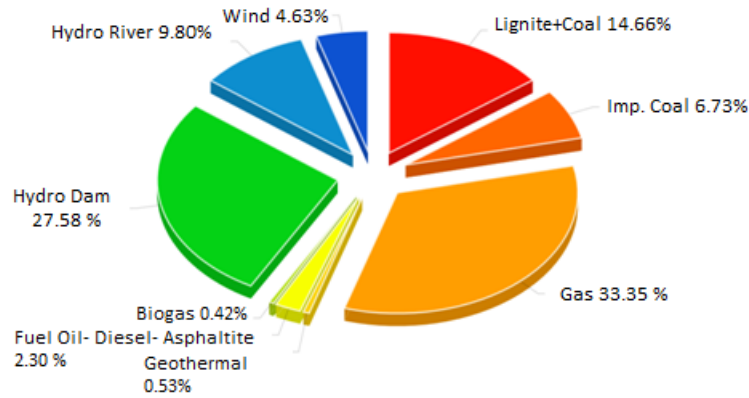


Figure 1.1 Energy source distribution in Turkey, 2013, TEI [4]

As it can be seen from the figure, most of the energy production is provided by the conventional systems like fuel based or hydro-energy based systems. However the interest of the renewable energies, are increasing rapidly, because the fact that the fossil fuels are running out fast. Therefore, renewable energies like wind, solar, etc. are being used more and more ($> 5\%$).

Figure 1.2 shows the energy consumption during a summer day in Turkey. The consumption has a significant difference between day time and night time. This difference is caused by the main working hours of the industrial plants, usage of mass transportation vehicles and usage of house based electrical devices. Therefore extreme amounts of energy are consumed during the day time.

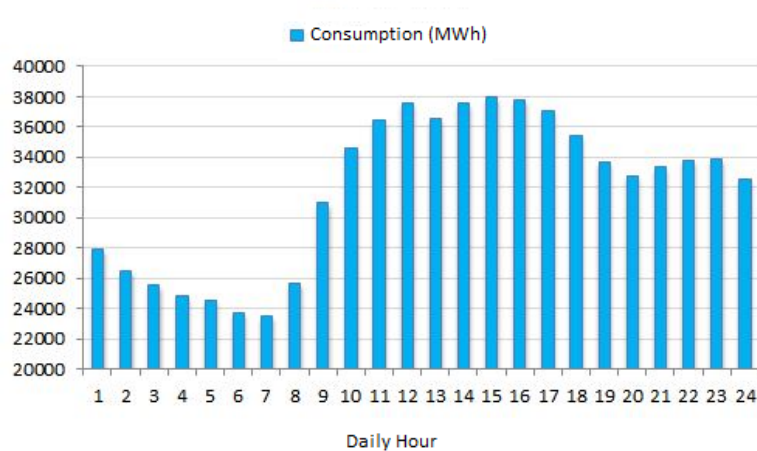


Figure 1.2 Energy consumption during the day in Turkey, July 2014, TEI [5]

As it was mentioned before, energy storage systems are required to supply sufficient energy to the electricity grid. They work as a buffer between providers and consumers. When the energy production exceeds the consumption, the excessive energy can be stored to be able to consume it later. Some energy sources are rarely fluctuant, but renewable energy sources, like solar and wind energy, are fluctuant during the day. Figure 1.3 shows daily production of solar energy of a standard solar panel. The figure illustrates the energy production of 1 m² panel during the day with comparing different times of the year. The solar energy is based mainly on clear skies and the sun's angle to the earth surface. Therefore this energy can't supply a constant energy to the grid. At this point an energy storage system is needed as a buffer between energy sources and consumers.

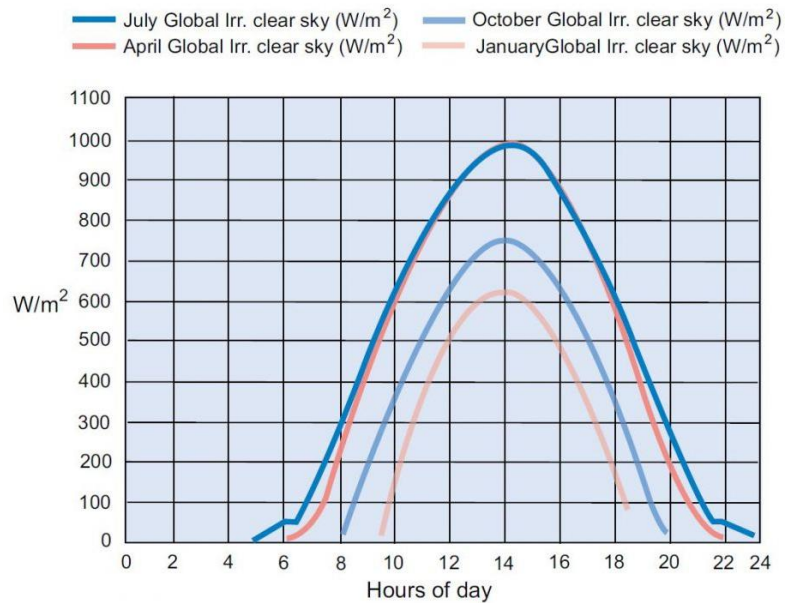


Figure 1.3 Daily solar energy production of a standard solar panel [6]

It can be seen so far that changes in energy production and consumption may be threatening for energy availability and reliability. In order to compensate the fluctuation of the energy and to generate qualified energy, storage systems can be used.

Electrical energy can be stored by several different methods, such as Pumped Hydro Storage (PHS), Compressed Air Energy Storage Systems (CAES), Super Capacitors (SC), Batteries and etc. Figure 1.2 shows the categorization of energy storage systems according to their working principle.

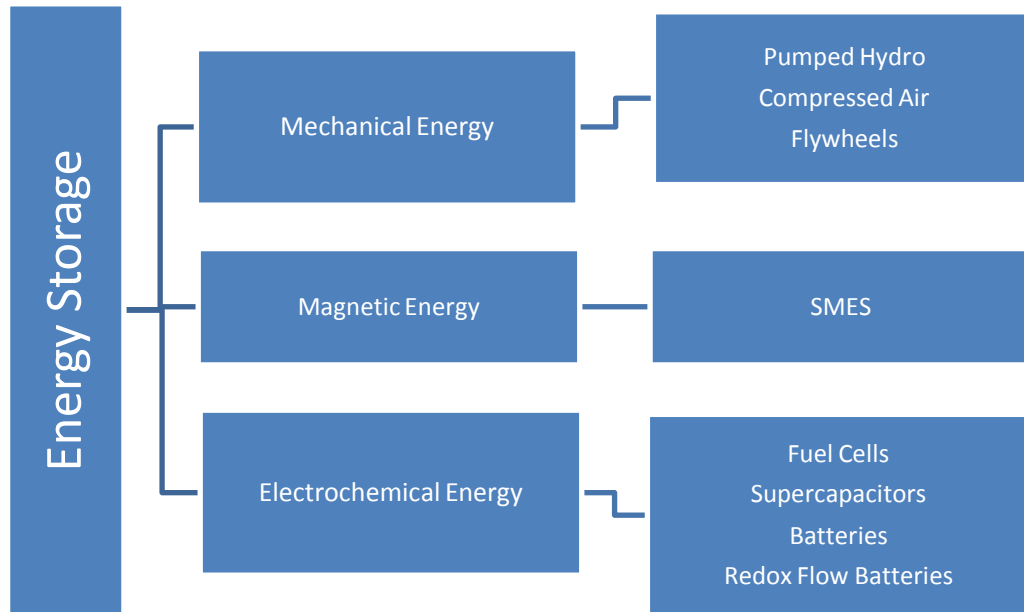


Figure 1.4 Energy storage system types

1.1 Mechanical Energy Storage Systems

Mechanical energy storage systems store electrical energy in different kinds of mechanical energy, such as pressure, elevation and others. Some of the frequently used systems are pumped hydro systems, flywheels, compressed air storage systems and superconducting magnetic energy storage systems.

Pumped Hydro Systems (PHS)

These systems are based on conversion of potential energy of a liquid to the electrical energy, as it is shown in Figure 1.3. Certain amount of water is pumped to high elevations in order to gain potential energy. The main advantage of pumped hydro systems is the working hours of these systems. Electricity prices are changing during the

day according to the consumption rates of the energy. During the evening hours electrical energy is the most expensive one through the day, because of the excessive usage of all consumers. The cheapest electrical energy is available during the late night. Pumped hydro systems generally use this price difference to store electrical energy and supply electrical energy. Discharge time range depends on the amount of liquid stored which changes with the day time. The disadvantages of these systems are the high capital costs and long construction times [3].

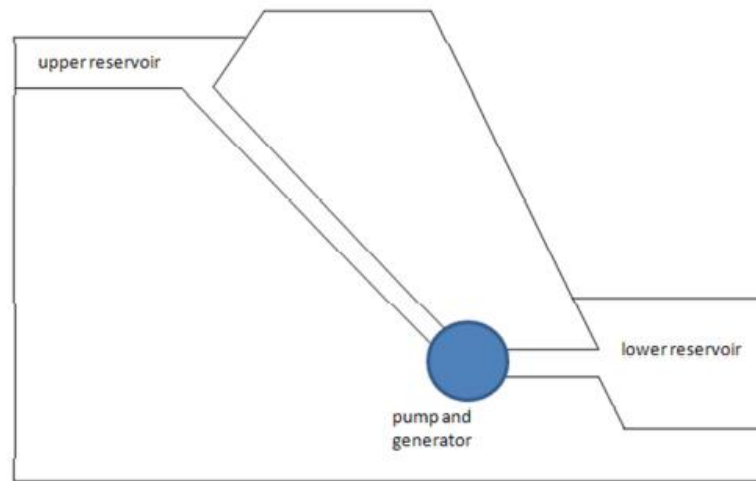


Figure 1.5 Pumped hydro systems [3]

Flywheels

Flywheels have been used for thousands of years. The earliest application is likely the potter's wheel. Perhaps the most common application in more recent times has been in internal combustion engines. A flywheel is a simple form of mechanical (kinetic) energy storage. Figure 1.4 represents scheme of a flywheel. Energy is stored by causing a disk or rotor to spin on its axis. Stored energy is proportional to the flywheel's mass and the square of its rotational speed. Advances in power electronics, magnetic bearings, and flywheel materials coupled with innovative integration of components have resulted in direct current flywheel energy storage systems that can be used as a substitute or supplement to batteries in uninterruptible power supply systems. Although generally more expensive than batteries in terms of first cost, the longer life, simpler maintenance,

and smaller footprint of the flywheel systems makes them attractive alternative to batteries [7].

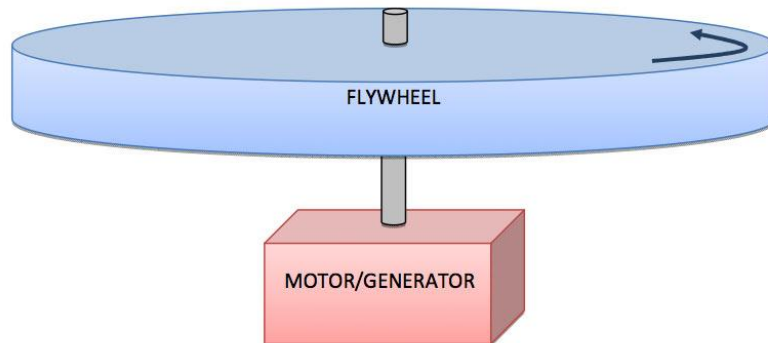


Figure 1.6 Basic scheme of a flywheel energy storage system [8]

Compressed Air Energy Storage Systems (CAES)

In this type of energy storage systems, electricity is generated by releasing the compressed air through a turbine. Compressed air is stored in underground caverns or ground vessels. A compressed air energy storage system figure is shown in Figure 1.5. Storage type depends on the power demand of the system. For high energy systems air is normally stored in caverns, for smaller systems, air is stored in above ground vessels. Compression of air is maintained with cheaper electrical energy during the night time and this energy is supplied to the consumers, when the price is more expensive. A recuperator is used to preheat the cold and pressurized air before it enters the expansion stage. A CAES plant can deliver about 75% of the energy used to compress the air. These energy storage systems are intensely relying on the geological structure of the plant and for this reason it is not suitable to build a CAES in unsuitable geography [3].

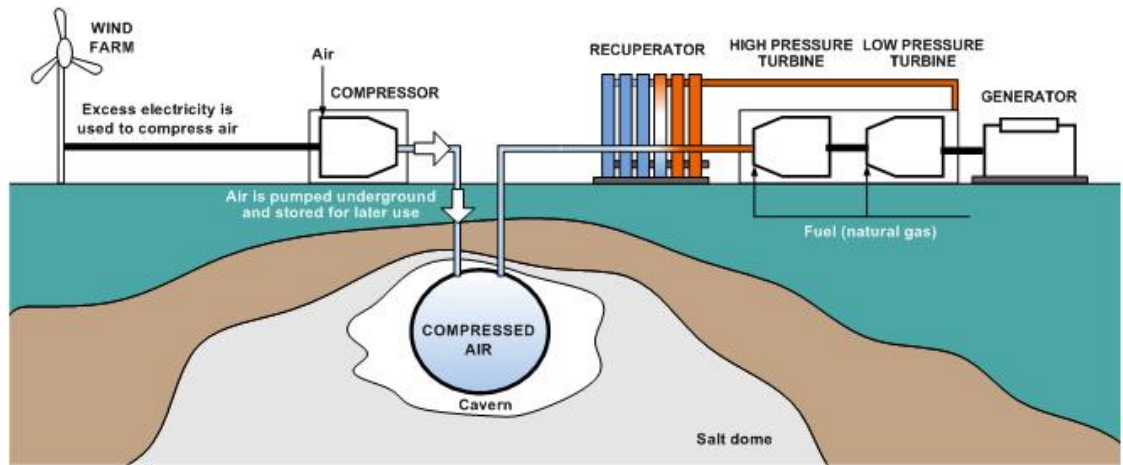


Figure 1.7 Compressed air energy storage system [9]

Super Conducting Magnetic Energy Storage (SMES)

A SMES device is a direct current device that stores energy in the magnetic field. Each unit of the system consists of a large superconducting coil and a cryogenic system. The coil is cooled to a low superconductivity temperature to minimize the electrical resistance. Figure 1.6 shows a common type SMES device. Total efficiency of these systems can be up to 90% [9]. SMES technologies have the ability of fast response; they can switch from charge to discharge state within seconds and they can be fully charged rapidly. Main disadvantage of SMES technology is the need of large amount of power to keep the coil at low temperatures. In addition this technology is economically suitable for short cyclic periods only, with a maximum of hours of duration in storage. This is due to a high self-discharge ratio for longer periods and mechanical stability problems [3].

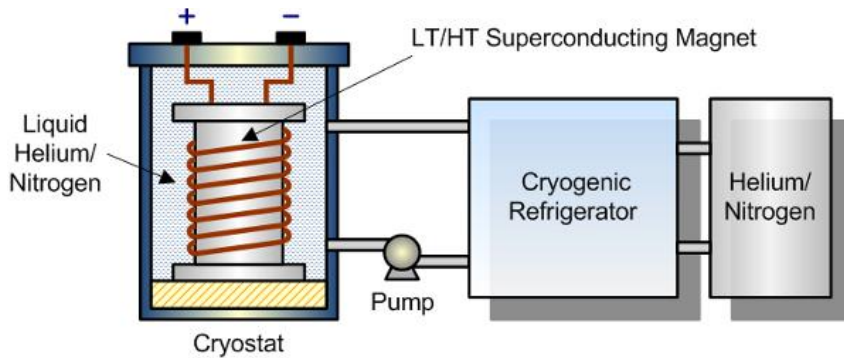


Figure 1.8 Superconducting magnetic energy storage [10]

1.2 Electrochemical Energy Storage (EES) Systems

Electrochemical energy storage systems are an alternative solution to the energy storage to overcome drawbacks of previously mentioned, conventional energy storage systems. Their ability to store large quantities of energy to compensate the energy demand of electricity grid makes them a good solution for energy storage systems.

An EES system or a battery stores chemical energy by converting electrical energy. These systems consist of an anode and a cathode. Oxidation and reduction reactions occur at these electrode surfaces with the presence of an electrolyte solution. Released electrons are transferred from anode to the cathode with an external circuit[3].

In the mid-1780's, in Italy, anatomist Luigi Galvani was studying the effects of atmospheric electrical discharge. Consequence of Galvani's experiment on a frog's muscle conductivity led to production of electrical current from the contact of two metals in a moist environment. But the first battery was invented by A. Volta in Italy, 1796. His invention, Voltaic Pile, can create a steady electric current with zinc and silver metals in brine solution. This invention became a breakthrough point and was further developed by other researchers[11]. Daniell Cell invented and developed the Voltaic Pile and made the battery provide the current for much longer time. W. Robert Grove built the first H₂-O₂ fuel cell in 1839. In 1866, G. Leclanche invented Carbon-Zinc cell which called today Leclanche Cell. By the year 1950's, the alkaline-manganese battery was developed by the Eveready Battery Company in USA. Alkaline batteries could supply more energy than the Leclanche Batteries [12]. At the end of the 20 century, the meaning of the electrochemical energy storage systems became wider than before. Fuel cells, flow batteries and hybrid systems are being used in every step of a daily life and today several types of EES systems are available as it is stated in Figure 1.7.

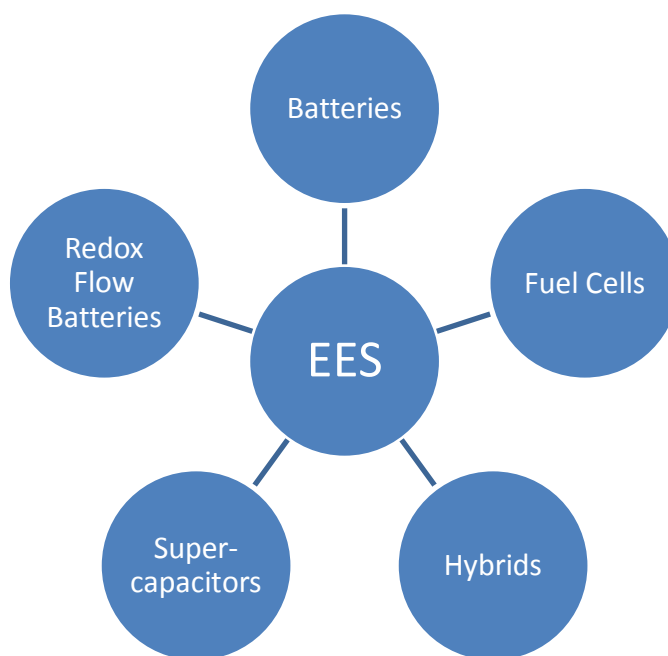


Figure 1.9 Electrochemical energy storage systems

Basic principles of electrochemical reactors and characteristics of EES systems are presented in Table 1.1.

Table 1.1 Battery characteristics[13]

Battery Characteristics	Definition	Unit
Open-Circuit Voltage	Maximum voltage in the charged state at zero current	Volt (V)
Energy Density	The energy that can be stored per unit volume or mass of the cell	Watt-hours per liter or kilogram (W h/dm ³ -kg)
Power Density	The power that can be derived per unit volume or mass of the cell	Watt per liter or kilogram (W/dm ³ - kg)
Charge Capacity	The theoretical capacity of a battery is the quantity of electrical charge involved per mass	Ampere-hours/gram (Ah/g)
Shelf Life	The time a battery can be stored inactive before its capacity falls to lower than 80%	Years
Service Life	The time a battery can be used at various loads and temperatures	Hours
Cycle Life	The number of discharge/charge cycles that the battery can undergo before its charge capacity falls lower than 80%	Cycles

Some of the important characteristic properties of the electrochemical energy storage systems are explained below.

Gibbs Free Energy

Gibbs free energy (ΔG) is the chemical potential that is minimized when a system reaches equilibrium state at constant pressure and temperature. The electrical energy produced by batteries is a result of this Gibbs free energy. Every reaction tends to lose Gibbs free energy, therefore the expression between Gibbs free energy and cell potential is calculated [14] as

$$\Delta G^{\circ} = -nFE \quad (1.1)$$

where

F: Faraday constant (-96500 C)

n: Number of electrons in reaction

E° : Standard potential, V

Voltage

The theoretical standard cell voltage can be determined as the difference between the standard potential of cathode and anode.

$$E^{\circ}(\text{cathode}) - E^{\circ}(\text{anode}) = E^{\circ}(\text{cell}) \quad (1.2)$$

Each active material has its individual standard potential for different oxidation and reduction reactions of the cell. Eq. 1.2 shows calculation of standard cell potentials [15]. Some of the standard reduction potentials of species are shown in Table 1.2. The theoretical cell voltage is controlled by the Nernst equation, which can be seen at Eq.

1.3. Nevertheless calculated voltage values are theoretical values that might be easily affected by material resistances, mass transport limitations and kinetic limitations [13].

$$E = E^{\circ} - RT \ln \frac{[C]^c [D]^d}{[A]^a [B]^b} \quad (1.3)$$

where,

E: cell potential (V),

E^o: standard cell potential (V),

R: ideal gas constant (J/mol-K),

T: temperature (K),

[A]-[B]: Concentration of reactants (M),

[C]-[D]: Concentration of products (M).

Table 1.2 Standard electrode potentials in an aqueous electrolyte at 298 K (Reduction Reactions)[13]

Reaction	E^o (V)
Na ⁺ + e ⁻ → Na	-2.71
Mn ²⁺ + 2e ⁻ → Mn	-1.18
Zn ²⁺ + 2e ⁻ → Zn	-0.76
Fe ²⁺ + 2e ⁻ → Fe	-0.44
V ³⁺ + e ⁻ → V ²⁺	-0.26
VO ₂ ⁺ + e ⁻ → VO ²⁺	1.00
1/2O ₂ + 2e ⁻ → H ₂ O	1.23

Theoretical Capacity

The capacity of a battery is the product of the current drawn from a battery and number of hours during the current flow [13]. Therefore, it is commonly used in terms of coulombs or ampere-hours. The quantity of capacity is related to the amount of active species in the cell. Capacity of some common electrode species can be seen from Table 1.3.

Table 1.3 Capacity of some electrode species

Material	Capacity, Ah/g
Anode Material	
Li	3.86
Na	1.16
Al	2.98
Zn	0.82
Cathode Material	
C	0.28
Mg	2.21
Cu	0.27
Pb	0.22

Energy Density and Power Density

The amount of energy that a battery can store per unit volume or mass is termed as energy density of the battery [14]. It can be calculated by integrating current and the operating voltage in one full discharge cycle. Due to the fact that both voltage and current can change during a discharge cycle, the calculation of energy expressed at equation 1.8.

$$E = \int V I dt \quad (1.8)$$

The unit of energy density defined as energy (Wh) per unit mass (kg) or volume (dm^3) [13].

Power density is the maximum available power per unit volume or mass of the cell. Power density can be defined as, rate of energy that can be given or taken from a battery. The unit of power density is Watts per liter or kilogram (W/L or kg). The relation between power and energy density is frequently expressed as a Ragone plot [13]. Ragone plots of several EES systems are shown in Figure 1.8.

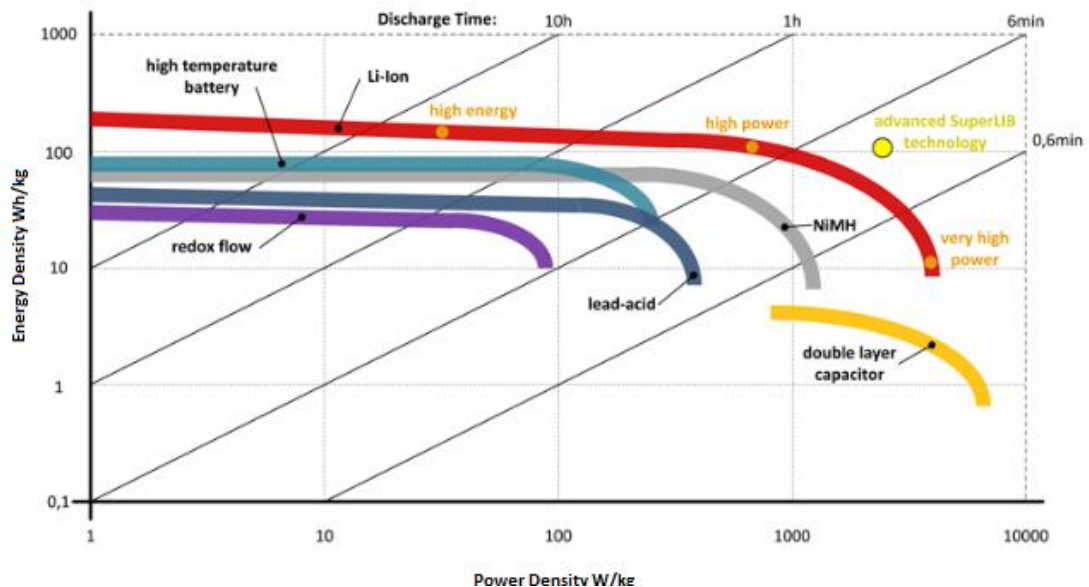


Figure 1.10 Ragone plot for energy storage systems [16]

1.2.1 Super Capacitors (SC)

Super capacitors store electrical energy within the electrostatic charge. They consist of two electrodes, which are separated with a separator and immersed in electrolyte solution. A scheme of a SC can be seen from Figure 1.10. Charge occurs along the electrode-electrolyte interface. By applying a voltage to the capacitor an electric double layer at both electrodes is formed, which has a positive or negative layer of ions

deposited in a mirror image on the opposite electrode. SC electrodes are generally made with high surface area materials and with an extremely thin electrolytic dielectrics to achieve capacitances in several orders of magnitude larger than other capacitor types [17] . A SC is mainly planted in series, thus higher voltages can be achieved. Energy efficiency is about 90 % [3]. The capacitance value is directly related to distance between two electrodes, which is only the thickness of the separator. This separator can be in nanometers, thus the capacitance of the system is exceptionally high. Their almost unlimited cycle life, high power densities and quick charging times makes them useful for systems which needs fast responses in weak electricity networks. Limiting factors of these systems are low energy densities and low voltages, even though they are connected in series[17].

$$C = \frac{\epsilon A}{d} \quad (1.9)$$

where;

C: Capacitance (F)

ϵ : Permittivity of dielectric

A: Surface area of plate (m²)

d: Distance between plates (m)

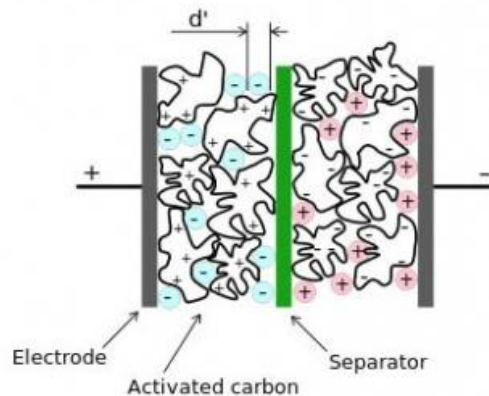


Figure 1.11 Supercapacitor [18]

1.2.2 Fuel Cells

A fuel cell is an energy conversion system that uses fuel combustion reactions to produce current [19]. A basic fuel cell process is shown in Figure 1.11. These cells consist of two electrodes and electrolyte. All chemical reaction occurs along the interface between electrodes and electrolyte. Oxidation occurs at the anode by consuming hydrogen and reduction occurs at the cathode by consuming the oxygen. Reaction products of hydrogen (electrons and protons) follow different paths, such as electrons follow external circuit and protons are transferred through the electrolyte. Both products react again at cathode to form water [19].

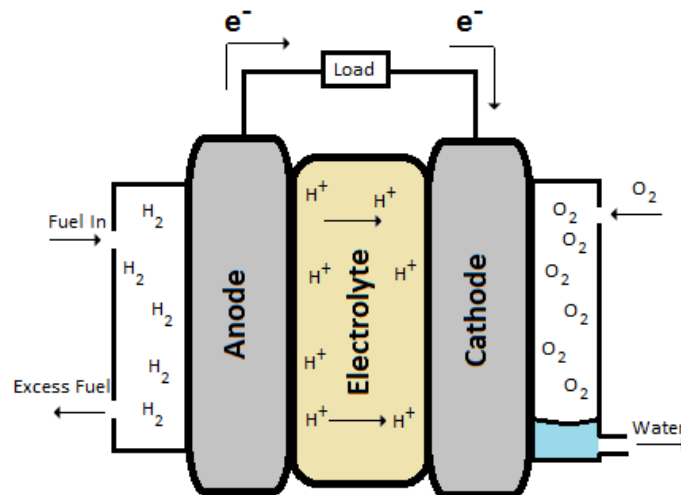


Figure 1.12 Basic fuel cell process

Polymer Electrolyte Membrane Fuel Cells (PEMFC)

In a PEMFC, two plates sandwich a poly electrolyte membrane to form a membrane electrode assembly (MEA), which is the core component of a PEMFC. Working principle of a PEMFC is shown in Figure 1.12. A polymer electrolyte membrane functions as a separator to prevent mixing of reactants, a conductor for protons from

anode to cathode and an electrical insulator to drive electrons through an external path to the cathode. Nafion type or Perfluorosulfonic acid polymers are mostly used as membranes in these technologies. Performance of the membrane affects the efficiency of fuel cell considerably [20]. Proton conductivity, mechanical and chemical stability of the membrane is the important criteria of PEMFCs. The membrane could achieve high proton conductivities, while they prevent the other materials to pass through, such as oxygen. Because of the fact that, oxygen crossover is highly challenging since it prevents the cathode reaction to occur. The other property that needs to be developed is the catalytic reaction on the electrodes. It has very high effect on fuel cell efficiency, therefore developing a suitable catalyst for electrodes are essential for these fuel cells [21].

Polymer electrolyte membrane fuel cells are promising as power supplies, due to their low operating temperature and high power density [22].

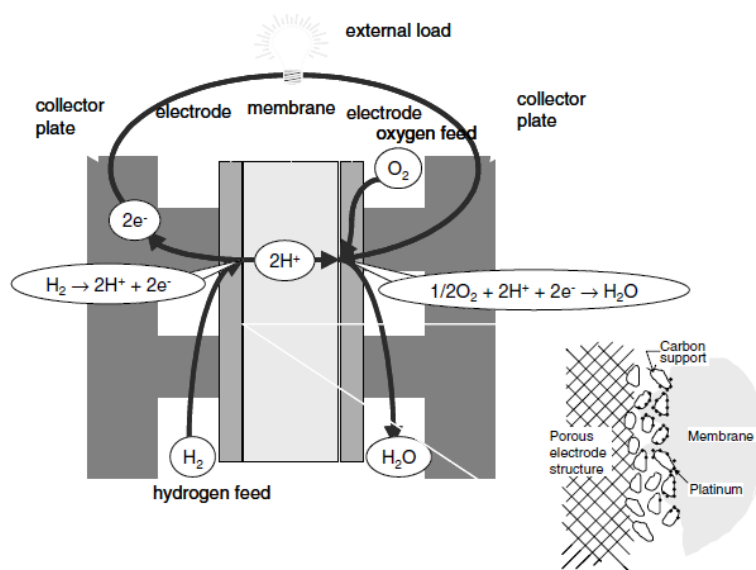
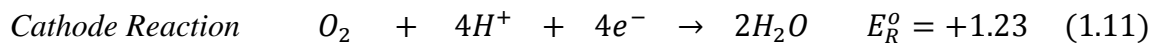
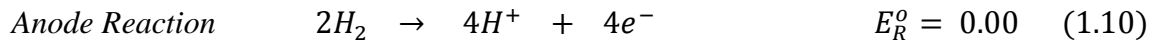


Figure 1.13 Polymer electrolyte membrane fuel cell [21]

- *H₂-O₂ Fuel Cell*

Hydrogen is a versatile energy carrier that can be used to power nearly every end-use energy need. These fuel cells use the combustion reaction of hydrogen and oxygen to reveal energy. Pure hydrogen fuel is fed to the anode. At the surface of anode, the hydrogen oxidation occurs, thus a proton and an electron forms. Electron follows the external circuit, while the proton transfers through the membrane to the cathode. Reduction occurs at cathode in the presence of oxygen and produces water as a product. H₂O₂ fuel cell reactions are given by equation 1.10 and 1.11. Main drawbacks about these systems are handling and storage problem of hydrogen gas [23].

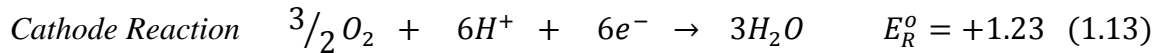
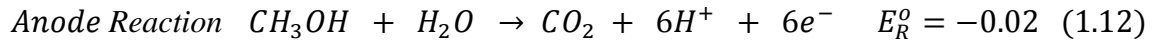


$$E^o = +1.23 \text{ V}$$

- *Direct Methanol Fuel Cell (DMFC)*

The other important type of the PEMFC is direct methanol fuel cell (DMFC). Methanol has significant characteristics as a liquid organic fuel. Such as, methanol releases six protons and electrons per molecule, works at low temperatures (up to 150°C) and easy to provide and store as it is liquid form. Therefore, supplying hydrogen by using methanol would be advantageous. Methanol is a cheap and easy producible fuel [24]. General limitation to store and produce Hydrogen could be overcome by using methanol directly in these fuel cells. Only difference from the H₂-O₂ fuel cells is, instead of using Hydrogen as feed, Methanol is supplied to the cell. Same as the PEMFCs, a DMFC cell has two electrodes, which separated with a proton exchange membrane. Methanol oxidation occurs at anode and oxygen reduction occurs at cathode. Protons moves from anode to cathode through the selective membrane and electrons transferred by an

external circuit to the same direction. Current is generated by this electron transfer [25]. Electrode reactions that occur during the DMFC process are written below:



$$E^o = +1.21 V$$

Main research areas about these fuel cells are; the slow oxidation kinetics that caused by CO_x sub-products; methanol crossover through the membrane, which slows down and blocks the reduction reaction at cathode; electrode and metal-oxide catalyst structure that can increase the activity of electrodes, thus the efficiency of the fuel cell [25].

Regenerative Fuel Cell (RFC)

A RFC, new innovative fuel cell type, is a specially-designed single stack of polyelectrolyte membrane cells for both electrolysis and fuel cell functions. Since the basic structure of a dedicated PEMFC stack is the same, the use of a single stack to perform both functions offers the view of extensive cost reductions. Advantage of this type of fuel cells is; energy and power can be gained separately. Temperature or cycle life is not effective on the cell discharge performance because fuels are stored outside the cell. Apparently this technology is comparably new among the fuel cells and still need to be developed to achieve high energy density than conventional fuel cells [26].

1.2.3 Batteries

Batteries convert chemical energy into electrical energy by using redox reactions. They are composed of one or more cells, each containing a positive electrode, negative electrode, separator and electrolyte. Generally batteries can be divided into two major types: primary and secondary. Primary batteries are not rechargeable and they need to be replaced after the discharge. Secondary batteries are rechargeable and require a power supply to charge the battery [13]. Some of the secondary type cells contains liquid electrolyte which can be stored outside the cell and re-circulate with a pump. This type of batteries is called as flow batteries.

Primary Batteries

A primary cell or battery is one that can't be recharged after one use and they must be replaced after the discharge. Most of the primary cells utilize electrolytes that are contained within absorbent material or a separator. Because of the disposal, these batteries are not environmentally safe and not cost effective. Some primary batteries are Leclanche, Manganese Alkaline, Carbon-Zinc, etc.

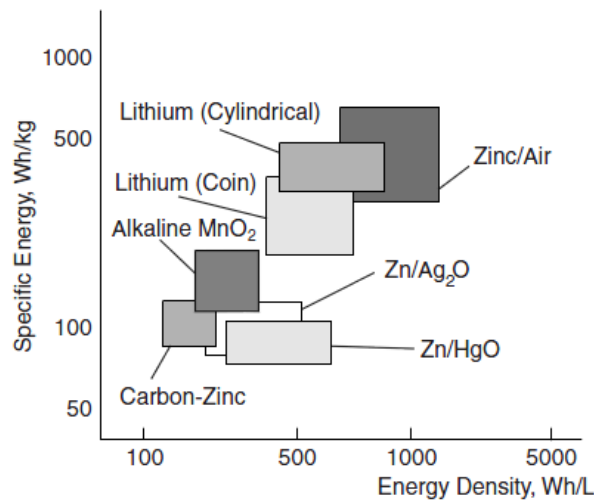


Figure 1.14 Comparison of primary batteries [27]

Secondary Batteries

A secondary battery is one that can be electrically recharged after the use to its original condition, by passing an electrical current through the circuit in the opposite direction to the current applied during the charge. By comparing with primary batteries, these are not environmentally safe but more cost effective than primary batteries. Some secondary batteries are Lead-Acid, Nickel-Cadmium, Lithium-Ion type and etc.

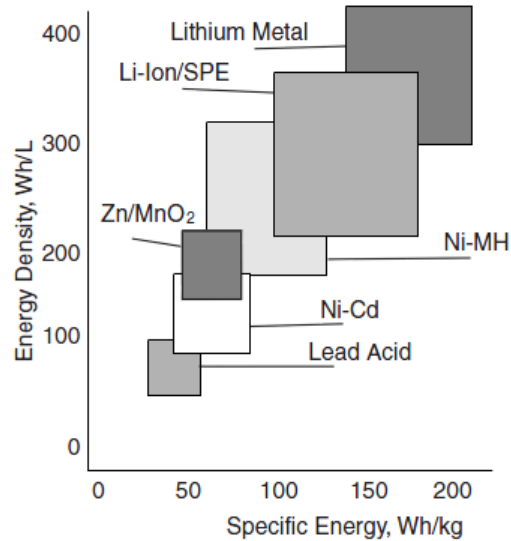


Figure 1.15 Comparison of secondary batteries[27]

1.2.4 Redox Flow Batteries (RFB)

Redox flow battery (RFB) is an attractive energy storage system for large-scale applications. The main difference between conventional batteries and RFBs is that the energy is stored only in electrolytes. A RFB scheme is shown in Figure 1.15. Instead of storing the electrolyte inside the cell stack, it is stored in external containers. Circulation of electrolyte between the electrolyte tanks and the cell is maintained by a pump [28]. This improvement in the battery system increases the flexibility, decreases the environmental threats and supplies an immediate response to the energy grid.

The cell consists of two separated electrodes, which are connected with an external circuit. Electrolyte solutions are separated with an ion-exchange membrane. Ion-exchange membrane works as a selective barrier between two half cells. While it lets the ions to pass, it prevents the electrolytes to mix. Electrical current is maintained by this transport of ions through the membrane [29]. Energy is stored in electrolytes in contrast to primary and secondary batteries, which the energy stored in electrodes. This ensures longer battery life for a RFB. Moreover, power and energy densities are independent.

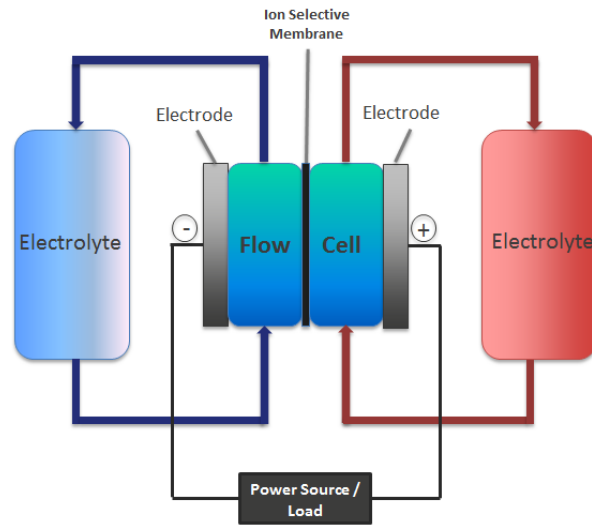


Figure 1.16 A redox flow battery energy storage system

Today many types of RFBs are known and used with applying different types of electrolytes as redox couples. Each redox couple has its specific redox potential and by combining two suitable redox couple a RFB can be operated. Table 1.4 includes some compatible redox couples.

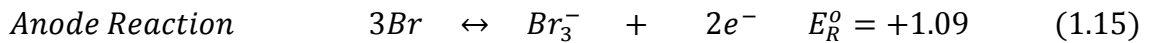
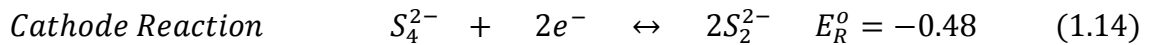
As it is stated before, these RFBs can be up-scaled. In order to get higher energies from the RFB, many cells can be connected in series. Furthermore, to be able to store more energy, more concentrated electrolyte or higher amounts of electrolyte can be used. For this reason both energy and capacity characterizations of the battery can be modified individually. Some of the RFBs such as; bromine polysulfide RFB; zinc bromide RFB and vanadium RFB, are the most promising redox couples in this technology.

Table 1.4 RFB redox reaction couples [29]

Negative Cell		Positive Cell		Total Cell	
Couple	Electrolyte	Redox Potential (V)	Electrolyte	Redox Potential (V)	Std. Cell Potential E° (V)
Fe/Ti	$Ti^{3+} + e^- \longrightarrow Ti^{2+}$	-0.9	$Fe^{2+} \longrightarrow Fe^{3+} + e^-$	0.771	1.7
Fe/Cr	$Cr^{3+} + e^- \longrightarrow Cr^{2+}$	-0.407	$Fe^{2+} \longrightarrow Fe^{3+} + e^-$	0.771	1.2
V/V	$V^{3+} + e^- \longrightarrow V^{2+}$	-0.255	$V^{4+} \longrightarrow V^{5+} + e^-$	0.991	1.2
Br/S	$S + 2e^- \longrightarrow S^{2-}$	-0.48	$2Br^- \longrightarrow Br_2 + 2e^-$	1.087	1.5
Zn/Br	$Zn^{2+} + 2e^- \longrightarrow Zn$	-0.763	$2Br^- \longrightarrow Br_2 + 2e^-$	1.087	1.9
V/O	$V^{3+} + e^- \longrightarrow V^{2+}$	-0.255	$2H_2O \longrightarrow O_2 + 4H^+ + e^-$	1.229	1.5

Bromine Polysulfide Redox Flow Battery

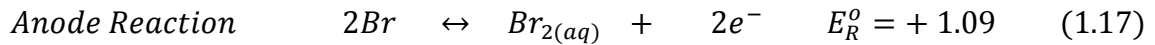
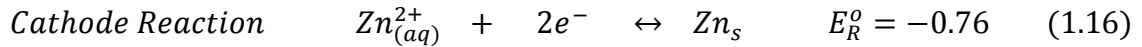
The bromine polysulfide RFB utilizes sodium bromide as the positive electrolyte and sodium polysulfide as a negative electrolyte. The common advantages of this system are high energy efficiencies and operating costs. The system suffers from the crossover of electrolytes, which causes precipitation of sulfur species. Moreover evolution of H₂S and Br₂ gases is another drawback that needs to be resolved [30]. Cell charge-discharge reactions are given at equation 1.14 and 1.15.



$$E^0 = +1.57 V$$

Zinc Bromine Redox Flow Battery

The zinc bromine RFB is made from a zinc-negative and a bromine-positive electrode. Cell is divided in to two compartments by a micro-porous membrane [29]. It has a difference from the other RFBs. This system involves a reaction that does not occur only in a liquid phase. Aqueous bromide is oxidized to bromine at negative electrode and it is deposited on the electrode as bromine. On the other side zinc metal is reduced and dissolved in the electrolyte [30]. Both electrolytes are re-circulated through the cell during the charge and discharge. Cell charge-discharge reactions occur according to equation 1.16 and 1.17.



$$E^{\circ} = +1.85 \text{ V}$$

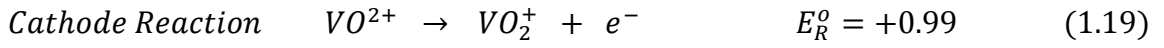
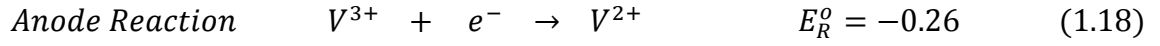
The Zinc-Bromine battery has very high cell voltage, good reversibility and low material cost as it does not need any complex membrane. Unfortunately, the toxicity of bromine and concentrated HBr is a challenge that needs to be resolved [30].

All-Vanadium RFB

All-Vanadium redox flow battery (V-RFB) was discovered in 1984 by Maria Skyllas Kazacos [31]. Working principal of V-RFB systems is based on two solutions of vanadium species. Figure 1.16 shows an all-vanadium redox flow battery. V(IV)/V(V) solution is applied in the positive electrolyte and V(II)/V(III) solution in the negative electrolyte. During charge process, V(IV) is reduced to V(V) at the positive electrode and V(III) is oxidized to V(II) at the negative electrode, as shown in Equation 1.18, 1.19 and discharge reactions occur to the reverse side as shown in Equation 1.20 and 1.21.

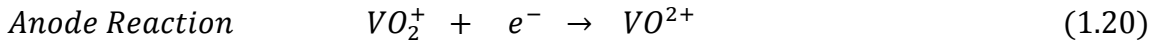
The standard voltage produced by the vanadium redox-flow battery system is 1.25 V [32].

Charge

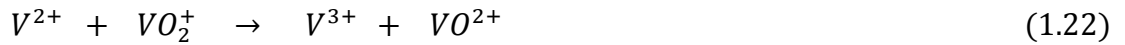


$$E^{\circ} = +1.25 \text{ V}$$

Discharge



Self-Discharge by Vanadium Crossover



Self-Discharge by Overcharge



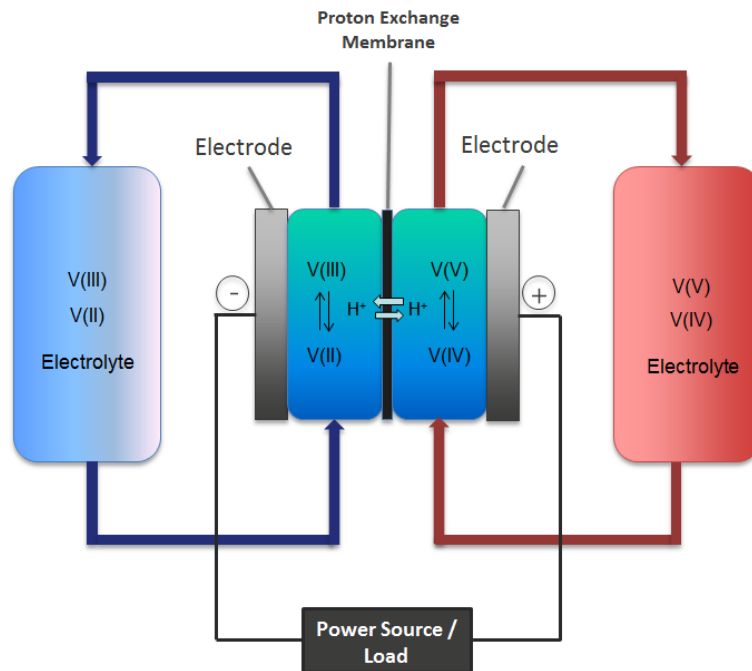


Figure 1.17 All-Vanadium redox flow battery

One of the main research areas in RFBs is polymer membranes, which is used as a separator. The membrane should be able to provide good proton conductivity, while it prevents the electrolytes to mix between two half cells. Another important characteristic of the membrane is the cross-over of vanadium species between the electrolyte reservoirs. Permeation of vanadium species through membrane causes a self-discharge in all-vanadium processes. The self-discharge occurs due to reactions between V(IV)/V(V) and V(II)/V(III). Reactions during self-discharge by crossover of vanadium ions are presented by Equation 1.22 and 1.23. These self-discharge reactions must be minimized to stabilize batteries efficiency by controlling the cross-over of V ions. Despite the fact that cross-over of electrolytes decrease the efficiency of the battery, the battery can be easily recharged and previous amounts of electrolytes can be produced. Additionally over-charging the battery can also result some parasitic reactions of the battery, such as electrolysis of water, as it is shown in equation 1.24 and 1.25. These reactions decrease the batteries efficiency. On the other side membrane's mechanical and chemical

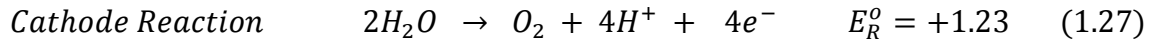
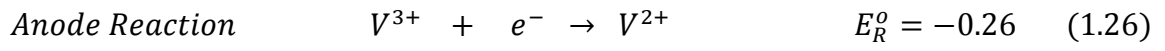
stability is a significant characteristic, since electrolytes involve concentrated acid and it can be extremely damaging to the membranes [33].

This invention solved the main concerns about the other redox flow batteries, such as the incompatibility and sensibility of two different redox couples. Other RFBs apply species that, when they cross into the other electrolyte, an irreversible reaction occurs between them. This kind of a redox couple loss does not only cause efficiency and capacity loss, it also necessitates an expensive electrolyte recovery by a separation process. Therefore, it may be really for the benefit of the battery to use redox couples that do not cause these kinds of difficulties. Vanadium offers an exact benefit that fits for this purpose with its four different oxidation level and the redox reactions between these levels. The crossover would only lead to a reversible efficiency loss, which can be corrected by a simple charging method [30]. In contrast to some other type of RFBs, in V-RFB, electrodes are not involved in redox reaction. Therefore, energy density and power density values might be independently regulated.

Air Vanadium Redox Flow Battery

Air-Vanadium Redox Flow Batteries (Air-VRFB) are becoming attractive in EES systems. An Air-VRFB consists of two electrode and electrolyte solution as All-VRFBs. The difference of Air-VRFB is; electrolysis reaction of humidified air is presented as positive cell reaction. The scheme of an Air-VRFB is shown at Figure 1.17. Two half cells are separated with an ion exchange membrane. Negative cell reactions occur as same as the All-VRFBs, but positive cell is fed with humidified air. Therefore, total volume of vanadium species are decreased to it half. The standard over potential of the system is about 1.49V. Charge and discharge reactions are shown in Equation 1.26, 1.27, 1.28 and 1.29 [27].

Charge



$E^{\circ} = +1.49 V$

Discharge

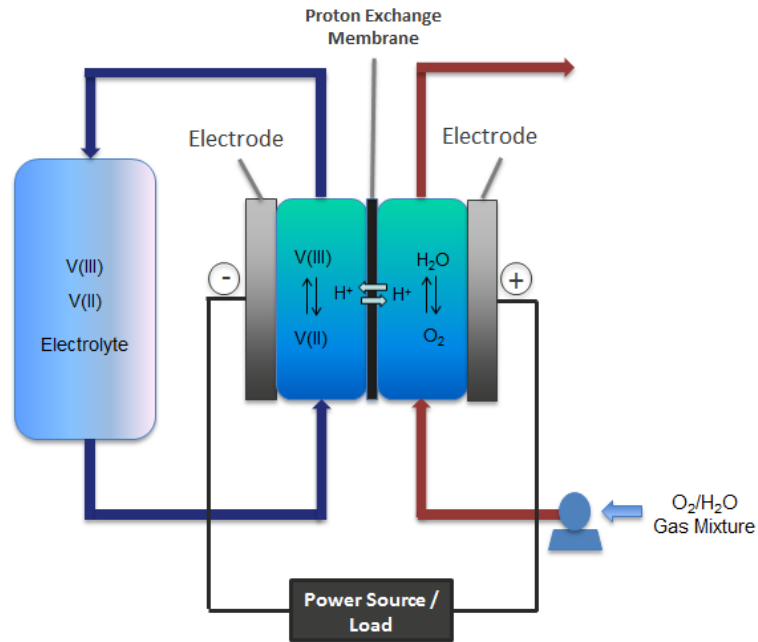
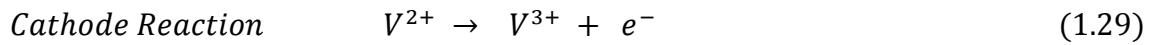
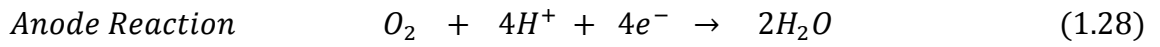


Figure 1.18 Air- Vanadium redox flow battery

Still there are a few studies about the Air-VRFB systems, which are mainly regarding the PEM or electrodes. During the charge of the cell oxygen is formed at the anode. Excess amount of oxygen in the water causes an osmotic pressure difference, thus crossover of oxygen to the negative cell occurs. Oxygen in the negative cell will set off a reaction of oxidation the V(II) ions to V(III). Other difficulty of these systems is the standard carbon or graphite electrode materials are not directly applicable to the positive cell. Carbon materials are not stable in the presence of oxygen and it causes corrosion on the surface of carbon electrode. Therefore, catalyst layer should be applied on the surface of electrode, such as titanium supported platinum or iridium [34].

2. Research Objectives

2.1 Incentive

Energy storage systems which are explained in introduction part have high efficiencies. Nevertheless high efficiencies are not the only sign for suitable storage systems. Suitability of energy storage devices also depends on storage capacities, resources and operating costs [35]. Therefore choice of the ESS should be done according to energy grid requirements. Figure 2.1 shows application ranges of different ESS according to their power output.

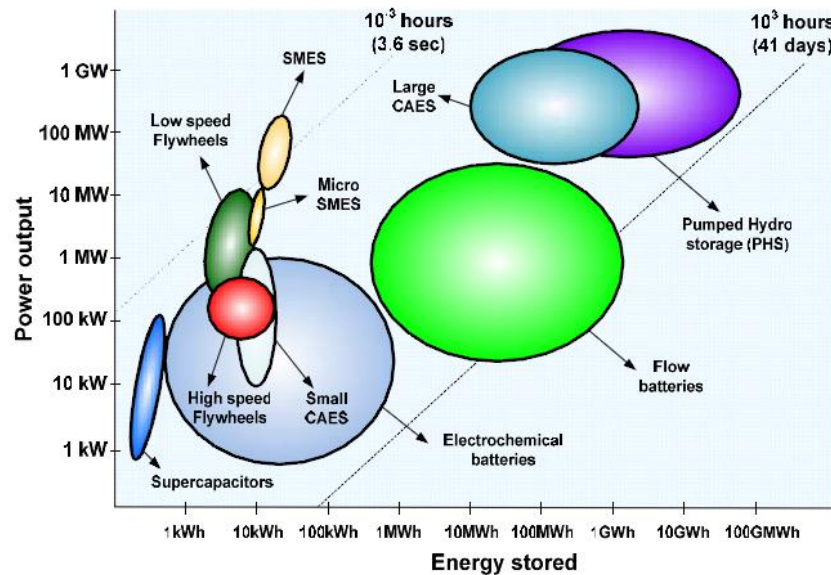


Figure 2.1 Application ranges for energy storage systems [9]

Figure 2.2 shows capital cost comparison of some ESS. Beside the fact that the capital costs are important parameters, operating cost of these systems are also substantial, therefore complete analysis should be done for most appropriate choice of energy storage system.

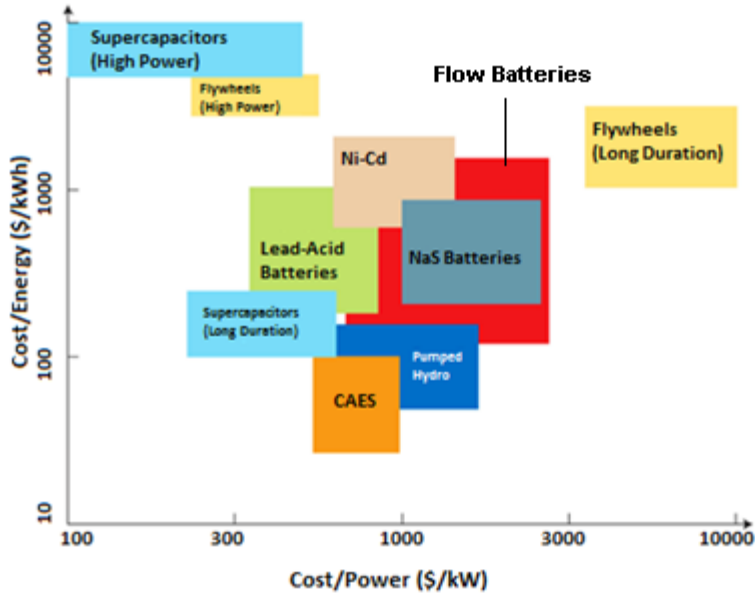


Figure 2.2 Capital costs per energy and power [36]

As it can be seen from both Fig. 2.1 and Fig. 2.2, RFBs serve an abroad energy and power range with accordance to affordable capitals costs. Furthermore their long cycle lives, flexible layouts and no hazardous emissions make them attractive more and more. Although these systems seem to be perfect for renewable energy storage systems, still cost effectiveness is a challenging issue that appears to be overcome. Figure 2.3 shows a low capacity RFB material costs effects on capital cost.

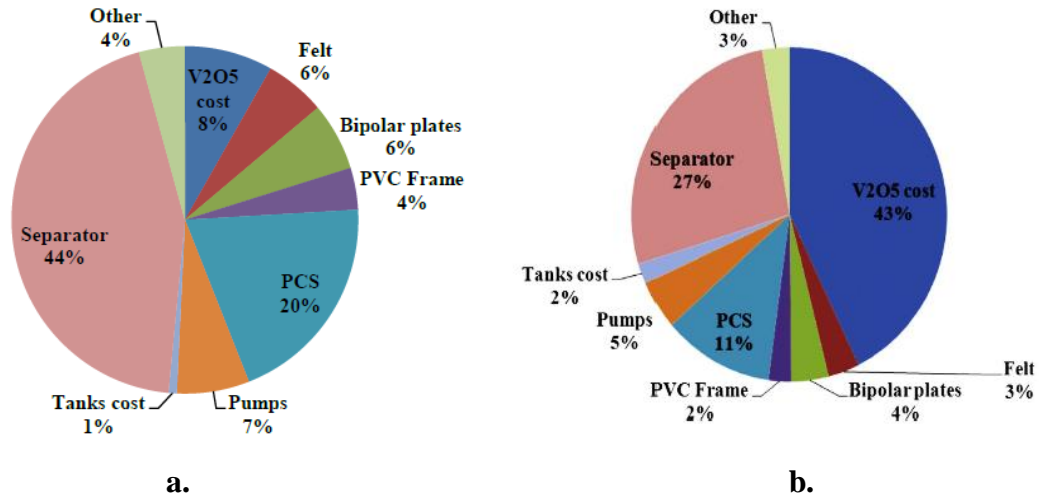


Figure 2.3 Component cost distribution of a VRFB **a.** 0.25 MWh system **b.** 4 MWh system [37]

Figure 2.3 (a) clearly states that especially in 0.25 h energy based V-RFB systems, polymer based membrane costs, such as Nafion, are higher than the any other components. On the other hand cell component costs comprise almost half of the total cost, such as PVC frames, bi polar plates, electrode felts and pumps. For 4 h energy storage systems, as shown in Figure 2.3 (b), the membrane cost are slightly less effective on capital cost, however, still electrolyte costs and other component costs keep its importance. Therefore, to be able to maintain more cost effective RFB it is essential to develop the following assets of a RFB system; the membrane technology that being used so far by using cost-effective material; lower amounts of electrolyte by integrating it into Air-VRFB; cell module by using a new design, which does not need any material that has no direct relation with the RFB, such as PVC frames, bipolar plates and electrode felts. Figure 2.4 (a)-(b) shows total capital costs for 0.25 h system and 4 h system. 0.25 h system costs showed almost 10 times higher values than the 4 h system. In addition, lower capital costs are expected in near term with the investigations and developments on these technologies. Moreover, even lower costs are predictable with the optimistic vision.

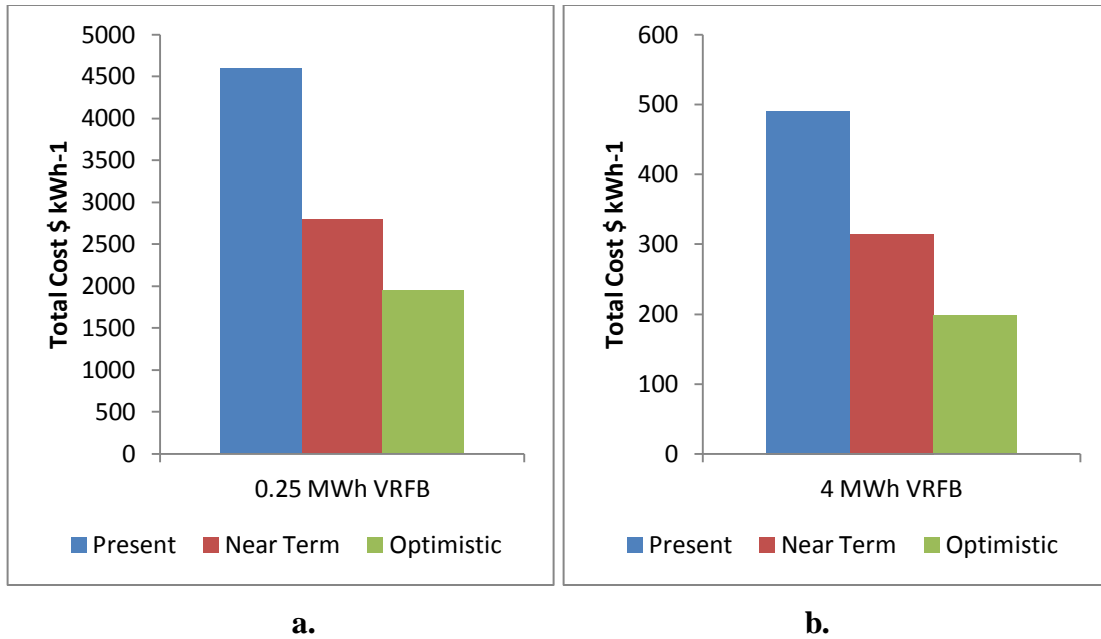


Figure 2.4 Total capital costs of 1 MW All-Vanadium RFBs **a.** 0.25 MWh **b.** 4 MWh [38]

One of the most promising battery technologies, V-RFB, is going to be studied during this master thesis. As it is mentioned before V-RFB consists of electrodes, electrolytes, membranes and cell compartments. Therefore developments are gathered around these specialties. This study will be performed in two parts. First part of the experimental part will be developing a novel polymer membrane for V-RFBs and second part will be developing a new cell module for the V-RFBs.

Project TubulAir±

A joint research project, TubulAir±, was founded on September 2012. Main objective of this project is to develop a cost-effective micro tubular redox flow battery. All-VRFBs has shown their good energy storage performance in many other researches. Nevertheless, comparatively low energy density and high costs of battery components require certain developments. Project TubulAir± suggests a new tubular module design for Air-VRFB, which would consume fewer electrolytes by replacing one side of the electrolyte with air/water steam and providing more conductive area between electrolyte and electrode interface by having a tubular MEA design. Therefore, energy density of V-

RFBs might be increased with high cost-effectiveness. Some of the project partners are; Hamburg University of Applied Sciences; Fau Erlangen-Nürnberg; DWI an der RWTH (Aachen); Fuma-Tech GmbH (St. Ingbert); Uniwell Rohrsysteme GmbH&Co.; DFI of DECHEMA; JRC-IET and project was supported by Federal Ministry of Education and Research [39].

This thesis was studied under the DWI an der RWTH. The objectives of DWI in this project are;

- Development of CNT electrodes,
- Development of tubular MEA,
- Catalyst application on electrodes,
- Application of membranes.

2.2 Membrane Development

Development and investigation of a novel proton exchange membrane will be represented in the first part of the thesis. In a V-RFB, the proton exchanging membrane separates the electrolytes while it still allows the protons to pass during charge and discharge. As it is explained before, during the operation of the battery electrons travels from external circuit while the protons transports from electrolyte through the selective proton exchange membrane. A suitable proton exchange membrane should have a low area resistance for good voltage efficiencies and it should be chemically stable in the highly oxidative vanadium solutions [40]. Generally perfluorinated sulfonic acids such as Nafion membranes (DuPont) are used as proton exchanging membranes. Structure of the Nafion membranes is shown in Figure 2.5. This kind of membranes has excellent proton conductivity and chemical stability under extreme conditions. Nevertheless, drawbacks like low Vanadium/Hydrogen ion selectivity and high purchasing cost of Nafion require many researches to search for more suitable membranes for this application [41].

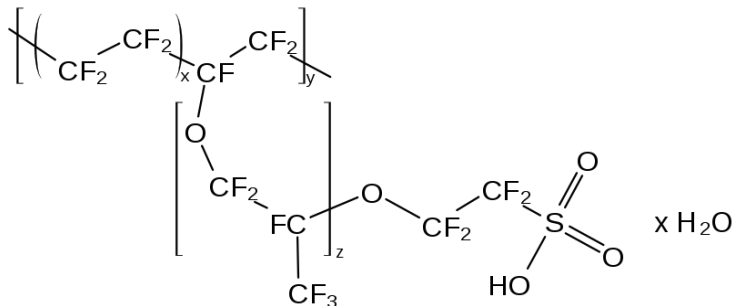


Figure 2.5 Structure of the Nafion (DuPont)

Alternatively sulfonated aromatic polymeric membranes have been suggested as proton exchanging membranes in early 2000s for RFB [42]. Sulfonated poly (ether-ether-ketone) (SPEEK) membrane is one of the most studied one, since sulfonation of PEEK (Poly-ether-ether-ketone) can be easily controlled. In comparison to Nafion, SPEEK has a less hydrophobic backbone and less acidic sulfonic groups, which produces narrower channels in the membrane [43]. Main advantages of using SPEEK membranes are; the low production costs, because of the aromatic backbone of the polymeric structure; high enough proton conductivity for a good proton conduction between electrolytes; higher selectivity between Vanadium / Protons as a result of tighter polymeric structure [42]. Sulfonation degree of the SPEEK membranes directly affects the mechanical stability of the membranes. High degree of sulfonation increases the swelling ratio of the membranes due to an increase in membrane hydrophilicity. This can lead to lost in membrane dimensional stability or even to dissociation in water [44]. In this work, we try to improve the mechanical stability of a highly sulfonated SPEEK membrane by SPEEK polymer blending with Polyaniline (PANI). PANI belongs to the intrinsically electronically conductive polymer class [45]. PANI based membranes and films were applied for actuators, gas separation, pervaporation, organic solvent nanofiltration and rechargeable batteries [46]. Polymer blends between SPEEK and PANI are homogeneous for up to 30 wt. % of PANI [47]. Polymer compatibility is based on an acid base reaction between one protonated sulfonic group of SPEEK polymer and 2 basic nitrogen atoms, per PANI repeating unit. Polymer structures and reaction between sulfonated groups and aniline groups can be seen from Figure 2.6, 2.7 and 2.8. This gives practically a physical crosslinking of SPEEK by PANI which, we assume leads to

a densified polymer matrix and therefore to improved mechanical stability and higher selectivity between the Vanadium ions and protons. The protonation reaction scarifies part of SPEEK sulfonic groups, nevertheless proton conductivity is expected to remain close to pure SPEEK as previously found for up to 33 wt. % PANI load [47].

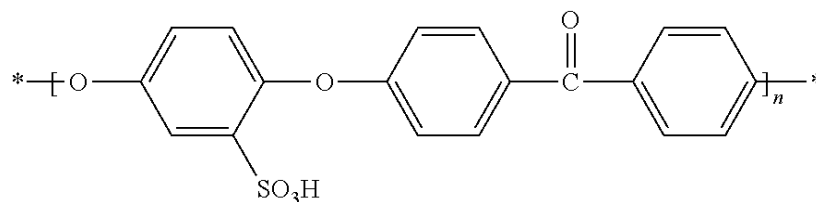


Figure 2.6 Chemical structure of sulfonated poly ether-ether-ketone

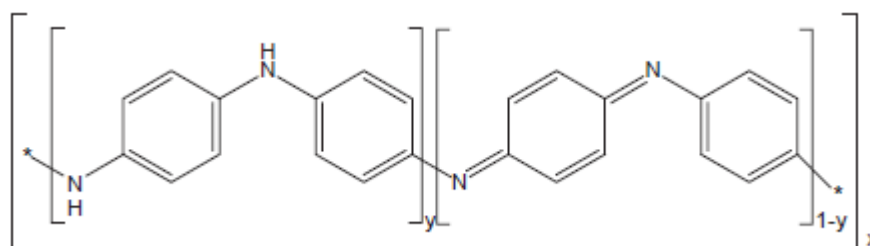


Figure 2.7 Chemical structure of polyaniline; if $y=1$ the structure is leucoemeraldine form, if $y=0.5$ the structure is emeraldine form and if $y=0$ the structure is pernigraniline form [48]

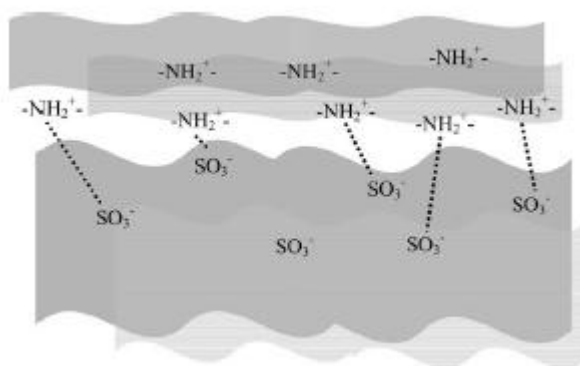


Figure 2.8 Schematic explanation of interaction between SPEEK and PANI [41]

Both sides' coated SPEEK membranes with PANI by polymerization, i.e. composite membranes, have already been produced for methanol fuel cell application [41]. The

composite SPEEK/PANI membrane had reduced methanol permeability when compared to pure SPEEK membrane. Nafion/PANI composite membranes with similar structure showed reduced cross transport of cations [49]. Nevertheless, lower proton conductivity and membrane degradation during battery cycling in a V-RFB system was observed. Membrane degradation was attributed to PANI and was concluded that this polymer was not suitable for V-RFB applications. Also, electrodeposited Polyaniline onto platinum showed PANI dissolution in V-RFB operation [50]. In the potential range of the V(IV)/V(V) electrolyte PANI also undergoes oxidation and reduction reactions. Nevertheless for the pH range 1-4, these reactions are reversible [51]. The chemical stability of PANI in V^{5+} solutions was never assessed. In both studies PANI was found as a bulk film on top of a membrane and electrode respectively. In contrast, SPEEK/PANI blend have an intimate mixing and polymer interaction. Therefore our hypothesis is that a stronger oxidation-resistant behavior is induced apart from an improved mechanical stability.

In this part of the work, SPEEK/PANI blended proton exchange membranes for V-RFB will be introduced. During the study, SPEEK/PANI blended membrane will be produced with different weight ratios and typical proton exchange membrane characterization methods will be applied on these membranes. Finally V-RFB performance of our membranes will be investigated.

Hypothesis

Hypothesis for the first part of the thesis is to development of a novel blended membrane for V-RFBs, which is cheaper than conventional type of membranes, without sacrificing any of the characteristic properties.

2.3 Tubular Module Development

Redox flow batteries were introduced during the introduction as suitable energy storage systems for renewable energy sources. Many other energy storage systems are currently being developed. Thus, expectations from RFB systems are growing rapidly. A novel proton exchange membrane was developed and characterized in first chapter. In this chapter a new tubular module and suitable electrode materials will be investigated and benefits of using these new materials will be studied.

A new tubular module for RFB idea was suggested due to improve low power density capability of the planar RFB. This tubular design consists of one large negative tubular electrode and a number of small positive tubular electrodes inside the negative one. A draft of the Tubular Module design can be seen at Figure 2.9. The tubular design of RFB with no extra component without the electrodes might decrease the capital cost of RFB that explained with Figure 2.2. Expected problem of this module might be the lower conductive area than typical planar redox flow batteries. In order to overcome lower conductive area problem, slurry electrode is suggested. It might improve conductivity between electrolyte and solid electrodes. After having proper negative and positive solid tubular electrodes, highly conductive particles as activated carbon or carbon nanopowder etc. will be mixed with both electrolyte solutions to maintain a slurry electrode.

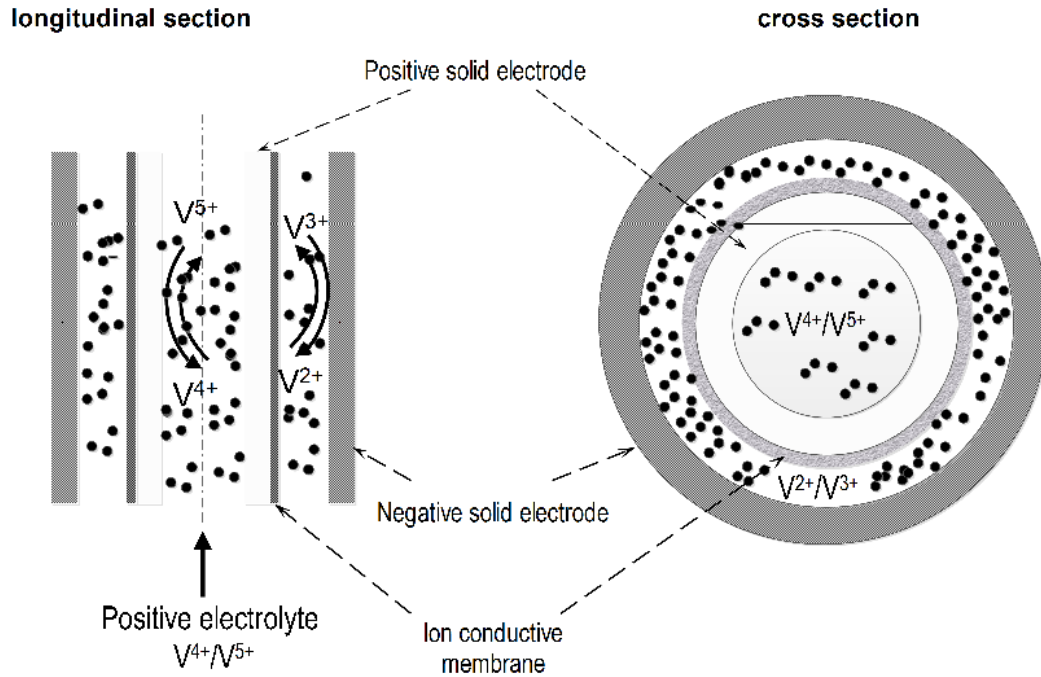


Figure 2.9 Tubular module of RFB

Electrode material should be an efficient combination of anode and cathode materials. In a basic system, the anode should be selected by considering these properties: efficient as a reducing agent, good conductivity, stability, ease of fabrication and low cost. On the other hand cathode material should be selected according to: efficiency as an oxidation agent, useful working potential and stability inside the electrolyte. Mostly carbon based materials are being used in Vanadium RFB [52]. Main concern point of these electrodes is the gas evolution by electrolysis of water. According to electrolysis reaction, hydrogen production occurs at cathode and oxygen production occurs at anode. Evolutions of these gases result self-discharge in the Vanadium RFB [53]. Therefore, selection of electrode materials plays a key role in the Vanadium RFB.

Carbon Nanotubes (CNT) were firstly introduced with the research of Iijama's [54]. CNTs have hexagonally bonded carbon atoms in its structure, which gives them unique shapes, sizes and physical properties. Generally CNTs being produced as single-walled

(SWCNT) or multi-walled (MWCNT) according to their number of layers [55]. Figure 2.10 shows structural image of the SWCNT and MWCNT respectively. They were suggested to use as electrodes in Fuel Cells, Lithium-ion batteries, super capacitors, redox flow batteries and etc.[56]. Currently, the physical properties of CNTs are still being discovered. In summary, three main properties of CNTs are specifically interesting for the industry: high electrical conductivity, mechanical endurance and thermal conductivity [55]. By integrating these properties, new variety of useful and beneficial applications may be accessible.

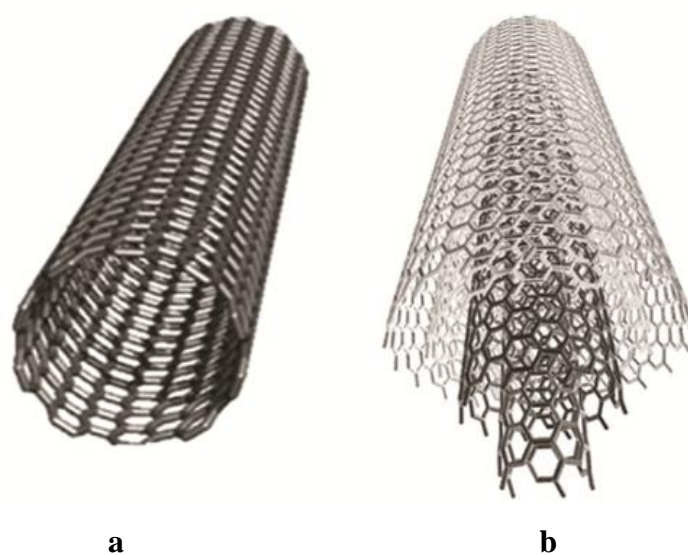


Figure 2.10 a. Structure of single-walled CNT, **b.** Structure of multi-walled CNT

Another electrode material, Titanium, has gained much interest recently. First use of Titanium has been started by mid 1950s [57]. By mid 1960s it has been used as a support material in brine electrolysis, but then researchers have found out that Titanium has good physical properties as an electrode material too. Currently planar-surfaced Titanium materials are being used for the industrial application of Fuel-Cells, Redox Flow Batteries and other electrochemical reactors. A new study of David [58] presents development of porous, tubular Titanium electrodes, which may have several important advantages better than planar Titanium products (meshes and felts); controllable geometry; porosity; pore size distribution and surface area.

It has been investigated that the functional groups on electrode materials can influence the electro-catalytic activity of these materials. Therefore a surface modification is suggested to improve the surface activity [59]. Oxygen functional groups on the electrode surface affect directly the reaction of vanadium RFB. Therefore, a heat treatment was offered to lower the adsorption of oxygen on carbon material. Sun et al. [59] reported chemically modified electrode material with solutions containing Pt, Pd, Au and Ir. The best electro-catalytic activity achieved by using iridium for V-RFB. These heat and chemical treatment of electrode materials may lead a significant improvement on V-RFB electrodes.

In the second part of the thesis new tubular module for V-RFB will be investigated by integrating different kind of electrode materials such as CNT, carbon fibers, graphite, titanium felt and titanium macrotubes. Pt/ Ir catalyst will be applied on positive electrodes with heat treatment to improve the surface catalytic activity. In order to achieve high conducting area, consequently high power density, slurry electrode will be introduced into the tubular V-RFB with different concentrations and standard V-RFB operations will be performed.

Hypothesis

Hypothesis of the second part of the thesis is to investigate a new designed tubular module for V-RFBs to able to achieve same surface area in a smaller volume of cell.

3. Materials and Methods

3.1 Membrane Development

This part of the master thesis includes respectively; preparation method of the dense polymeric membranes from Sulfonated Polyether-ether-ketone and Polyaniline blend, pre-treatment method of dense membranes, membrane characterizations and vanadium redox flow battery performance of the blended membranes.

3.1.1 Membrane Preparation

Sulfonated polyether-ether-ketone SPEEK (E600-E700) was kindly provided by FuMA-Tech GmbH. Polyaniline (PANI) was synthesized according to a procedure reported in the literature [60]. N-methylpyrrolidone (NMP, 99 wt%, Acros Organics) was used as a solvent for membrane preparation. Prior to use, the polymers were dried in a vacuum oven at 30 °C for 14 h, all other chemicals were used without further treatment.

Different weight ratios of polymer mixture were prepared as shown at Table 3.1.

Table 3.1 SPEEK/ PANI wt. ratios for blended membranes

SPEEK	PANI
100	0
98	2
95	5
80	20

Totally 50 g of the mixture was prepared with 15 wt% of polymer (SPEEK/PANI) solution in NMP at 50 °C. A mechanical stirrer (Heidolph RZR 2052) in a Pyrex® vessel was used to mix the polymers for 24 h and an air condenser was attached to the

vessel to avoid solvent evaporation. The Pyrex® vessel was weighted before and after mixing to ensure that there is no solvent evaporation.

Mixing process was followed by a mechanical filtration to separate insoluble parts of polymer blend. A 15 μm sintered metallic filter (Bekipor STAL3 Bekaert) was used under high pressure. After filtration of polymer solution, there can be some trapped gas inside the viscous polymer solution. To release these gases, a vacuum pump and a closed vessel were used. Polymer solution was placed in this vacuumed vessel for 1-2 h, until getting a pure visual appearance. If still there were some bubbles, degassing repeated for 2 h more. Mixing device, filtration device and degassing pump are shown at Figure 3.1.

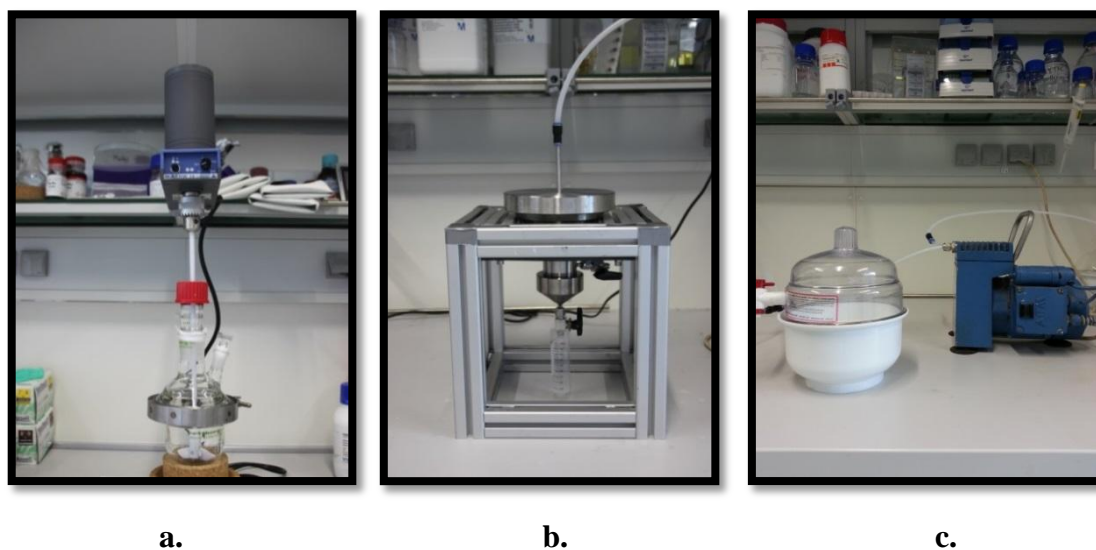


Figure 3.1 a. Mixing device, b. Filtration device, c. Degassing pump and vessel

Membranes with comparable thickness ranging from 23 μm to 40 μm were prepared by casting the polymer solution on a dust and scratch free glass plate using a casting knife. Dry films of comparable thicknesses were prepared by using a casting knife with a gap size of 500 μm for the bare SPEEK polymer while a casting knife with a gap size of 200 μm was used for the blends. Excess polymer solution was kept for possible usage of membranes by deep coating. The casted membranes were dried for 24 h at room

temperature in a nitrogen box. This Nitrogen box was laid down on a flat surface to avoid changes in thicknesses of membranes. Air was emptied from this box by maintaining a very slow flow rate of N₂. Then, the casted membranes were further dried in a vacuum oven at 60 °C and 90 mbar for minimum 3 days to fully evaporate the excess NMP solvent inside the membrane. Dried membranes were removed from the glass plates by immersing into water and pulled gently. All ready membranes were stored in vacuum oven.

3.1.2 Pre-treatment

SPEEK / PANI blended membranes were immersed in a 3 vol. % H₂O₂ solution at 60°C for 1 hour. This step of pre-treatment helps to remove fouling on membrane surface. After having clean and proper membranes, they all immersed in 0.5 M H₂SO₄ for at least 48 hours to fully protonation of sulfonated groups on membrane.

3.1.3 Characterization Methods

In view of the membrane application in all vanadium redox flow battery the basic membrane properties such as: swelling degree, water uptake, proton exchange capacity, proton conductivity and vanadium diffusion coefficient were measured. These experiments have been carried out for three different samples of the same membrane. In addition the battery performance was also evaluated.

Vanadium Permeation

Vanadium permeation method is to determine V (IV) permeation rate through the membrane. In this experiment a H-Cell was used as in Figure 3.2. A pre-treated membrane was placed between two compartments of the cell. The active area of the membrane was 5.72 cm². One compartment was filled with 100 ml 1.0 M VOSO₄, 2.5 M H₂SO₄ solution and the other with 100 ml 1.0 M MgSO₄, 2.5 M H₂SO₄ solution. MgSO₄ was added to equalize the ionic strengths and osmotic pressure difference between the

compartments [40]. Mixing was provided by recirculating each solution with a peristaltic pump (Masterflex L/S Cole Parmer) at a flow rate of 100 mL min^{-1} . Samples of solution from MgSO_4 compartment were taken at regular time intervals and the concentration of VO^{+2} analyzed by UV-Visible Spectrophotometer (Genesys 10S). 10 different V (IV) solutions (0.00 - 0.04 M) were prepared to draw a calibration curve for calculation of V (IV) amount in the MgSO_4 solution.

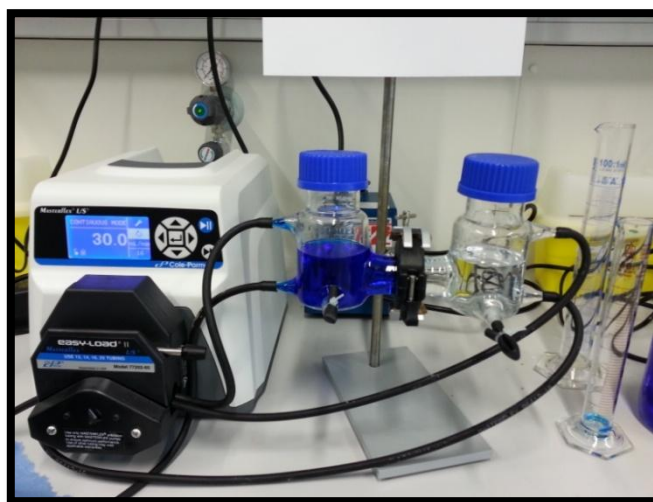


Figure 3.2 H-Cell and peristaltic pump

The diffusion coefficients of vanadium ions across different membranes were calculated according to Fick's Law of Diffusion (Eq. 3.1).

$$\text{Fick's Law of Diffusion; } J = -D * \frac{dC}{dx} \quad (3.1)$$

Ion Exchange Capacity

Ion exchange capacity (IEC) of a membrane is relevant with sulfonation degree of the membranes, as high sulfonated membrane can transfer more ions than lower sulfonated membranes. To measure IEC, first the pre-treated membrane was immersed into 100 ml 2.0 M NaCl solution for 24h. Then, to be sure that all H^+ within the membrane were ion-exchanged with Na^+ , the NaCl solution was renewed with fresh one and the membrane was left for 4h more. The membrane was removed and the acidic solutions were mixed

and diluted to a volume of 500 ml. H^+ concentration was measured by titration (Titrand 905 Metrohm) As titrant freshly prepared 0.01 M NaOH solution was used. The IEC was calculated according to the following Equation 3.2:

$$\text{Ion Exchange Capacity (IEC)} = \frac{\text{Moles of } H^+}{\text{Dry Weight of Membrane}} \quad (3.2)$$

Where, IEC is defined in terms of millimole of H^+ / gram of dry membranes.

Swelling and Water Uptake

Water uptake and swelling ratio of the membrane were determined by comparison of dry and wet physical properties. Pre-treated membranes were cut and shaped like stripes (10 cm length - 1 cm width). First dry membranes measured and then they all immersed in water at room temperature for 24 h. Wet membranes were weighed and length-width measurement were taken again. Water uptake and swelling ratio were calculated as follows:

$$\% \text{ Water Uptake} = \frac{W_{Wet} - W_{Dry}}{W_{Dry}} * 100 \quad (3.3)$$

$$\% \text{ Swelling Ratio} = \frac{L_{Wet} - L_{Dry}}{L_{Dry}} * 100 \quad (3.4)$$

Chemical Stability

Long term chemical stability plays a critical role on membrane's operational life. In a V-RFB system, V (V) is highly oxidizing and if the chemical stability of membranes is not confidential enough, it would mean that V-RFB is not going to work at same conditions after a certain time. Thus, the chemical stability was measured by immersing pre-treated samples into 10 ml 1 M V (V) solution for 30 days. The V (V) solution was prepared by charging the V (IV) in a V-RFB. The increase in V (IV) concentration was monitored by UV-Visible Spectrophotometry (Genesys 10S) at a wavelength of 750 nm. 10 times

sample dilution was done to obtain more accurate values. 5 different V (IV) solutions (0.00 - 0.01 M) were prepared to draw a calibration curve for calculation of V (IV) amount in the V (V) solution. After 30 days, samples were washed and dried again to be able to calculate the weight loss by chemical degradation.

Proton Conductivity

Proton conductivity is a crucial criterion for evaluating RFB performance as well as the practicability of novel proton exchanging membrane materials. Conductivity measurements were carried out by AC impedance spectroscopy using a four-probe conductivity cell (Bekktech BT-112) at room temperature and 100% humidity. Four-Probe conductivity cell can be seen at Figure 3.3.

Pretreated membrane was cut into a rectangular (1 cm x 3 cm) shape and placed into a conductivity cell with 0.42 cm distance between two working electrodes. Then the cell was introduced into UV-water at room temperature to guarantee that the membrane was fully hydrated. The impedance measurements were carried out in the frequency region from 1 Hz to 500 kHz using frequency work station (response analyzer and power supply) (ZAHNER® IM6 Electrochemical Work Station).

Proton conductivity calculations were made by following equations,

$$Z(w) = \frac{1}{R} + iwC \quad (3.5)$$

$$\sigma = \frac{RA}{L} \quad (3.6)$$

Where Z is impedance (Ω), R is resistance (Ω), σ is resistivity (cm S^{-1}), C is capacitance (F), w is the frequency (Hz), L is distance between working electrodes and A is the lateral area of placed membrane (cm^2). Proton conductivity (S cm^{-1}) was calculated as

the reciprocal of resistivity, $1/\sigma$. The Four-probe proton conductivity cell can be seen at Figure 3.3.

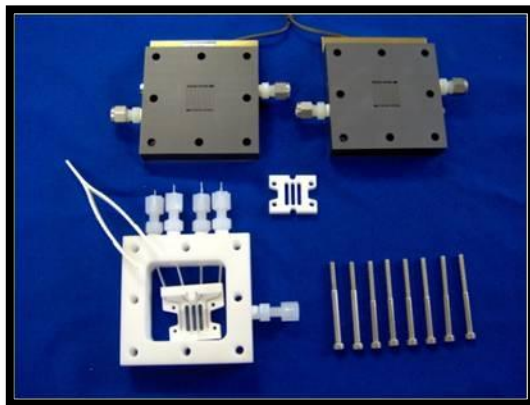
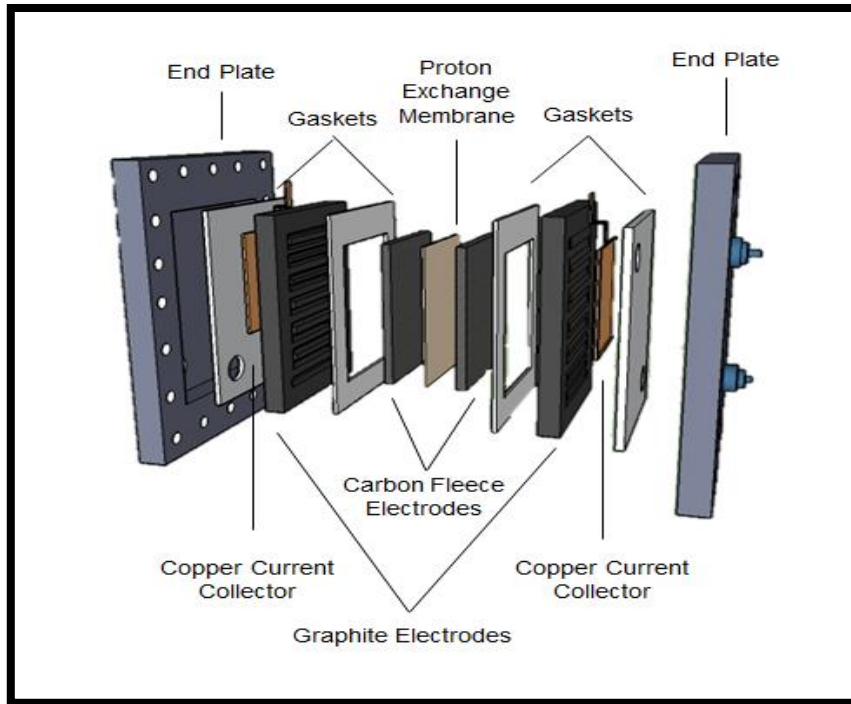


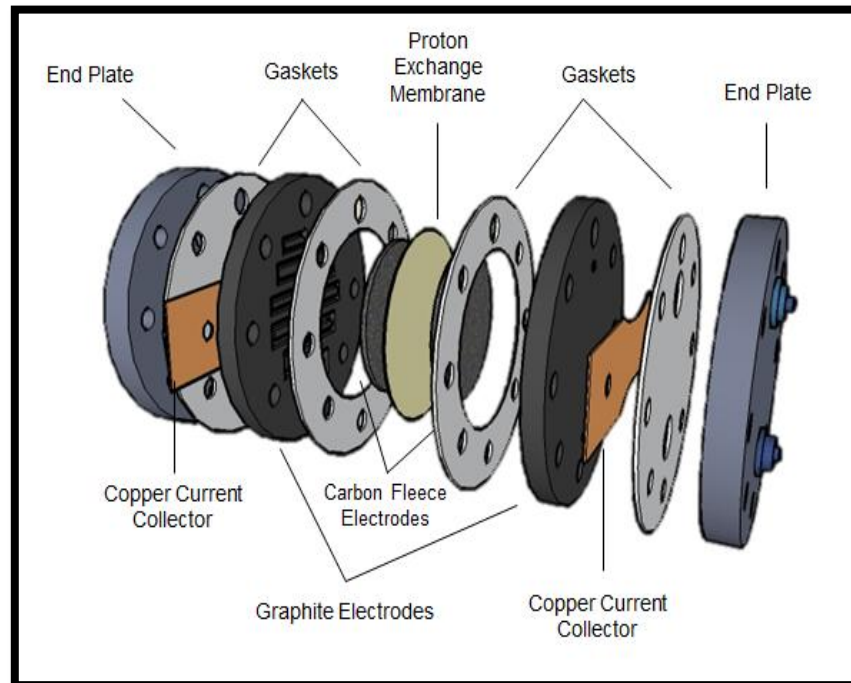
Figure 3.3 Four-Probe proton conductivity cell

3.1.4 Battery Performance

Two planar redox flow battery were constructed as mentioned in [61]. Their design was developed to have minimum contact resistance loss by having “zero-gap” configuration. According to this configuration, plates, electrodes and membrane are in a directly contact to able to decrease resistance occurred by empty volumes. In our construction a rectangular planar design and a circular planar design were developed. Graphite plates were purchased from Novotech Inc. (Germany) and Epoxy Impregnated graphite plates were purchased from Müller & Rössner GmbH & Co. (Germany). Plates have flow channels (1.5 mm depth, 1.5 mm wide and 600 mm overall length) to distribute the conducting area on the surface and both act as an electrode and a current collector. A copper plate was used as an exterior current collector. The membrane was sandwiched between two carbon fleece electrodes, which were purchased from SGL Group (Germany). The carbon fleeces (2 mm uncompressed thicknesses) were activated by thermal treatment at 400 °C for 6 h. In order to fill the area between graphite plates and membrane, 2 layers of carbon fleece was used. PVC gaskets were used to fasten the membrane between electrodes. Outer housing was constructed with PVC and had screw holes in order to fasten the assembly together. 3D drawing of our RFB assembly can be seen at Figure 3.4.



a.



b.

Figure 3.4 a. Rectangular redox flow battery design; **b.** Circular redox flow battery design

VO_2SO_4 was purchased from Sigma-Aldrich Co., Germany, which gives VO^{2+} ions into solution as V (IV). As electrolyte solution 1 M VO_2SO_4 solution was prepared. Vanadium ions are not soluble in water; therefore solution was prepared with 2.5 M H_2SO_4 . Battery electrolyte volume was determined as 20 ml for both electrolyte vessels.

Despite the fact that purchasing Vanadium (III) solution was really challenging, it was initially produced by charging the battery with VO^{2+} . According to V-RFB reactions, V (IV) at positive the electrode oxidizes to V (V) and V (IV) at negative electrode reduces to V (III) and V (II) respectively. It means twice amounts of electrons were consumed at positive electrode. Thus, twice amount of V (IV) electrolyte solution was filled in positive side to equalize this difference. After the first fully charge, excess amount of charged positive electrolyte (20 ml) was emptied from the vessel.

Each electrolyte vessel was de-aerated with continuous flow of N_2 to avoid the chemical oxidation of the electrolyte solutions. Entire RFB systems can be seen from Figure 3.5.

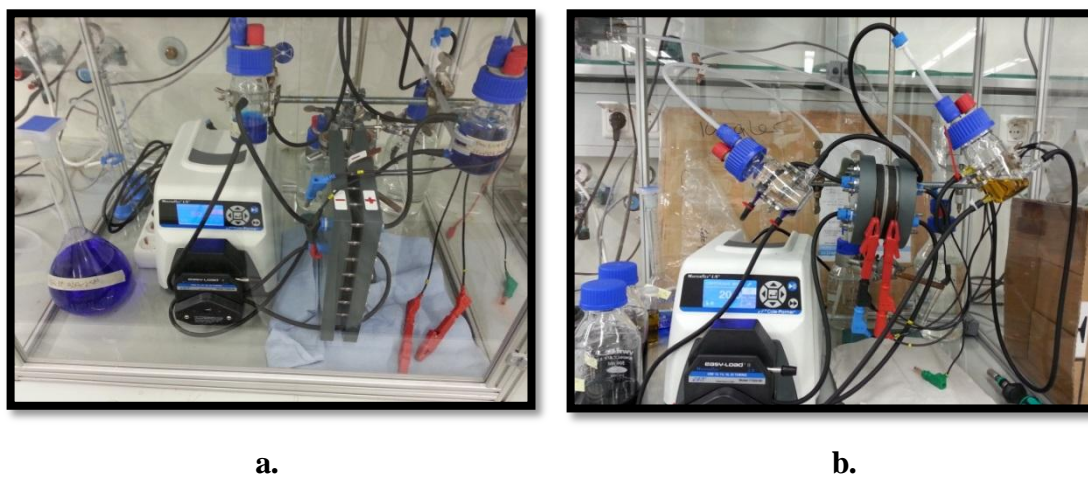


Figure 3.5 a. Rectangular planar RFB; b. Circular planar RFB

A potentiostat/galvanostat (PGSTAT302N - Metrohm GmbH) equipped with data analysis software Nova 1.9v was used to charge and discharge the battery. For each membrane sample, such as SPEEK, SPEEK /PANI blends, Nafion 112 and Fumapem 14100 (Fumatech Co.), same charge and discharge properties were applied. Battery was

charged at a constant current density of 40 mA cm^{-2} and discharged at different current densities. Respectively 20, 30, 40 and 50 mA cm^{-2} current densities were used for discharge. Charge and discharge cycles were maintained 30 times for 40 mA cm^{-2} and 5 times for the other current densities.

A cut-off point was applied at 1.7 V during the electrolyte production (first charge at 40 mA cm^{-2}). After cut-off point, a constant voltage at 1.7 V was applied on the battery and this time cut-off was set to 10 mA to be sure that battery was fully charged. Besides colors of the electrolytes were observed as they perfectly show fully charge state (at positive electrolyte light yellow, at negative electrolyte dark purple) and fully discharge state (positive electrolyte dark blue, at the negative electrolyte dark green). Apart from that charging was always stopped at 1.7 V and discharging was stopped at 0.8 V.

The software of the potentiostat/galvanostat was set to collect time (s), voltage (V), current (A), charge (C) and power (W) values automatically. The values were determined for each half second. According to this values energy efficiency, voltage efficiency, coulombic efficiency and charge capacities were calculated by using all collected data. Efficiency equations can be seen from Table 3.2.

Finally, the self-discharge of the battery was evaluated by tracking the open circuit voltage decrease in time of a fully charged battery. All data were collected until open circuit voltage dropped below 0.8 V to the discharge state of the battery.

Table 3.2 Efficiency equations

Energy Efficiency	$\eta_{Energy} = \frac{\int_0^{t_{Discharge}} I_{Discharge} * E_{Discharge} * dt}{\int_0^{t_{Charge}} I_{Charge} * E_{Charge} * dt}$
Coulombic Efficiency	$\eta_{Coulombic} = \frac{\int_0^{t_{Discharge}} I_{Discharge} * dt}{\int_0^{t_{Charge}} I_{Charge} * dt}$
Voltage Efficiency	$\eta_{Voltage} = \frac{V_{Discharge}}{V_{Charge}}$

3.2 Tubular Module Development

3.2.1 Membrane Electrode Assembly

The tubular shaped RFB (Figure 2.9) design was built with two suitable electrodes which are combined together. Outer electrode was a negative solid electrode and inner electrode was a positive solid electrode. Positive electrode was coated with proton exchange membrane solution to allow proton exchange. Positive electrolyte was circulated through the inner tube, while negative electrolyte was circulated between two tubular electrodes. Oxidation and reduction reactions were occurred at electrodes and then proton exchange was maintained by the PEM.

Electrodes

The characteristics of the negative and positive electrodes determine both the power density and energy density of the battery. As a battery converts its chemical energy to electrical energy, electrodes are altered important physical and chemical changes which affect its electrical performance. In this experiment different types of electrodes were studied. These electrodes were carbon nanotubes, carbon fibers, graphite tubes, epoxy impregnated graphite tubes, titanium felts and titanium macrotubes were used as electrode materials. Electrode materials can be seen in Table 3.3.

Table 3.3 Electrode materials

Material	Electrode
CNT	Positive & Negative Electrode
Carbon Fibers	Negative Electrode
Titanium Felt	Positive Electrode
Graphite & Epoxy Imp. Graphite	Negative Electrode
Titanium Macrotube	Positive Electrode

Carbon Nanotubes were provided via infiltration of carbon nanotubes suspension through a microfiltration hollow fiber membrane as mentioned in Y. Gendel et al. [56]. Carbon fibers were purchased from SGL Group (Germany). Titanium felt (ST/Ti/20/150/85) was purchased from Bekaert Co. (Belgium). Graphite tubes were purchased from Novotech Inc. (Germany) and Epoxy Impregnated graphite tubes were purchased from Müller & Rössner GmbH & Co. (Germany). Tubular macroporous titanium membranes prepared via a dry-wet spinning process from a poly-ethersulfone solution loaded with Ti particles and a subsequent sintering process at various sintering temperatures and sintering times. The processing method was explained at Oana David et al. [58]. Physical properties of CNT and Titanium Macrotube electrodes were stated in Table 3.4.

Table 3.4 Physical properties of electrode materials

Electrode	Outer	Wall	BET	Porosity	Electrical
	Diameter	Thickness			Conductivity
	(mm)	(μm)	(m^2/g)	(%)	(S/cm)
CNT	1.7	100-300	~200	48-67	~25
Titanium Macrotube	1.9	340	0.028	30	3457

Pre-treatment

Pretreatment was applied only on Titanium Felt and Titanium Macrotubes to clean out impurities and possibly synthesized TiN and TiO₂. Firstly pre-weighed tubes were immersed into 6 M HCl at 100 °C. Optimization of acid pretreatment was obtained by studying on 5 different tubes with different immersion time (1 to 5 min). Then the tubes and felts were weighed again to be able to see weight loss during the pretreatment. Tubes were dried in a vacuum oven for 1 hour. After that Platinum/Iridium (wt. 70/30) catalyst was prepared according to thermo-decomposition method, which was reported in Raghu et al [62]. Catalyst coating was maintained with simply brushing the catalyst on the tubes and felt. Then electrodes were dried at 160 °C for 15 min in the oven. This coating procedure was repeated for 10 times to get complete coating on the electrodes. A last activation of catalyst was provided with a heat treatment at 450 °C for 1 h in the oven and final weights of the tubes were observed to be able to calculate the amount of implanted catalyst.

Membrane Coating & Membrane Pretreatment

As a proton exchange membrane Fumion F-950 (FuMA-Tech GmbH, Germany) solution was used. A glass tube was filled with membrane solution and CNT and Titanium Microtubes dipped into this solution. Dip-Coating was repeated for 5 times and tubes were dried between each coating for 20 min. After that a heat treatment was applied on membrane coated tubes. The best performance of the polymer membrane solution treatment was achieved at 150°C for 6h. This heat treatment is highly effectible on membrane performance, since it is reported that different type of treatments might change the ionic conductivity and mechanical stability of the polymeric membranes [63].

FE-SEM Analysis

Field Emission Scanning Electron Microscopy (FESEM) (Hitachi S-4800) was used to observe visual appearance of the surface and the cross-sectional area of the Titanium tubes. Respectively non-coated tubes, acid pre-treated tubes, catalyst implanted tubes and membrane coated tubes were analyzed with different scanning magnifications.

3.2.2 Construction of Tubular All-Vanadium RFB

Three different MEA were constructed as it follows:

CNT and Carbon Fibers

In this type of MEA, CNT was used as a positive electrode. A 25 cm long CNT was wrapped from each ends with a Titanium wire current collector (0.25 mm thickness), which was purchased from Alfa Aesar (Germany). Then membrane dip-coating was applied on CNT. As a negative electrode, carbon fibers were rolled around Titanium wire and again same current collector material was used and connected from each side of the carbon fibers. Lastly MEA was placed into a PVC tube with suitable PVDF connectors for each direction of electrolyte flow. Positive electrolyte was flowed through the CNT and negative electrolyte was flowed between tubes. Electrode materials and MEA can be seen from Figure 3.6.



Figure 3.6. Carbon fibers, CNT and Ti wires

CNT and Titanium Fleece

In this design CNT was used as a negative electrode. In this assembly CNT tube was fully wrapped with Ti wire and they were dip-coated together with membrane solution. As a positive electrode, pre-treated titanium felt was used and it was rolled around the CNT. Titanium wire was connected to collect currents from each ends of Titanium felt. This MEA was placed into a glass tube, which has two inlets and outlets. Negative electrolyte was flowed through the CNT and positive electrolyte was flowed between glass and CNT. MEA materials and the tubular battery can be seen from Figure 3.7.

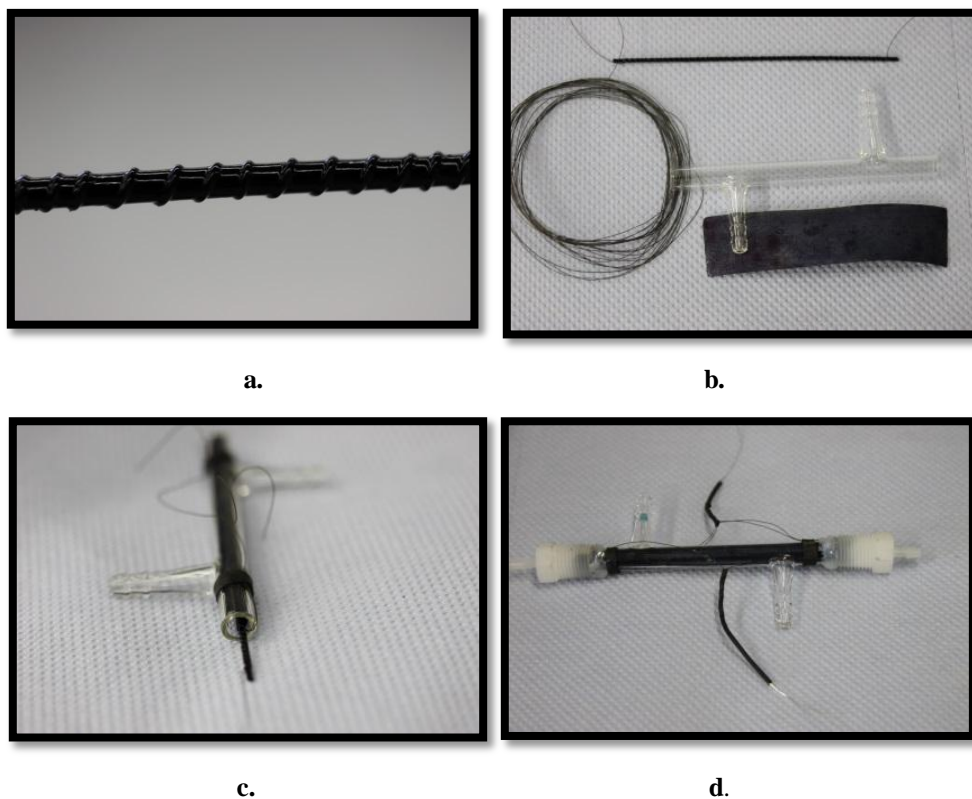


Figure 3.7 a. CNT and titanium wire with membrane coating b. MEA materials c. Side view of the tubular RFB d. Front view of the tubular RFB

Titanium Macrotube and Epoxy Impregnated Graphite Tube

Titanium Macrotubes were used as a positive electrode in this construction. Tubes were first pre-treated and then dip-coated with membrane solution. Each end of the tubes was left uncoated with membrane to be able to connect current collector wires. Each side was wrapped with Titanium wire and a non-conductive tubing material was glued on the current collector to separate the wire with negative electrode. Conductive glue (Leit-C, Fluka Co. Germany) was used for this purpose. Epoxy impregnated graphite tube was used as a negative electrode and housing of the tubular battery, which is wrapped with Titanium current collector. Graphite tubes were constructed as they could directly connect with a suitable connector. Teflon connectors were used as connector for each side. Finally a non-conductive tape was used to cover the current collector. Positive electrolyte was flowed through the Titanium Macrotube and negative electrolyte was flowed between Graphite and Titanium tubes. MEA materials and the tubular battery can be seen from Figure 3.8.

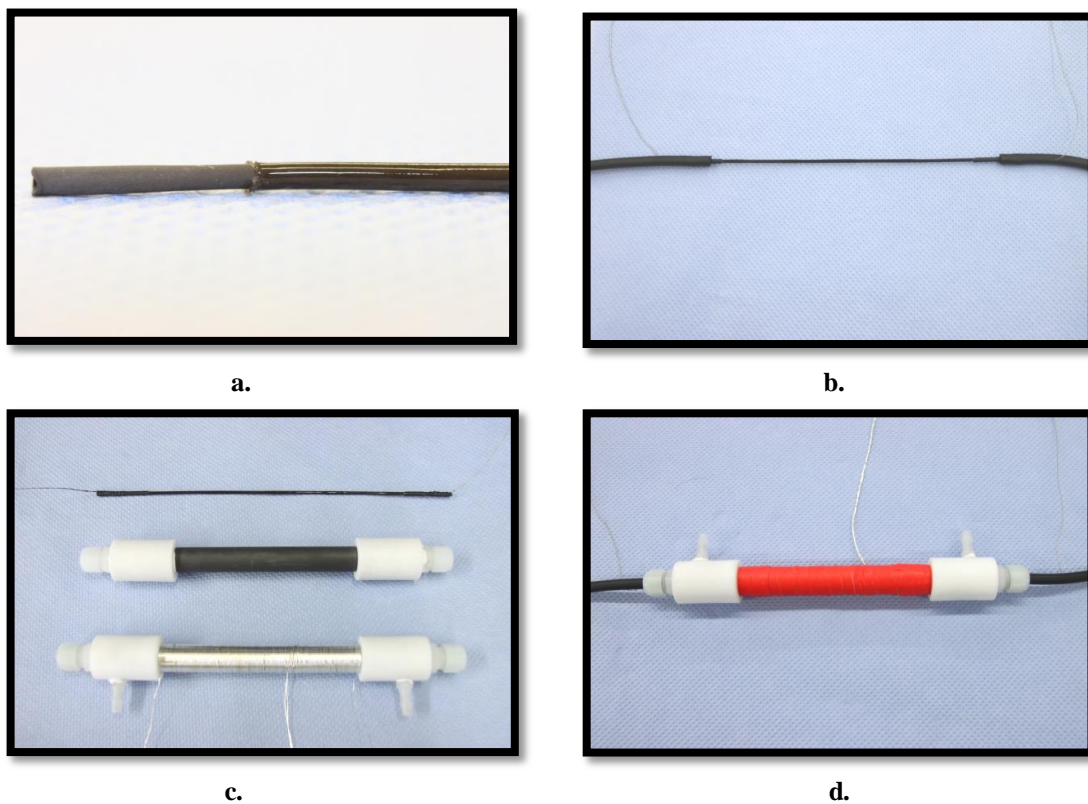


Figure 3.8 a. Titanium macroporous tube with membrane coating b. Titanium m. tube with current collectors c. Titanium m. tube, Epoxy impregnated graphite tube with Teflon connectors and epoxy impregnated graphite tube with current collectors d. Tubular RFB with all connections

3.2.3 Tubular All-Vanadium RFB Operation

Electrolyte production was carried out as explained before in §3.1.4. Battery performance of the tubular MEA analyzed with a potentiostat/galvanostat (PGSTAT302N - Metrohm GmbH) equipped with data software Nova 1.9v. Each different MEA had its own active surface area according to titanium macrotubes length and diameter. Therefore, different current densities were applied on each MEA. Charging was applied as maximum operable voltage (1.7V) and current was detected during the charge. Charging was stopped when the current dropped down below 20 mA. Discharging was applied with constant current in a range of 20-50 mA, according to the currents that tracked during the charge. The cut off point for discharge was set up to 0.8 V, which a V-RFB was assumed as almost fully discharged.

Tubular All-Vanadium Redox Flow Battery with Slurry Electrodes

Two different types of slurry materials applied in electrolyte solution; activated carbon and graphite powder. Basic properties of slurry materials can be seen from Table 3.5.

Table 3.5 Basic properties of slurry materials

	Particle Size (μm)	Surface Area (m^2/g)	Pore Diameter (nm)
Activated Carbon	<1700	~600	15-25 * 10^5
Graphite Powder	<150	~20	50-200

Slurry effect on MEA's conductive area was studied step by step adding slurry material into electrolyte solution by volumetric ratio. Before starting the standard battery application, slurry materials were pre-treated for 6h at 400°C. First vol. 5% of slurry was added into negative electrolyte and a charge-discharge cycle was applied on the tubular battery. Then vol. 5% of slurry was mixed on positive electrode and another charge-discharge cycle was applied on the battery. In every time vol. 5% more slurry was added

into electrolyte and after each slurry addition, a charge-discharge procedure was applied to be able to observe the development on current density of tubular MEA.

As it is mentioned during the previous title (§3.1.4), the software of the potentiostat/galvanostat was set to collect time (s), voltage (V), current (A), charge (C) and power (W) values automatically. According to these values energy efficiency, voltage efficiency, coulombic efficiency, charge capacities and energy& power densities were calculated. Efficiency equations can be seen from Table 3.2.

Finally, the self-discharge of the battery was evaluated by tracking the open circuit voltage decrease in time of a fully charged battery. All data were collected until open circuit voltage dropped below 0.8 V to the discharge state of the battery.

4. Results and discussion

4.1 Membrane Development

The blended membranes were successfully prepared according to method, which explained in the experimental part of this chapter. Blends that had higher SPEEK concentration than 80 % were dissolved completely and formed smooth blended polymers. The one with the highest weight ratio of PANI (80-20% SPEEK/PANI) was jellified during the mixing process of the polymers. It is previously reported; increasing amount of the PANI concentration in the polymer mixtures causes gelation [60]. De-gelling agent (Totally 6 wt. 4-methyl piperidine) was used to maintain a non-gellified polymer solution. Nevertheless some amount of the polymer blend had still gel parts. Same procedure was applied on the remaining (non-gellified) part of the polymer blend. After all other production processes some small defects on the membranes were detected. But these defects were found on almost every blend. Therefore it is concluded that, this defects were not due to formation of the gel. One possible reason that the membranes have these defects is not having a perfectly cleaned glass plates or casting knives. Some of the membranes on the glass plates can be seen from Figure 4.1.

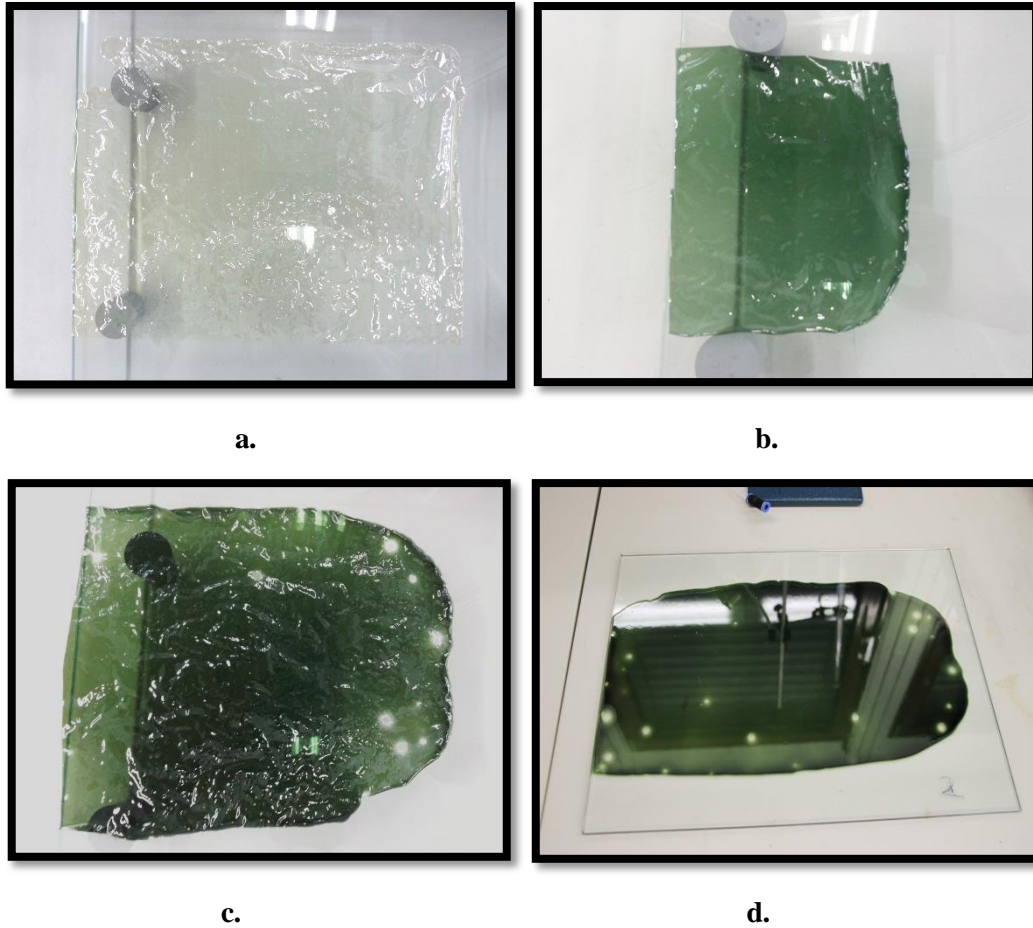


Figure 4.1 a. SPEEK-E600 (100/0) b. SPEEK-E600/PANI = 98/2 c. SPEEK-E600/PANI = 95/5 d. SPEEK-E600/PANI = 80/20

4.1.1 Membrane properties

The swelling, water uptake, ion exchange capacity (IEC), proton conductivity and $V(IV)$ diffusion coefficient results for two pure SPEEK unblended membranes (SPEEK-E600 and SPEEK-E700) with different sulfonation degrees and for SPEEK-E600/PANI blends are listed in Table 4.1. Also own and literature results are added for reference materials: Nafion 112 and Nafion 117 respectively.

Table 4.1 Experimental results for swelling degree, water uptake, proton exchange capacity, proton conductivity and vanadium diffusion coefficient for the membranes characterized at room conditions.

	Swelling degree (%)	Water uptake (%)	Ion exchange capacity (mmol g ⁻¹)	Proton Conductivity (mS cm ⁻¹)	V4+ diffusion coefficient x 10 ⁷ (cm ² min ⁻¹)
SPEEK-E600	6.66	27.63	1.50 ± 0.06	71.12 ± 7.24	6.88 ± 0.70
SPEEK-E600/PANI = 98/2	6.74	26.88	1.58 ± 0.02	59.86 ± 7.41	4.00 ± 1.45
SPEEK-E600/PANI = 95/5	5.52	26.65	1.54 ± 0.01	57.27 ± 4.74	3.25 ± 0.54
SPEEK-E600/PANI = 80/20	5.56	20.99	1.44 ± 0.01	54.15 ± 4.67	2.67 ± 0.51
SPEEK-E700	7.26	24.80	1.33 ± 0.01	40.28 ± 2.66	1.21 ± 0.53
Nafion 112	6.83	13.94	0.97 ± 0.11	81.51 ± 0.27	15.9 ± 0.43
Nafion 117*	11.00	14	0.91	83	16.7**

*data taken from [1].

** data taken from [40]

All the results listed in Table 4.1 for Nafion 112 are experimentally determined in our work and are in accordance with literature data for Nafion 117 [64]. Considering that the only difference between Nafion 112 and Nafion 117 is the membrane thickness (50 μm and 175 μm respectively), we prove the reliability of our testing equipment and experimental methodology.

As expected, for SPEEK membranes, the swelling degree and water uptake depend on the sulfonation degree (SD) of the starting polymer. The SD is reflected by the IEC. Membranes made from SPEEK-E600 have a higher IEC than membranes made from SPEEK-E700 and thus a higher swelling degree and water uptake. A higher sulfonated PEEK is more hydrophilic and therefore it is expected to have higher water uptake in the polymer matrix. The SD can be calculated from the ratio between the molecular weight of the polymer repeating unit and the IEC. All the sulfonic groups are not necessary active for the ion exchange, thus the real SD can be slightly higher. The calculated SD for SPEEK-E600 and for SPEEK-E700 is of 46 and 41 % respectively. Sulfonated PEEK with similar SD was reported not to form stable membranes due to solubility in water [65].

Both membranes have a higher IEC than Nafion 112, therefore a higher swelling degree and water uptake is expected. It can be seen from Table 4.1, that water uptake values of the SPEEK and PANI blended membranes are slightly higher than Nafion 112 membranes, but swelling degree values of the membranes are almost same as Nafion 112 membranes. The measuring method of the swelling ratio was not literally reliable, due to the fact that the membrane surfaces were considerably bended, which made the measurements problematic and untrustworthy. Still we can conclude that, swelling ratio of Nafion 112 and the other membranes are comparable with Nafion 117.

Blending PANI with SPEEK-E600 up to 80/20 wt. ratios does not produce a significant decrease in the ion exchange capacity, while the swelling degree and water uptake values are decreased. The IEC of the SPEEK-E600 membrane is 1.50 mmol/g. For SPEEK/PANI 98/2 and 95/5 membranes, the values are slightly larger, 1.58 and 1.54 mmol/g respectively; for the 80-20 membrane, IEC is just smaller, 1.44 mmol/g. Increase on the SPEEK/PANI 98/2 and 95/5 membranes can be clarified with the experimental errors. A decline on the IEC was expected as it can be seen between SPEEK-E600 and SPEEK-E600/PANI = 80/20 membranes. The observed decrease of IEC is most probably a result of the crosslinking between imine groups in emeraldine PANI and sulfonic groups in SPEEK. Some parts of the sulfonic groups are consumed in the crosslinking reaction with PANI. Thus it is ordinary to have less ion exchangeable ions than SPEEK-E600 membrane. On the other hand IEC value of the SPEEK-E700 membranes are considerably low, 1.33 mmol/g. This decline of the IEC was explained before with the SD of the membranes.

Nafion type polymers have higher proton conductivity than SPEEK type membranes, because of the good conductive ability of the Teflon backboned polymer [43]. As it can be seen from table 4.1, proton conductivity of the SPEEK-E600 is 71 mS/cm² and it is comparably lower than Nafion 112 membrane, which has 81.51 mS/cm² proton conductivity. The proton conductivities of the blended membranes were encountered a decline compared with the E600 SPEEK membrane. It decreases with the increasing amount of the PANI in the blends, due to the loss of some sulfonated groups during the

protonation of the blend. SPEEK-E700 membranes showed slightly lower proton conductivities than the other membranes.

For the application of PEM in Vanadium RFB, lower crossover rate of vanadium species is a desired property which would indicate longer self-discharge of the battery. The diffusion coefficient of V (IV) across Nafion 112 membrane is $12.40 \text{ cm}^2/\text{min}$. Through blend of PANI, the diffusion coefficients are reduced for E600 SPEEK membrane from $6.88 \text{ cm}^2/\text{min}$ to $2.67 \text{ cm}^2/\text{min}$. It can be seen from the Table 4.1 that the diffusion coefficient of V (IV) decreases with higher amounts of PANI. The reduced vanadium crossover rate is a result of tighter crosslinking between PANI and sulfonic groups of SPEEK.

4.1.2 Chemical Stability of Membranes

Chemical stability of membranes was investigated with the data of V (IV) concentration produced in the V (V) solution. The equation between the concentration and the absorbance of the V (IV) ions are evaluated with a calibration curve. The calibration graph can be seen from Figure 4.2. A linear equation was derived from the data of this graph and it can be seen from Equation 4.1.

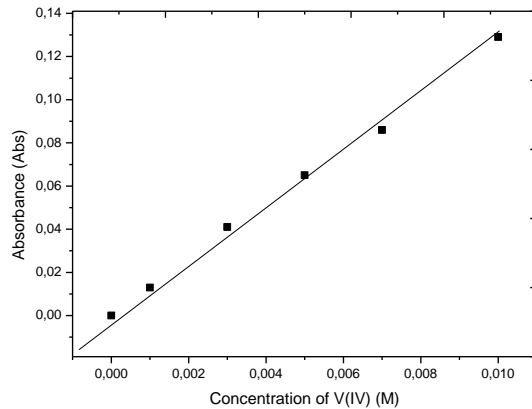


Figure 4.2 Calibration graph for chemical stability measurement

$$\text{Absorbance} = 12.70 \times \text{Concentration of V(IV)} \quad (4.1)$$

The chemical stability of membranes was tested by immersion of membranes in 1 M V (V) solution. Figure 4.3 shows the concentration increase of V (IV) ions when membranes were placed in 1 M V (V) solution at room temperature. The highly oxidative V (V) ions generated at the positive side of battery during charging are generally thought to cause the degradation of membranes, and consequently performance deterioration of battery [42]. When membranes were exposed to V (V) solution, the oxidation of membrane polymer material was accompanied by reduction of V (V) to V (IV). So, the concentration increase of V (IV) is indicative of the oxidation rate of the membranes. Another method of measuring chemical stability for PEM membranes was reported by T. Mohammadi and M.S.Kazacos [66]. Our method is a static method, which only includes immersion of membranes in V(V) solution. But when it is considered, membranes do not contact with the V(V) solution all the time during the operation of a V-RFB. Only full contact occurs, when the battery is entirely charged. According to T. Mohammadi [66] more dynamic method, which includes real working standards of the V-RFB, provides more accurate chemical stability data.

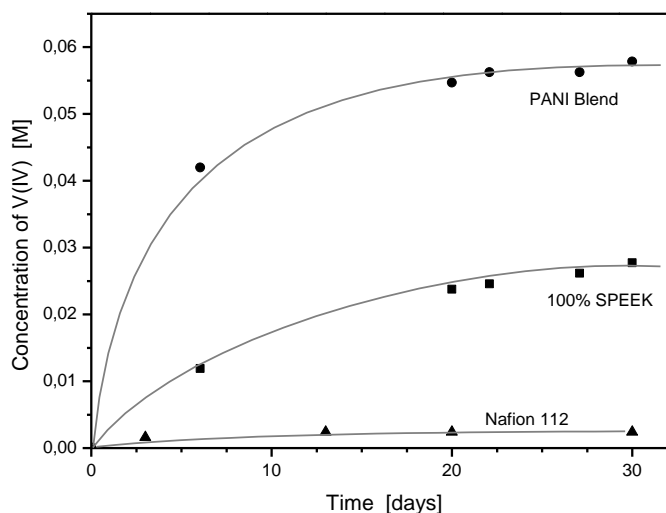


Figure 4.3 Concentration increase of V(IV) with time in acidic vanadium solutions immersed with membranes at room temperature. The initial concentration of acidic vanadium solution is 1 M V(V), 2.5 M H_2SO_4 .

For both the SPEEK-E600 and SPEEK-E600/PANI = 80-20 membranes, the V(IV) concentrations increased quickly during the beginning 7 days; after around 3 weeks the V(IV) concentrations increased slowly and leveled off thereafter, which indicated possible equilibrium state. The higher V(V) production rate at the beginning and higher equilibrium concentration of SPEEK-E600/PANI = 80-20 membrane compared with the SPEEK-E600 membrane after 30 days long-term immersion test are resulted from the presence of PANI in the blend. It was reported that PANI layer coated on surface of Nafion would be dissolved in 0.1 M V(V) solutions within 7 days [49]. However, different from PANI surface layer which would impose intensive direct contact of V (V) ions in solution to thin surface layer, blend method creates PANI-sulfonic group interaction throughout the whole cross-section of the membrane and stronger oxidation-resistant behavior would be expected. As shown in Figure 4.3, the equilibrium V(IV) concentrations for the SPEEK-E600 and SPEEK-E600/PANI = 80-20 membranes after around 3 weeks imply no obvious further oxidation of membrane materials. On the other hand, only 5.6% and 2.6% V(V) ions were reduced after 30 days of test. Chemical

stability samples (100 % SPEEK and 80-20% SPEEK/PANI) in V(V) solution visuals can be seen from Figure 4.4. According to these images it is clearly obvious that after 30 days blended membranes caused V(IV) formation in V(V) solution. Mohammadi *et al.* [66] performed long-term test with membranes immersed in 0.1 M V(V) for 60 days, in which the concentration increase of V(IV) ions were almost linear with time for the cation exchange CMV membranes (Asahi Glass Co., Japan) during the 60 days.

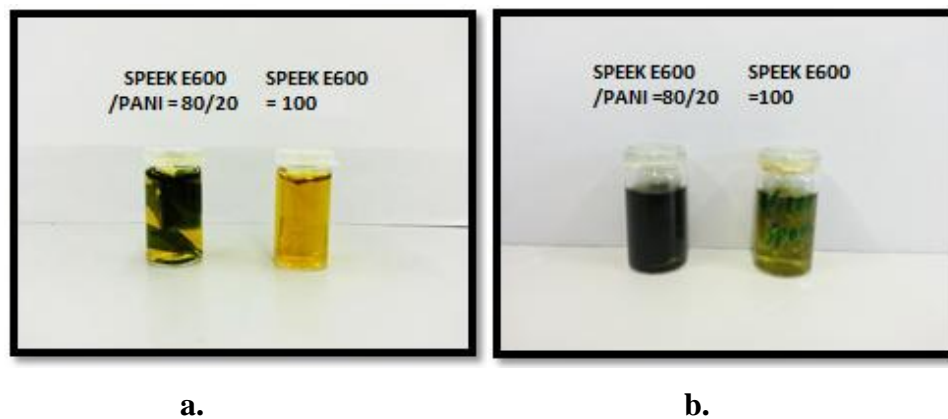


Figure 4.4 a. Newly immersed membrane samples in V (V) solution **b.** Membrane samples immersed in V (V) for 30 days

For some reported ion exchange membrane materials, such as sulfonated polysulfone(Radel®), sulfonated poly(fluorenyl ether ketone), sulfonated poly(arylene thioether)s and quaternary ammonium functionalized poly(fluorenyl ether), none of these membranes can survive when immersed in 1 M V(V) + 2 M H₂SO₄ solutions for 3 days at 40 °C [67]. Investigation of the degradation of S-Radel had shown that the membranes in 0.1 and 1.7 M V(V) + 5.0 total sulfate solutions in detail. Besides the production of V(IV) in solution, the S-Radel membranes broke into small pieces in both 0.1 and 1.7 M V(V) solutions, and the breakage was more severe in 1.7 M V(V) solution. This breakage of membranes was proposed to be a result of chain scission and was confirmed by the viscosity analysis of S-Radel membrane after immersion test [67]. However, in this investigation, both the SPEEK-E600 and blend membranes remained contact and flexible after immersion test in 1 M V(V) solutions at room temperature for

30 days. From this long-term *ex-situ* chemical stability evaluation of the SPEEK-E600 and SPEEK-E600/PANI = 80-20 membranes, it can be concluded that even though there is some oxidation of the two membranes by high concentration V(V) ions as is a common problem for hydrocarbon based polymer membranes, the two membranes still show promising potential during *in-situ* battery operation.

4.1.3 Single Battery Performance

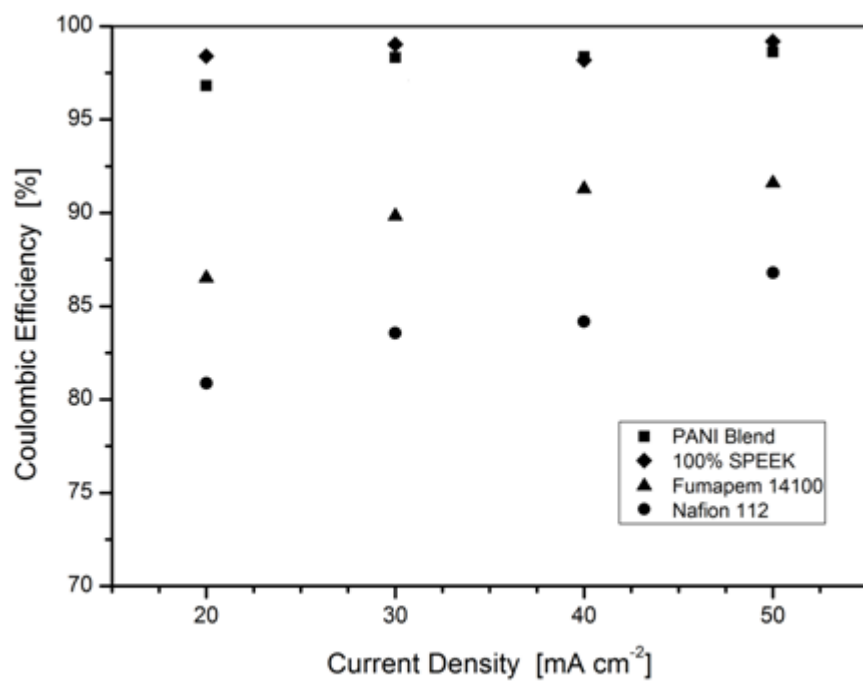
A rectangular and a circular redox flow battery were constructed as it mentioned in experimental part. There was an obvious leakage during the rectangular RFB construction with graphite plates. It was concluded that leakage occurred across the graphite plate's pores. Therefore new non-liquid-permeable epoxy impregnated graphite plates ordered and a circular RFB was constructed with these new plates.

Table 4.2 Battery efficiencies of different membranes at a current density of 40 mA cm⁻²

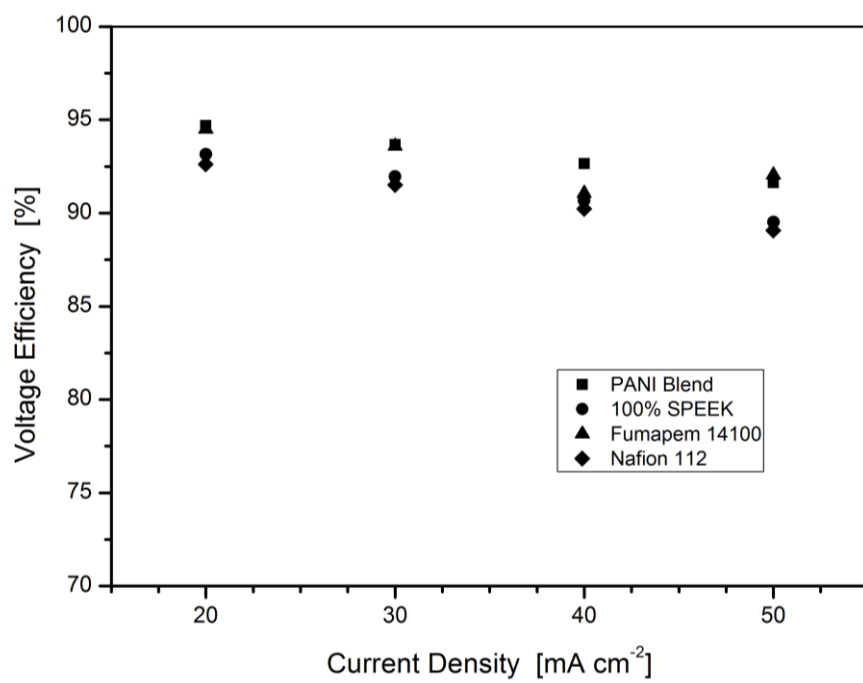
Membranes	Coulombic Efficiency %	Voltage Efficiency %	Energy Efficiency %
SPEEK-E600	98.18	90.67	89.01
SPEEK-E600/PANI= 80/20	98.43	92.76	91.31
Fumapem 14100	91.30	90.23	82.38
Nafion 112	85.41	90.98	77.70
Nafion 117*	93.8	90.7	85.0

*data taken from [40].

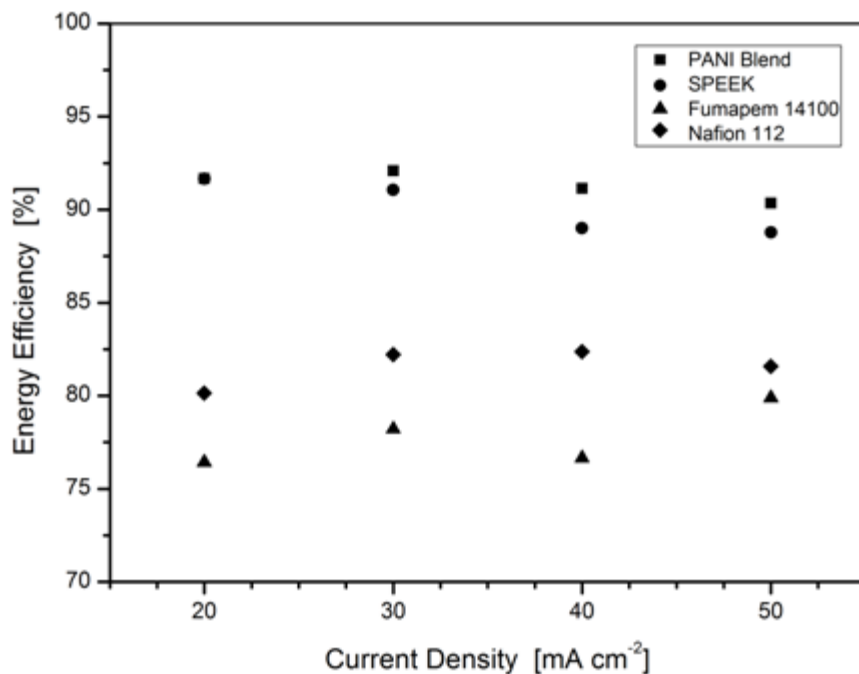
The performance of vanadium redox flow battery assembled with different membranes was evaluated with three parameters: Coulombic efficiency (CE), voltage efficiency (VE) and energy efficiency (EE). The batteries were both charged and discharged at a current density of 40 mA cm^{-2} and the efficiencies were listed in Table 4.2. The Coulombic efficiencies with SPEEK-E600 and SPEEK-E600/PANI= 80/20 membranes are 98.18% and 98.43%, respectively. These very high Coulombic efficiencies indicate low cross-over rate of vanadium species during battery charging and discharging, and this is implied by the low values of determined V(IV) cross-over rates in diffusion test for SPEEK-E600 and SPEEK-E600/PANI= 80/20 membranes (Table 4.1). As also indicated by the high V(IV) cross-over rate shown in Table 4.1, the Coulombic efficiency of battery with benchmark Nafion 112 membrane is only 85.41%, much lower than those obtained with SPEEK-E600 and SPEEK-E600/PANI= 80/20 membranes. The voltage efficiency of battery with ion exchange membranes is determined to a large extent by the internal electrical resistance, of which electrical resistance of membranes constitutes most. For all the membranes, high voltage efficiencies of around 90% are achieved. The area resistances of SPEEK-E600, SPEEK-E600/PANI= 80/20 and Nafion 112 membranes calculated from data in Table 4.1 are 0.58, 0.68 and $0.62 \Omega \text{ cm}^2$, respectively. Though SPEEK-E600 and SPEEK-E600/PANI= 80/20 membranes are less conductive than Nafion 112, but thinner membranes with enough mechanical strength can be used. Nafion 112 membrane that has high conductivity and also relatively high swelling degree has a wet thickness of $61 \mu\text{m}$. To avoid serious vanadium cross-over and ensure mechanical strength of membranes used in this flow battery, too thin Nafion membrane is not suggested. In this study, the low swelling degree of SPEEK-E600 and SPEEK-E600/PANI= 80/20 membranes allows employment of thinner membranes to be used in the battery. Because of higher Coulombic efficiencies and similar voltage efficiencies of SPEEK-E600 and SPEEK-E600/PANI= 80/20 membranes compared with Nafion 112, there is large improvement ($\sim 12\%$) of the energy efficiencies for the batteries with these two membranes as shown in Table 4.2.



(a)



(b)

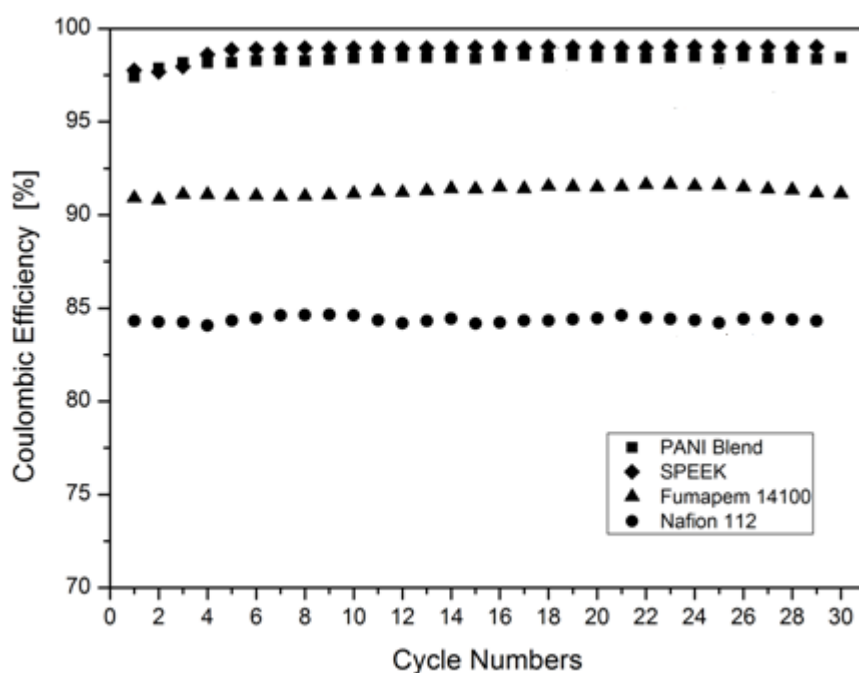


(c)

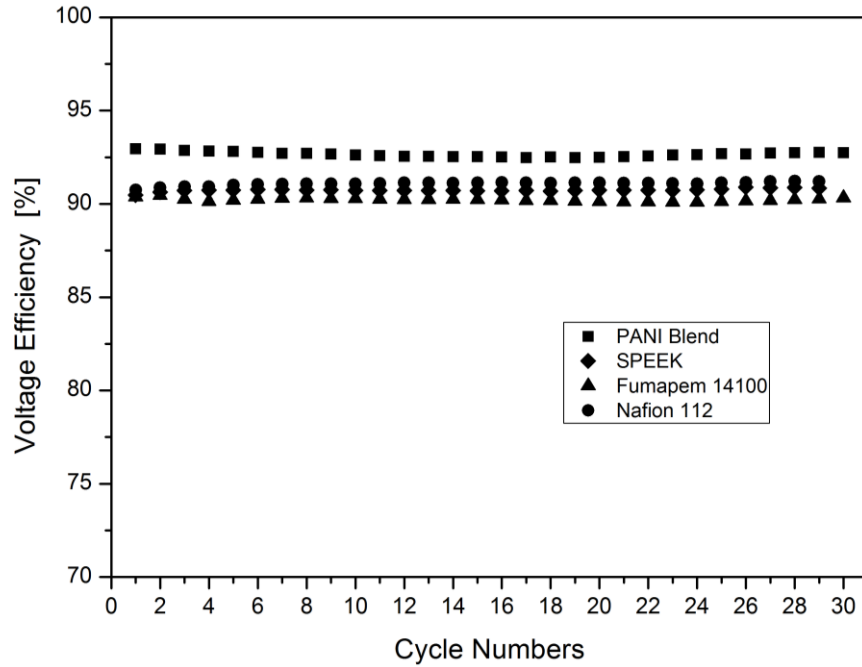
Figure 4.5 a. CE, b. VE, c.EE of batteries with SPEEK-E600/PANI= 80/20 membrane(■), SPEEK-E600 membrane(●), Nafion 112(◆) and Fumapem 14100 membrane (▲) at current densities of 20, 30, 40 and 50 mA cm⁻²

To characterize the influence of current density, V-RFB batteries with different membranes were discharged at different current densities. Figure 4.5 shows the efficiencies of batteries at different discharging current densities, and all the charge was performed at a constant current density of 40 mA cm⁻². In Figure 4.5(a), Coulombic efficiencies of Nafion 112 increase with current density. This is because of relative short discharge time when the discharging current density is high. Since the vanadium cross-over rate is very low for SPEEK-E600 and SPEEK-E600/PANI= 80/20 membranes, even at such small discharging current density as 20 mA cm⁻² for SPEEK-E600/PANI= 80/20 membrane, the Coulombic efficiency remain 96.8%. This value is close to 98.6% for this membrane at the current density of 50 mA cm⁻². As expected, the voltage efficiencies of three batteries depicted in Figure 4.5(b) all decrease when the current density increases, due to the ohmic polarization resulted from the battery internal resistance. Since thinner SPEEK-E600 and blend membranes with adequate mechanical

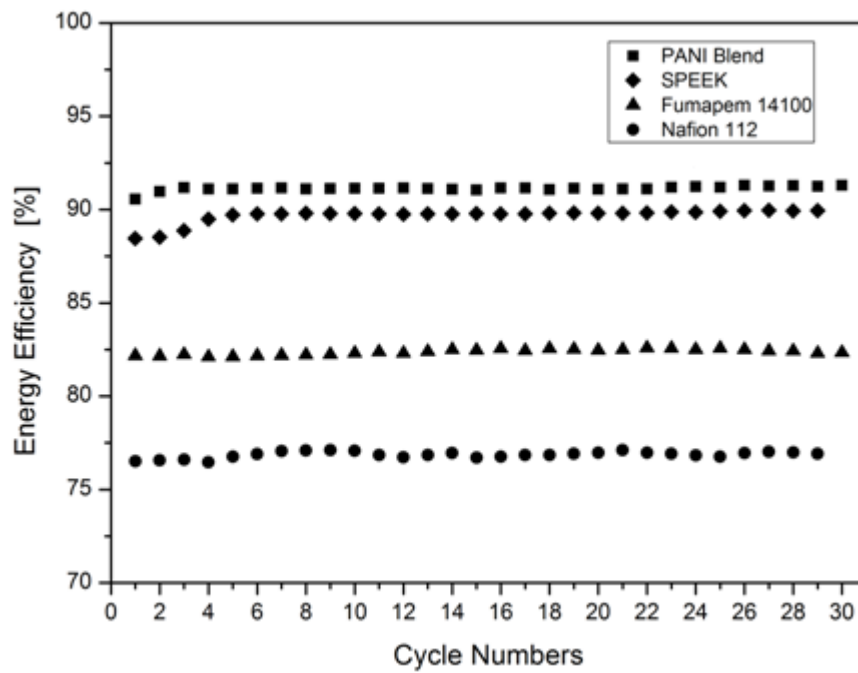
strength can be applied, the common disadvantage of lower proton conductivity for hydro-carbon based membranes compared with Nafion can be mitigated. As a result of higher Coulombic efficiencies and comparable voltage efficiencies, the overall energy efficiencies of batteries with SPEEK-E600 and SPEEK-E600/PANI= 80/20 membranes are much higher than those of Nafion 112 under all the investigated current densities, as shown in Figure 4.5(c). For both the SPEEK-E600 and SPEEK-E600/PANI= 80/20 membranes, energy efficiencies of around 90% at the current density of 50 mA cm^{-2} are higher compared with data reported in literature[40], [42].



(a)



(b)



(c)

Figure 4.6 a. CE, b. VE, c.EE of batteries with different membranes during charge-discharge cycles (The charge and discharge current densities are both 40 mA cm^{-2} .)

The *in-situ* stability of membranes was investigated in charge-discharge cycles of V-RFB battery. The battery performance was also expressed in terms of three efficiencies as depicted in Figure 4.6. The CE, VE of batteries with SPEEK-E600 and SPEEK-E600/PANI= 80/20 membranes were as stable throughout the 30 cycles as those for Nafion 112. Higher Coulombic efficiencies and comparable voltage efficiencies are maintained for batteries with SPEEK-E600 and SPEEK-E600/PANI= 80/20 membranes. In this investigation, after the charge-discharge cycles, the SPEEK-E600 and SPEEK-E600/PANI= 80/20 membranes were still in good shape and remained mechanically intact. These results demonstrate the *in-situ* stability of SPEEK-E600 and SPEEK-E600/PANI= 80/20 membranes in dynamic charge and discharge operation of batteries, and shows good prospect for long-term application of these membranes in V-RFB.

V-RFB capacity loss during the 30 cycles was investigated with 40 mA/cm² current density. Total discharge current of the battery was followed. Figure 4.7 shows discharge capacity loss of the SPEEK-E600, SPEEK-E600/PANI= 80/20, Fumapem 14100 and Nafion 112 membranes. After 30 cycles almost 5 % capacity loss was detected for SPEEK-E600 membrane, 10 % for Fumapem 14100 membrane, almost 20 % for both SPEEK-E600/PANI= 80/20 and Nafion 112 membranes. First reason to have a capacity loss is imbalance of Vanadium ions, caused by crossover through the membrane. Another possible reason is asymmetrical valence of the Vanadium ions [68]. It is stated that especially negative electrolyte utilization decreases with charging higher SOC's (>90 %). Moreover, high SOC that resulting hydrogen evolution in negative electrode is another reason to have accelerated capacity loss. In the light of these facts, it is expected to have lower capacity loss for SPEEK-E600 membranes than Nafion 112 and Fumapem 14100 membranes. The other fact is SPEEK-E600/PANI= 80/20 membranes showed higher capacity loss than SPEEK-E600 membranes. It can be explained with the chemical degradation of the PANI. Degradation was occurred gradually during the charge and discharge, thus the capacity in each cycle decreased.

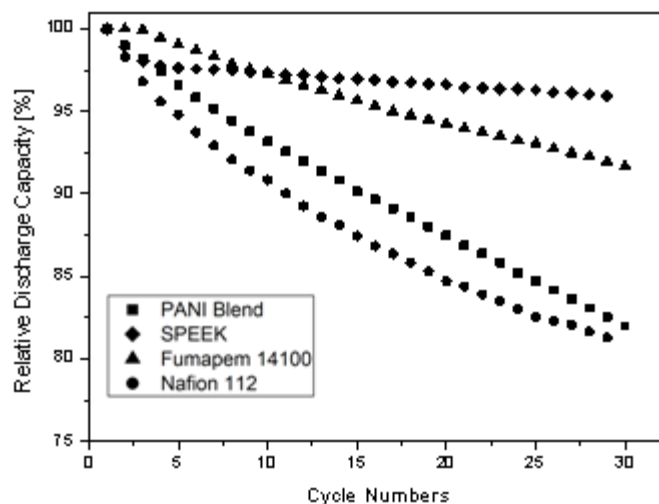


Figure 4.7 Discharge capacity loss graph

The open circuit potential (OCP) was monitored to observe the self-discharge rate of V-RFB batteries. Figure 4.8 shows the results of V-RFB batteries with different membranes. The batteries were charged to 100% state of charge (SOC) and then the OCV decrease with time was followed. As can be seen, the OCV of Nafion 112 drops quickly and only after 9 hours the voltage is below 0.8 V, which corresponds to SOC of 0%. Compared with Nafion 112, the self-discharge rate of V-RFB with SPEEK-E600 and SPEEK-E600/PANI= 80/20 membranes is much slower, as the OCV sustains above 0.8 V around 120 and 132 hours for SPEEK-E600 and SPEEK-E600/PANI= 80/20, respectively. Slow cross-over rate of vanadium ions through the membranes results in longer self-discharge time and higher Coulombic efficiency. The longer self-discharge time of batteries with these two membranes is consistent with the determined cross-over rate of V(IV) ions across different membranes in Table 4.1. This result demonstrates that by employing membranes based on hydrocarbon polymer SPEEK-E600, the self-discharge rate of V-RFB battery could be reduced a great deal; with SPEEK-E600/PANI blend, the self-discharge rate could be reduced further.

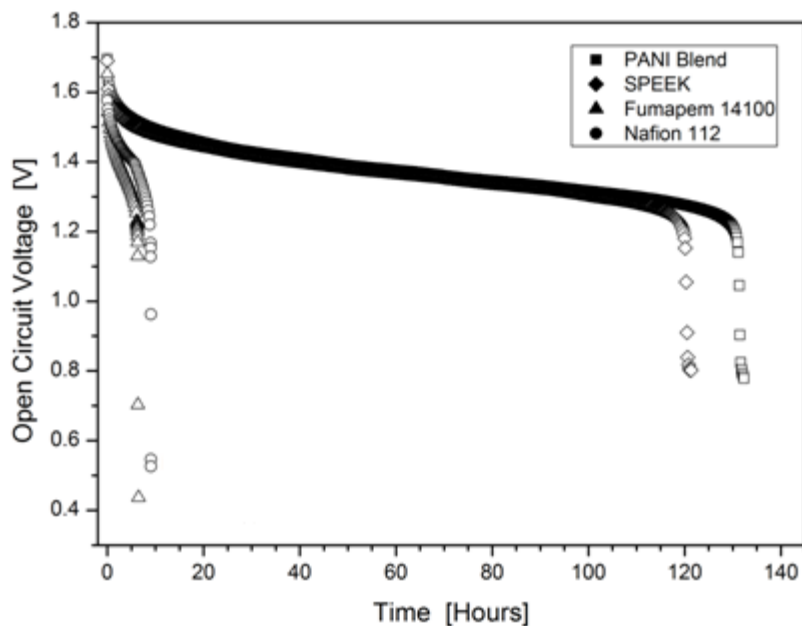


Figure 4.8 Open circuit voltage of V-RFB batteries with different membranes.

4.2 Tubular Module Development

All electrode materials were purchased or produced successfully as it is mentioned in part §3.2. Produced electrodes, such as CNT and Titanium macrotubes were investigated with FeSEM device to observe outer and inner surface of the electrodes.

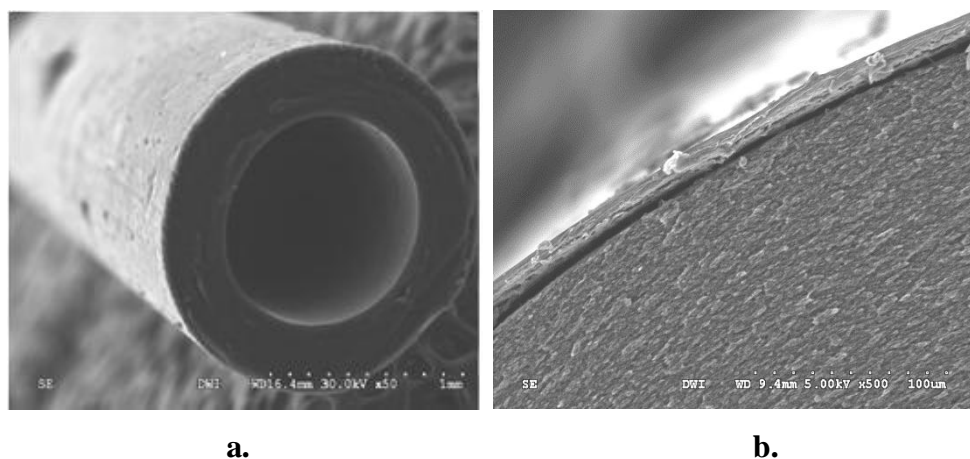
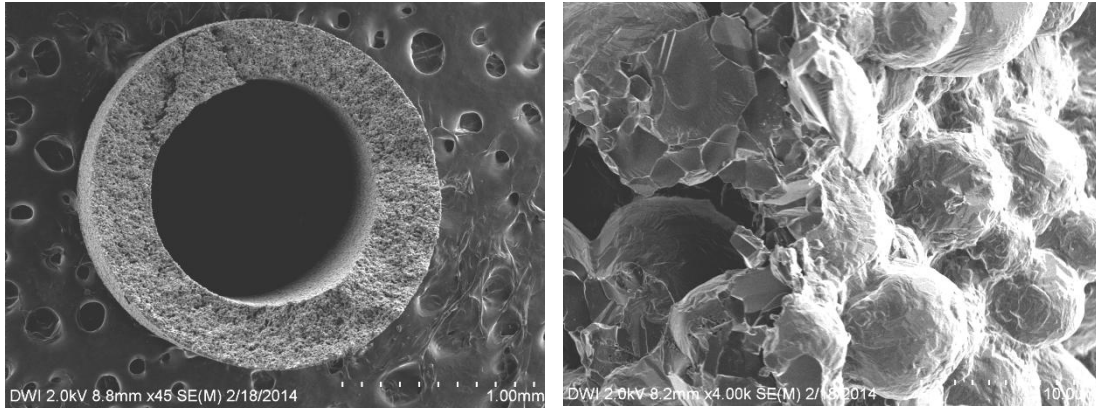


Figure 4.9 FeSEM images of Carbon Nanotubes (CNTs) – 50x **a.** Perspective view **b.** Cross-sectional view with membrane

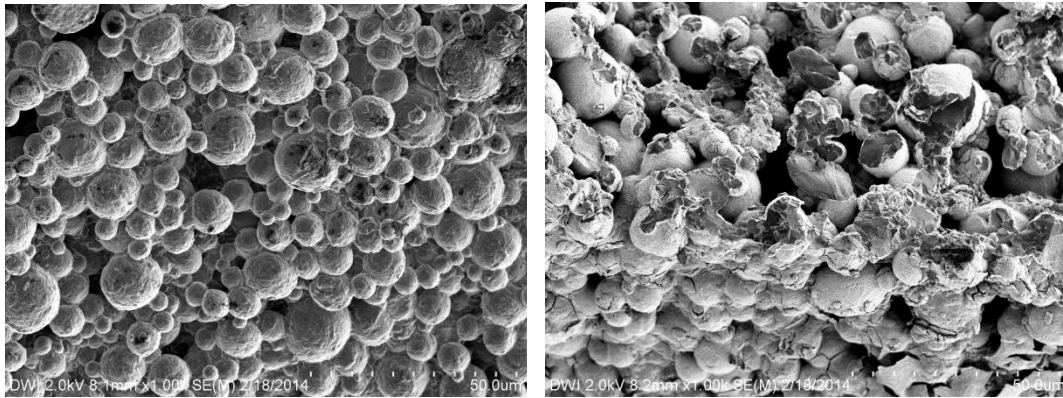
Figure 4.9 shows FeSEM images of dense structured CNT tubes, which were used in tubular module construction. Polymer membrane layer, which was dip-coated, can be seen from figure 4.9 (b). The cracks in the membrane structure were occurred during the preparation of SEM sample.

Figure 4.10 shows FeSEM images of preparation of titanium macrotubes, which includes non-treated tubes, acid treated tubes, catalyst coated tubes and membrane coated tubes. Highly porous titanium macrotubes, which would provide high conduction area, can be seen from Figure 4.10 (a). Closer view of the surface layer is presented at Figure 4.10 (b). The acid pre-treatment with 6 M HCl was successfully applied on the titanium materials. The tubes were cracked after 2.5 minutes acid treatment and after 4 minutes they were dissolved in acid. Thus, immersion time in acid was decided as 2 minutes. The effect of acid pre-treatment can be observed by the difference between Figure 4.10 (b) and (c). The impurities on the titanium particles, such as TiN and TiO₂, were removed by the acid treatment. After this stage, tubes were painted with Pt/Ir (wt. 70/30) catalyst and the load of Pt/Ir can be seen from Figure 4.10 (d). 7 mg/cm² catalyst load on Ti tube was accomplished according to the weight measurements after 10 times of Pt/Ir treatment. Finally membrane dip coating was applied and successfully thin layer of polymer membrane was coated on titanium tubes. Layer of membrane is shown in Figure 4.10 (e).



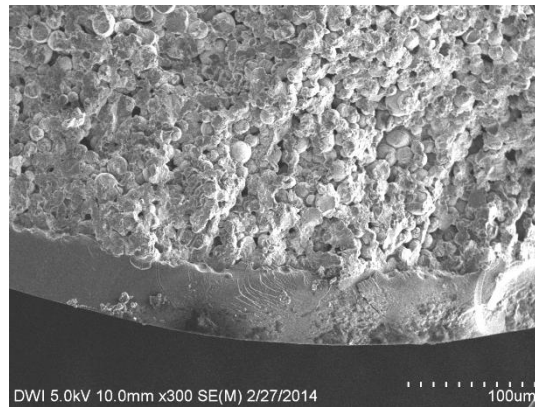
a.

b.



c.

d.



e.

Figure 4.10 FeSEM images of titanium macrotubes **a.** Non-pretreated tubes, cross-sectional view **b.** Non-pretreated tubes, outer surface **c.** Pre-treated tubes, outer surface **d.** Pt/Ir coated tubes, outer surface **e.** Membrane coated tubes, cross-sectional view

4.2.1 Battery Performances

Charge and discharge results of each MEA were presented below.

CNT-Carbon Fibers

Construction of CNT electrodes with carbon fibers was completed successfully. Charge of the battery was maintained with constant potential, 1.7V. However, the current that generated during the charge was extremely low, so that charge could never be completed. The reason behind this fact could be explained with the poor conductive area between carbon fibers and titanium wire. Moreover, inner conductivity of CNTs was low too. Therefore, generated electricity could not be stored inside the electrolyte.

CNT-Titanium Fleece

Successfully constructed CNT-Titanium fleece MEA was firstly charged at constant potential, 1.7V. During the charge, excess amount of gas evolution was observed at positive side of the battery. Therefore, the voltage was decreased to 1.5, 1.4, 1.3 and 1.2 V respectively. Still, decreased voltage did not affect gas evolution; even the potential was 1.2V, which there could be no oxygen evolution by electrolysis. Thus, it was concluded that the hydrogen was produced by electrolysis at CNT. Despite the fact that CNT electrode was the inner electrode (negative electrode) in MEA, the hydrogen gases was observed at outer (positive) electrolyte vessel. This could only mean that membrane layer on the CNT did not worked during the charge. Hydrogen gases transferred to the positive side of the battery. Nevertheless, a charge was completed, although there was gas evolution. Charge was obtained with constant voltage, 1.5V and resulting currents were collected until battery had reached the charged state. Figure 4.11 states charging graph of the tubular CNT-Ti fleece MEA. Especially positive electrolyte was charged almost 100 %, which was understood by the clear yellow color of positive electrolyte. On the other side, negative electrolyte was still dark green, which means it was not

completely charged. Thus, it was concluded that, titanium coated Pt/Ir catalyst could work effectively as positive electrode in this kind of tubular battery.

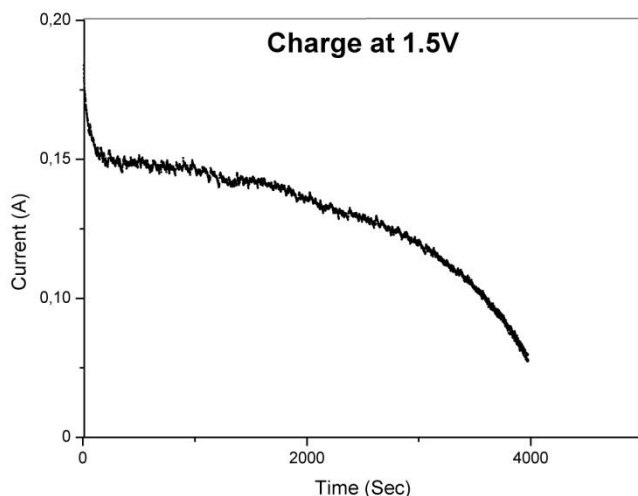


Figure 4.11 Current change graph during the charge at 1.5V

Titanium Macrotube and Epoxy Impregnated Graphite Tube

Tubular battery was constructed as it mentioned before and active electrode area was measured as almost 7 cm^2 . First time charging was done with constant potential, 1.7V. Charge was successfully completed without gas formation and current values are collected until it decreased down to 10 mA, which means the battery was almost fully charged. Charging and discharging graph is stated at Figure 4.12. As it can be seen from graph too, the average charging current is very low, such as 40 mA and therefore, the charging time is extremely long for 20ml of electrolyte solution, such as 27h.

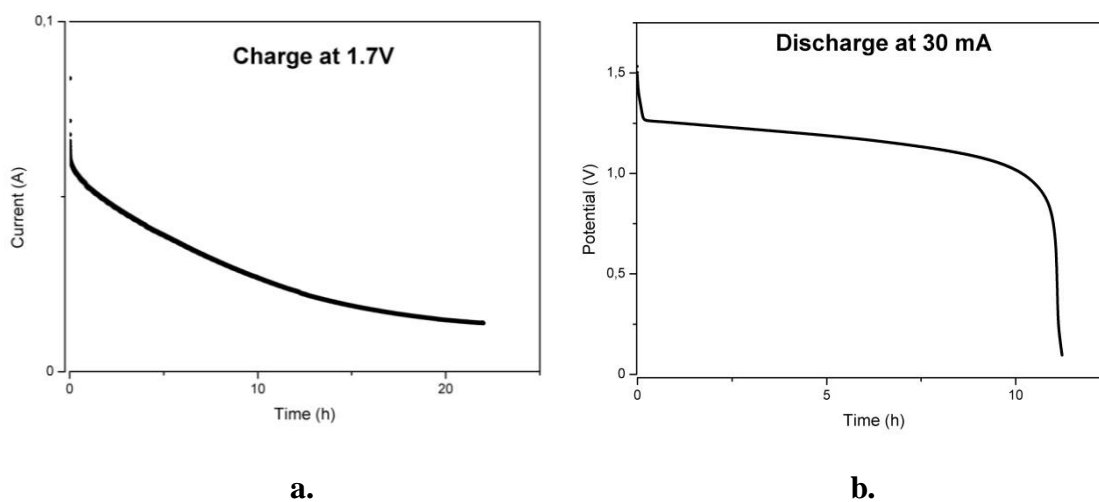


Figure 4.12 a. First Charge at 1.7V, **b.** First Discharge at 30mA

On the other hand, fully charged state was understood by the color change of the solutions. Negative electrolyte, which was V(II), was purple and positive electrolyte, which was V(V), was completely yellow. Fully charged electrolytes can be seen from Figure 4.13.

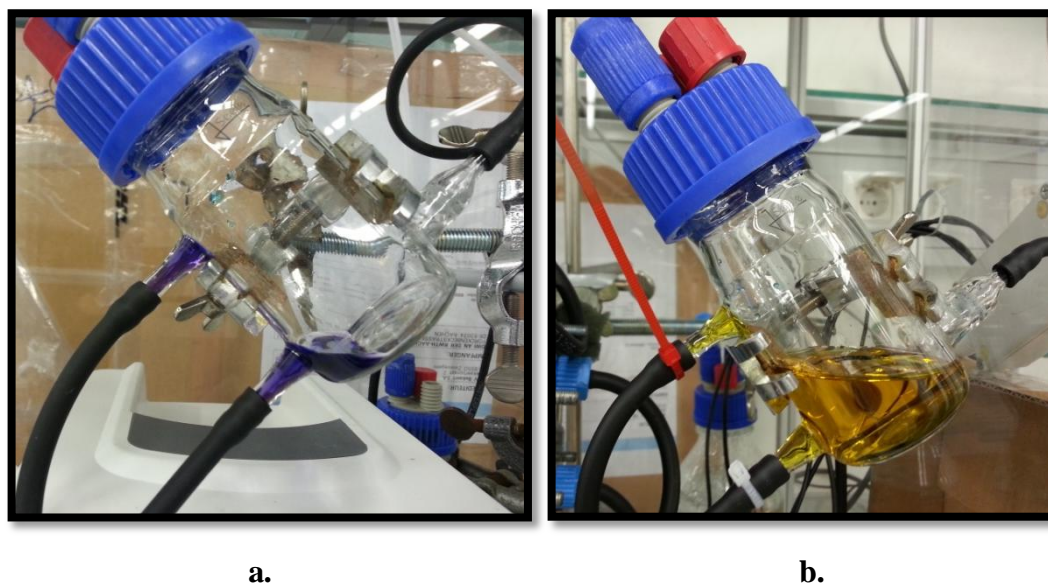


Figure 4.13 a. Negative electrolyte, V(II), **b.** Positive electrolyte, V(V)

After first charge, discharge was applied on the tubular battery. Constant current, 30 mA, was given to the system and cell voltage was detected until it decreases down to 0.8 V, which is generally at the range of safely discharge of V-RFBs [61]. It can be seen from figure 4.12 (b). Average potential was observed around 1.25 V, which is precisely expected.

For the second charge, active carbon was prepared as slurry electrode. Firstly 5% of active carbon was mixed to the negative electrolyte and charge discharge cycle was repeated. Charge and discharge graph of slurry mixed tubular RFB can be seen from Figure 4.14. In addition the comparison of charging statement of non-slurry electrode and 5% slurry electrode is stated in Figure 4.15. During the first 10 hours, where actual charge was in progress, 5% slurry electrode currents are higher than the non-slurry electrode currents.

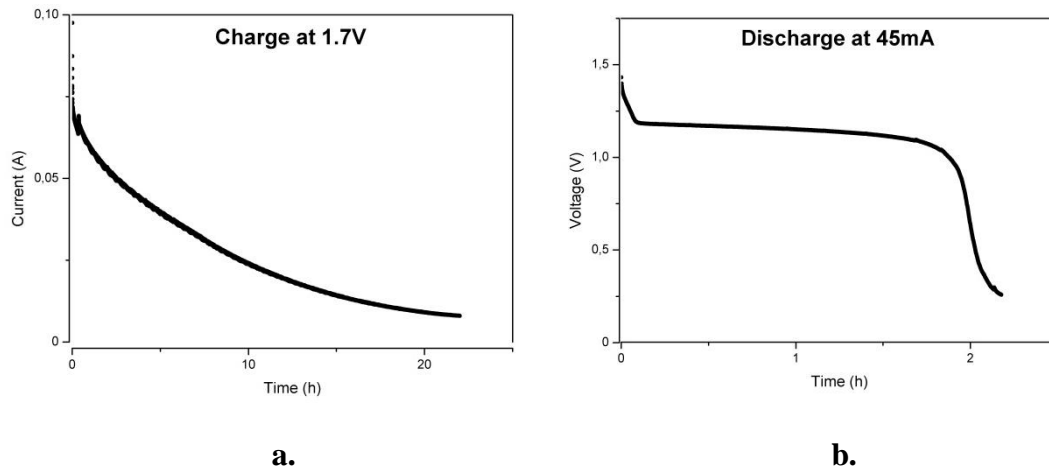


Figure 4.14 a. Charge of 5 % slurry mixed electrolyte, **b.** Discharge of 5 % slurry mixed electrolyte

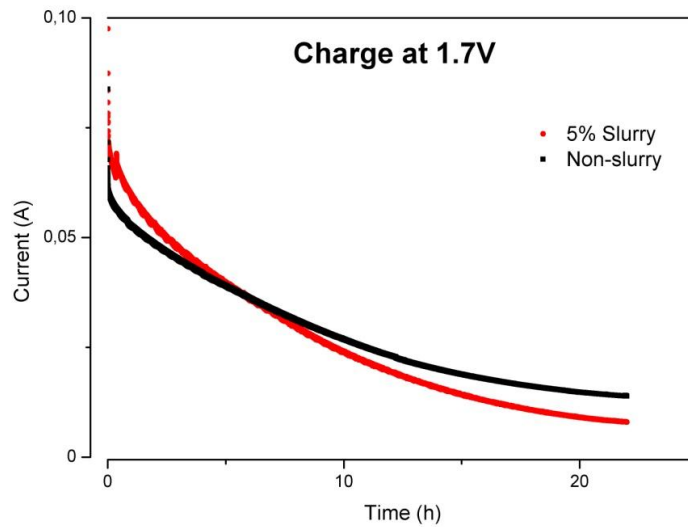


Figure 4.15 Charge with slurry and non-slurry electrode at 1.7V

Table 4.3 states efficiencies and densities of these two battery trials. The maximum achieved current density is still much lower than a standard planar RFB, which was generally around 20-50 mA/cm². During the discharge, there were serious charge losses of the battery. Therefore, the energy efficiency and the columbic efficiency are extremely low. The main reason for this charge loss might be the long charging time. The vanadium crossover was certainly high with these membranes, which was proved at part §4.1. Thus, charge loss was occurred during the long charging and discharging sessions. Furthermore, charge loss caused decrease on energy density too. But still power density found as a bit improved, which could lead that slurry electrode could help to improve the power density of the tubular battery.

Table 4.3 Densities and efficiencies of the tubular RFB

	Current Density, mA/cm²	Energy Density, Wh/L	Power Density, W/L	Energy Efficiency, %	Coulombic Efficiency, %	Voltage Efficiency, %
Non-Slurry	4,6	29.4	2.2	33.3	49.7	67.1
5% Activated Carbon*	8,9	9.7	2.4	10.7	17.5	61.4

*Only in negative electrolyte

As a next step 5 % active carbon was added to the positive electrolyte to see the difference of slurry at each electrode. Before starting to charge, circulation of electrolyte at positive electrode was plugged. The titanium positive electrode was too thin to circulate the slurry electrode. Consequently, active carbon slurry material was given up and another slurry material, graphite powder, which has smaller particle size, was chosen to carry on with the experiment. Figure 4.16 shows the comparison of graphite powder addition to the electrolyte solution.

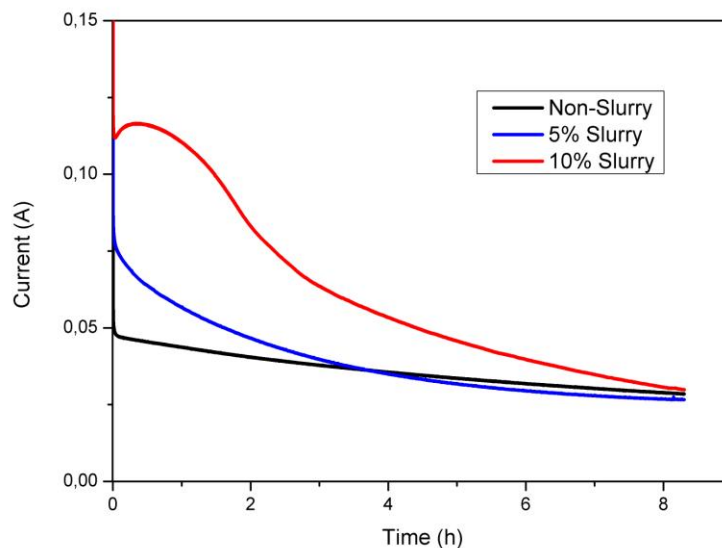


Figure 4.16 Comparison of graphite powder addition to the electrolyte

As it can be seen from this figure too, the slurry addition had improved the currents. The non-slurry electrolyte was carried around 40 mA. Addition of 5 % graphite powder into the electrolyte increased the currents to almost it's twice amount for a certain amount of time. As it is expected the 10% slurry addition had increased the currents again in more certain way, which was started around 120 mA. The affect of the slurry addition to the electrolyte is apparently encouraging. Nevertheless, to reach the same current conductivity potential as a planar redox flow battery, tubular cell should have the same current densities. Table 4.4 indicates the current density improvement by every graphite powder addition. However there is an improvement on current densities, still it is not enough to have same current densities as planar RFB (20-50 mA/cm²). Therefore the slurry addition was going to be increased more, but a false step was carried out during the first pretreatment of the membrane layer on the positive titanium electrodes. This led us to that all experiments with graphite powder were not held with standard electrodes as before. However, the improvements of the slurry electrodes are undeniable as the collected currents were increased.

Table 4.4 Current density improvement of graphite addition in electrolyte

	Non-Slurry	5% Slurry	10% Slurry
Current Density, mA/cm²	4.6	7.8	10.2

5. Conclusions

5.1 Membrane Development

New SPEEK/PANI blended membranes for V-RFB applications were successfully produced with different weight ratios. Crosslinking of two materials were accomplished until higher weight ratios of PANI. Significant performance improvements were obtained with SPEEK E600 membranes when compared to the commercialized Nafion membranes. Furthermore, addition of PANI polymer into the blend had showed tighter polymer matrix, thus higher selectivity between H^+/V ions. As it is suggested, lower crossover of vanadium ions were achieved by having more cross-linked polymer matrix. Such as, Nafion membranes had shown almost 3 times more permeability than SPEEK E600 membranes and SPEEK E600 membranes had shown almost 3 times more permeability than SPEEK E600/PANI = 80/20 blended membranes. IEC and proton conductivity of the membranes were also showed suitable results like the increasing amount of the PANI in the blend caused decrease on IEC and proton conductivity. However, lower chemical stability of PANI affected the long-term performance of the cell, because of the high effectiveness of $V(V)$. As well as the well characteristics of the blended membranes, battery performance values, such as energy, coulombic and voltage efficiencies were obtained around optimum values (>90). Moreover OCP performance of the membranes had shown that longer self-discharge might be achieved, even though the blended membranes had poor chemical stability. Considering all these results and in addition the price of the SPEEK polymer is certainly cheaper than Nafion membranes, SPEEK/PANI blended membranes might be perfect for Air-VRFBs, thus for the project Tubulair±. Since there is no $V(V)$ inside an Air-VRFB, the chemical stability of polymer membrane would not be an issue for these batteries. But nevertheless, the low chemical resistance of membranes is a limiting property for the applications of All-VRFBs, which needs to be overcome.

5.2 Tubular Module Development

Electrode materials were obtained successfully and membrane electrode assemblies were constructed with CNT-Carbon Fibers, CNT-Titanium fleece and Graphite-Titanium Macroporous Tubes. The first MEA (CNT-Carbon Fibers) was unsuccessful due to the poor contact area between fibers and current collectors. The second MEA (CNT-Titanium fleece) was successful in only positive electrode which was titanium. There was gas evolution on the negative electrode which was CNT. Therefore, titanium made electrodes were accepted as a suitable positive electrode for Vanadium RFBs. The last MEA (Graphite – Titanium Macroporous Tubes) was successful in both sides. Proper charge and discharge cycles could maintain at both electrodes. After then cyclic analysis were held on the last MEA. The efficiencies of the battery were found lower than usual (<40%), which explained as: even the tubular battery has higher current density with the slurry electrodes, the charge and discharge time is too long. The higher self-discharge rate causes serious energy loss, thus lower battery efficiencies. Moreover these analyses had shown that the current density of the tubular MEA ($\sim 4 \text{ mA/cm}^2$) was low for the standard Vanadium-RFBs ($20\text{-}50 \text{ mA/cm}^2$). As it was planned, a slurry material was added to the electrolyte solution to increase the conductive area of the tubular MEA. Respectively activated carbon and graphite powder was used with increasing weight ratios. Both slurry materials showed positive effect on the currents. The activated carbon particles were larger than graphite powder particles; it caused a blockage inside the macroporous titanium tube. Therefore the experiments were continued with graphite powder. A non-negligible improvement on current density was obtained, even though the electrodes were not properly pre-treated. By using proper electrodes and higher slurry addition, the low current densities can be increased to standard Vanadium RFB current densities.

REFERENCES

- [1] J. F. K. Anne-Marie Borbely, *Distributed Generation: The Power Paradigm for the New Millennium*. CRC Press, **2001**, p. 416.
- [2] M. Armand and J.-M. Tarascon, “Building better batteries.,” *Nature*, vol. 451, no. 7179, pp. 652–7, Feb. **2008**.
- [3] D. D. Supervisor and F. Wallin, “Flow Batteries: Status and Potential,” Mälardalens University, Sweden, **2011**.
- [4] T. E. Enstitüsü, “Türkiye’nin Kurulu Enerji Gücü,” 2013. [Online]. Available: <http://enerjienstitusu.com/turkiye-kurulu-elektrik-enerji-gucu-mw/>. [Accessed: 10-Nov-2014].
- [5] T. E. Enstitüsü, “Elektrik İstatistikleri ve Trendler,” 2013. [Online]. Available: <http://enerjienstitusu.com/avrupa-elektrik-istatistikleri-yenilenebilir-enerji-elektrik-fiyatlari/>. [Accessed: 11-Nov-2014].
- [6] C. University, “Solar Panels in Cambridge.” [Online]. Available: <http://www.cambridge-solar.co.uk/solar-pv-cambridge/>. [Accessed: 15-Nov-2014].
- [7] P. Tsao, “An integrated flywheel energy storage system with homopolar inductor motor/generator and high-frequency drive,” University of California, Berkeley, **2003**.
- [8] A. E. Efficiency, “Thermal Energy Storage,” 2013. [Online]. Available: <http://www.areous.com.au/uncategorized/thermal-energy-storage-how-it-fits-in-with-the-other-energy-storage-systems/>. [Accessed: 08-Jul-2014].
- [9] J. I. S. Martín, I. Zamora, J. J. S. M. V Aperribay, and P. Eguía, “Energy Storage Technologies for Electric Applications,” no. 2, **2011**.
- [10] M. G. Molina, “Dynamic Modelling and Control Design of Advanced Energy Storage for Power System Applications,” in *Dynamic Modelling*, Alison V. ., Intech Co., **2010**, p. 300.
- [11] F. C. Bakewell, *Electric Science: Its History, Phenomena, and Applications*. **1853**, pp. 27–31.
- [12] K. J. Laidler, *The world of physical chemistry*. New York, New York, USA: Oxford University Press, **1995**, pp. 219–220.

- [13] R. V. Kumar and T. Sarakonsri, "Introduction to Electrochemical Cells," in *High Energy Density Lithium Batteries: Materials, Engineering, Applications*, Weinheim: Wiley-VCH Verlag GmbH & Co., **2010**.
- [14] E. J. Cairns, "Batteries, Overview," California, **2004**.
- [15] D. Linden and T. B. Reddy, *HANDBOOK OF BATTERIES*, 3rd ed. New York, New York, USA: McGraw-Hill, **2002**.
- [16] S. Co., "Dual-cell Battery Concept." [Online]. Available: <http://www.superlib.eu/index.php?spid=en&site=preview&id=020000>. [Accessed: 15-Jul-2014].
- [17] B. E. Conway, *Electrochemical Supercapacitors : Scientific Fundamentals and Technological Applications*. Ottawa: Springer Science, **1999**.
- [18] R. Burks, "Supercapacitors: The (near-ish) future of batteries," *Dvice*, 2013. [Online]. Available: <http://www.dvice.com/2013-5-3/supercapacitors-near-ish-future-batteries>. [Accessed: 20-Jul-2014].
- [19] C. Rayment, "Introduction to Fuel Cell Technology," **2003**.
- [20] S. S. Kocha, "Polymer Electrolyte Membrane (PEM) Fuel Cells, Automotive Applications," in *Encyclopedia of Sustainability Science and Technology*, R. A. Meyers, Ed. New York, New York, USA: Springer, **2012**.
- [21] F. Barbir, "PEM Fuel Cells," in *PEM Fuel Cells: Theory and Practice*, 2 nd., USA: Elsevier, **2005**, pp. 27–51.
- [22] F. C. Today, "PEMFC." [Online]. Available: <http://www.fuelcelltoday.com/technologies/pemfc>. [Accessed: 11-Jul-2014].
- [23] M. Cifrain, K. Kordesch, A. Lamm, and H. A. Gasteiger, "Hydrogen / oxygen (Air) fuel cells with alkaline electrolytes Chapter 14 Hydrogen / oxygen (Air) fuel cells with alkaline electrolytes," vol. 1, pp. 267–280, **2003**.
- [24] A. S. Aricò, V. Baglio, and V. Antonucci, "Direct Methanol Fuel Cells : History , Status and Perspectives," in *Electrolysis of Direct Methanol Fuel Cells*, Weinheim: Wiley-VCH Verlag GmbH & Co, **2009**, pp. 3–25.
- [25] A. Hacquard, "Improving and Understanding Direct Methanol Fuel Cell (DMFC) Performance By," Worcester Polytechnic Institute, **2005**.
- [26] G. L. Soloveichik, "Regenerative Fuel Cells for Energy Storage," *Proc. IEEE*, vol. 102, no. 6, pp. 964–975, Jun. **2014**.

- [27] S. S. Hosseiny, "Vanadium / Air Redox Flow Battery," University of Twente, Enschede, The Netherlands, **2011**.
- [28] T. Shigematsu, "Redox Flow Battery for Energy Storage," **2011**.
- [29] P. De Boer, "Flow batteries," *Leonardo Energy*, pp. 1–9, **2007**.
- [30] A. Z. Weber, M. M. Mench, J. P. Meyers, P. N. Ross, J. T. Gostick, and Q. Liu, "Redox flow batteries: a review," *J. Appl. Electrochem.*, vol. 41, no. 10, pp. 1137–1164, Sep. **2011**.
- [31] R. R. Maria Skyllas-Kazacos, Miron Rychick, "All-vanadium redox battery," 4786567, **1988**.
- [32] X. Xie, "Vanadium Redox-Flow Battery," California, **2011**.
- [33] G. Kear, A. A. Shah, and F. C. Walsh, "Development of the all - vanadium redox flow battery for energy storage : a review of technological , financial and policy aspects," **2011**.
- [34] and S. A. M. L. L. Swette, A. B. LaConti, "Proton-exchange membrane regenerative fuel cells," *J. Power Sources*, vol. 47, pp. 343–351, **1994**.
- [35] A. Oberhofer and P. Meisen, "Energy Storage Technologies & Their Role in Renewable Integration July 2012," California, **2012**.
- [36] D. Herman, "Comparison of Storage Technologies for Distributed Resource Applications," California, **2003**.
- [37] V. Viswanathan, A. Crawford, L. Thaller, D. Stephenson, S. Kim, W. Wang, G. Coffey, P. Balducci, Z. Gary, L. Li, and V. Sprenkle, "Estimation of Capital and Levelized Cost for Redox Flow Batteries," pp. 1–16, **2012**.
- [38] V. Viswanathan, A. Crawford, D. Stephenson, S. Kim, W. Wang, B. Li, G. Coffey, E. Thomsen, G. Graff, P. Balducci, M. Kintner-Meyer, and V. Sprenkle, "Cost and performance model for redox flow batteries," *J. Power Sources*, vol. 247, pp. 1040–1051, Feb. **2014**.
- [39] / J. R. P., "Tubulair," 2012. [Online]. Available: http://www.tubulair.de/1/project/?no_cache=1. [Accessed: 15-Aug-2014].
- [40] Q. Luo, H. Zhang, J. Chen, D. You, C. Sun, and Y. Zhang, "Preparation and characterization of Nafion/SPEEK layered composite membrane and its application in vanadium redox flow battery," *J. Memb. Sci.*, vol. 325, no. 2, pp. 553–558, Dec. **2008**.

- [41] R. K. Nagarale, G. S. Gohil, and V. K. Shahi, "Sulfonated poly(ether ether ketone)/polyaniline composite proton-exchange membrane," *J. Memb. Sci.*, vol. 280, no. 1–2, pp. 389–396, Sep. **2006**.
- [42] S. Winardi, S. C. Raghu, M. O. Oo, Q. Yan, N. Wai, T. M. Lim, and M. Skyllas-Kazacos, "Sulfonated poly (ether ether ketone)-based proton exchange membranes for vanadium redox battery applications," *J. Memb. Sci.*, vol. 450, pp. 313–322, Jan. **2014**.
- [43] H. Prifti, A. Parasuraman, S. Winardi, T. M. Lim, and M. Skyllas-Kazacos, "Membranes for Redox Flow Battery Applications," *Membranes (Basel)*, vol. 2, no. 4, pp. 275–306, Jun. **2012**.
- [44] B. P. Tripathi and V. K. Shahi, "Surface redox polymerized SPEEK–MO₂–PANI (M=Si, Zr and Ti) composite polyelectrolyte membranes impervious to methanol," *Colloids Surfaces A Physicochem. Eng. Asp.*, vol. 340, no. 1–3, pp. 10–19, May **2009**.
- [45] A. G. Manohar, S.K., Macdiarmid, "Polyaniline: pernigraniline, an isoable intermediate in the conventional chemical synthesis of emeraldine," *Synth. Met.*, pp. 711–714, **1991**.
- [46] Z. Fu, Z. Wei, X. Lin, T. Huang, and A. Yu, "Polyaniline membranes as waterproof barriers for lithium air batteries," *Electrochim. Acta*, vol. 78, pp. 195–199, **2012**.
- [47] J. Roeder, H. Silva, S. Nunes, and a Pires, "Mixed conductive blends of SPEEK/PANI," *Solid State Ionics*, vol. 176, no. 15–16, pp. 1411–1417, May **2005**.
- [48] J. Roeder, V. Zucolotto, S. Shishatskiy, J. R. Bertolino, S. P. Nunes, and A. T. N. Pires, "Mixed conductive membrane: Aniline polymerization in an acid SPEEK matrix," *J. Memb. Sci.*, vol. 279, no. 1–2, pp. 70–75, Aug. **2006**.
- [49] and J. L. Schwenzer B, S Kim, M Vijayakumar, Z Yang, "Correlation of Structural Differences between Nafion/Polyaniline and Nafion/Polypyrrole Composite Membranes and Observed Transport Properties," *J. Memb. Sci.*, vol. 372(1–2), pp. 11–19, **2011**.
- [50] S.-K. M. RYCHCIK M, "Evaluation of electrode materials for all-vanadium redox flow cell," *J. Power Sources*, vol. 19, pp. 45–54, **1987**.
- [51] A. G. Macdiarmid, J. C. Chiang, and A. F. Richter, "Polyaniline: a new concept in conducting polymers," *Synth. Met.*, vol. 18, no. 1–3, pp. 285–290, **1987**.

- [52] M. Skyllas-Kazacos, “New All-Vanadium Redox Flow Cell,” *J. Electrochem. Soc.*, vol. 133, no. 5, p. 1057, **1986**.
- [53] C.-N. Sun, F. M. Delnick, L. Baggetto, G. M. Veith, and T. a. Zawodzinski, “Hydrogen evolution at the negative electrode of the all-vanadium redox flow batteries,” *J. Power Sources*, vol. 248, pp. 560–564, Feb. **2014**.
- [54] S. Iijima, “Helical microtubules of graphitic carbon,” *Nature*, vol. 354, no. 6348, pp. 56–58, **1991**.
- [55] M. F. L. De Volder, S. H. Tawfick, R. H. Baughman, and a J. Hart, “Carbon nanotubes: present and future commercial applications,” *Science*, vol. 339, no. 6119, pp. 535–9, Feb. **2013**.
- [56] W. M. Gendel, Y., David, O, “Microtubes made of carbon nanotubes,” *Carbon N. Y.*, vol. 68, pp. 818–820, **2014**.
- [57] P. C. S. Hayfield, “Development of the Noble Metal / Oxide Coated Titanium Electrode,” *Platin. Met. Rev.*, vol. 42, no. 1, pp. 27–33, **1998**.
- [58] W. M. David, O, Gendel, Y., “Tubular macro-porous titanium membranes,” *J. Memb. Sci.*, vol. 461, pp. 139–145, **2014**.
- [59] M. Sun, B., Skyllas-Kazacos, “Modification of Graphite Electrode Materials,” *Electrochim. Acta*, vol. 37, no. 1, pp. 1253–1260, **1991**.
- [60] P. Chapman, X. X. Loh, a. G. Livingston, K. Li, and T. a C. Oliveira, “Polyaniline membranes for the dehydration of tetrahydrofuran by pervaporation,” *J. Memb. Sci.*, vol. 309, no. 1–2, pp. 102–111, Feb. **2008**.
- [61] D. S. Aaron, Q. Liu, Z. Tang, G. M. Grim, a. B. Papandrew, a. Turhan, T. a. Zawodzinski, and M. M. Mench, “Dramatic performance gains in vanadium redox flow batteries through modified cell architecture,” *J. Power Sources*, vol. 206, pp. 450–453, May **2012**.
- [62] S. Chandrabose Raghu, M. Ulaganathan, T. M. Lim, and M. Skyllas Kazacos, “Electrochemical behaviour of titanium/iridium(IV) oxide: Tantalum pentoxide and graphite for application in vanadium redox flow battery,” *J. Power Sources*, vol. 238, pp. 103–108, Sep. **2013**.
- [63] S. Vengatesan, E. Cho, H.-J. Kim, and T.-H. Lim, “Effects of curing condition of solution cast Nafion® membranes on PEMFC performance,” *Korean J. Chem. Eng.*, vol. 26, no. 3, pp. 679–684, May **2009**.

- [64] Q. Luo, H. Zhang, J. Chen, P. Qian, and Y. Zhai, "Modification of Nafion membrane using interfacial polymerization for vanadium redox flow battery applications," *J. Memb. Sci.*, vol. 311, no. 1–2, pp. 98–103, Mar. **2008**.
- [65] T. Soboleva, Z. Xie, Z. Shi, E. Tsang, T. Navessin, and S. Holdcroft, "Investigation of the through-plane impedance technique for evaluation of anisotropy of proton conducting polymer membranes," *J. Electroanal. Chem.*, vol. 622, no. 2, pp. 145–152, Oct. **2008**.
- [66] S. K. Mohammadi, T., M., "Evaluation of the chemical stability of some membranes in vanadium solution," *J. Appl. Electrochem.*, vol. 27, pp. 153–160, **1997**.
- [67] M. Chen, D. , Hickner, "V⁵⁺ degradation of sulfonated Radel membranes for vanadium redox flow batteries," *Phys. Chem. Chem. Phys.*, vol. 15, no. 27, pp. 11299–11305, **2013**.
- [68] Q. Luo, L. Li, W. Wang, Z. Nie, X. Wei, B. Li, B. Chen, Z. Yang, and V. Sprenkle, "Capacity decay and remediation of nafion-based all-vanadium redox flow batteries.," *ChemSusChem*, vol. 6, no. 2, pp. 268–74, Feb. **2013**.

CURRICULUM VITAE

Credentials

Name, Surname : Korcan Perçin
Place of Birth : Seyhan, TURKEY
Marital Status : Single
E-mail : korcanpercin@hotmail.com
Address : Barbaros mah. J.F.Kennedy cad. No:68/10 Ankara

Education

BSc. : Gazi University, Chemical Engineering
MSc. : Hacettepe University, Chemical Engineering (As an
Exchange Student in RWTH Aachen,Germany)
PhD. :

Foreign Languages

English : Reading : Advanced
Writing : Advanced
Listening : Advanced
Speaking : Upper Intermediate

German : Reading : Upper Intermediate
Writing : Upper Intermediate
Listening : Intermediate
Speaking : Intermediate

Work Experience

- Internships : Aselsan A.Ş. , Deionized Water Production Systems (20 days), 2011
Sanovel A.Ş., Quality Control Lab. for pharmaceuticals (25 days), 2009
- Others : Ergin Jewelry Shop, Silivri, Istanbul as Salesman (2005-2012, for every summer university break)

Areas of Experiences

- Electrochemical Batteries : Redox Flow Batteries were studied during the MSc. thesis research at CVT, RWTH Aachen, (Sep. 2013- Sep. 2014)
- Composite Membranes : Pd-Ag Composite Membranes were studied during the BSc. Thesis at Gazi University (Sep. 2011- June 2012)

Projects and Budgets

- Projects : Tubulair , a joint research project in Germany. Worked as a MSc. MSc. Student for one year at CVT, RWTH Aachen, (Sep. 2013- Sep. 2014).

Publications

David O, Percin K., Gendel Y., Wessling M., “Proton-exchange membranes based on sulfonated poly(ether ether ketone)/polyaniline blends for all- and air-vanadium redox flow battery applications” , *Journal of Energy Storage*, (Not published yet)

Oral and Poster Presentations

Gendel Y., David O., Roth H., Percin K., Rommerskirchen A., Wessling M. (2014)
Tubular Electrochemical Membrane Reactors. 15th Aachener Membrane Kolloquium.
Aachen, Germany. November 12-13, 2014 (Paper and Presentation)